N72-12871

NASA CR-111984

VIBRATION ANALYSIS OF A 1/15 SCALE
DYNAMIC MODEL OF A
SPACE SHUTTLE CONFIGURATION

By E. A. Thornton

Prepared under Grant No. NAS1-9434-20 by
OLD DOMINION UNIVERSITY
Norfolk, Va.

for Langley Research Center

NATIONAL AERONAUTICS AND SPACE ADMINISTRATION

ABSTRACT

The natural frequencies and mode shapes of a 1/15 scale space shuttle dynamics model are analytically determined. The model, a parallel beam type structure with delta wings, is dynamically representative of the stiffness and mass properties of an early space shuttle design. Important characteristics of the model are elastic interfaces with adjustable spring rates.

Normal mode computations are made using the finite element modeling technique as implemented in the NASTRAN (NASA Structural Analysis) computer program. The feasibility of neglecting elastic deformations in the lower modes was investigated using a rigid body model.

Using NASTRAN, natural frequencies and mode shapes were first calculated for the booster fuselage, orbiter fuselage, and both delta wings in a free-free condition. Next, the fuselages were connected for various spring rates. Then the wings were attached to each fuselage, and the booster and orbiter were analyzed as separate airplanes. Finally, the two airplanes were elastically joined, and the complete model was analyzed.

In the complete model for an interface nominal spring constant of 10^3 lb/in there were forty modes with frequencies less than 200 HZ. The coupling of the booster and orbiter motions were found to be significantly affected by the spring interface stiffnesses.

ACKNOWLEDGEMENT

The work report in this report was sponsored by NASA under Master Contract Agreement NASI-9434, Task Order No. 20 through the Langley Research Center, Hampton, Virginia. During the early phase of this work Mr. Howard Adelman of the NASTRAN Management Office acted as contract monitor. The final phase of the work was completed under the direction of the Loads Division with Mr. John L. Sewall acting as monitor. The principal investigator is indebted to these engineers for their assistance as well as to Mr. S. Leadbetter of the Loads Division who is conducting the experimental investigation.

TABLE OF CONTENTS

	Page
LIST OF FIGURES	vi
LIST OF TABLES	vii
NOMENCLATURE	ix
INTRODUCTION	1
DESCRIPTION OF MODEL	3
COMPLETE MODEL	3
FUSELAGE COMPONENTS	3
WING COMPONENTS	4
ELASTIC INTERFACE	4
FUSELAGE-WING INTERFACE	5
ANALYSIS	6
NASTRAN ANALYSIS	6
FUSELAGE COMPONENTS	6
WING COMPONENTS	8
ELASTIC INTERFACE	10
FUSELAGE-WING INTERFACE	11
BOOSTER AND ORBITER AIRPLANES	13
COMPLETE MODEL	
RIGID BODY ANALYSIS	14
RESULTS AND DISCUSSION	15
COMPONENT MODES	15
ELASTICALLY CONNECTED FUSELAGES	19
BOOSTER AIRPLANE	23
ORBITER AIRPLANE	23
COMPLETE MODEL	24
CONCLUSIONS	28
REFERENCES	29
APPENDIX A-ANALYSIS OF ELASTIC INTERFACE	30
APPENDIX B-RIGID BODY ANALYSIS	44

List of Figures

Figure	Title	Page
1	Photograph of 1/15 scale space shuttle model.	52
2	Schematic of 1/15 scale space shuttle model.	53
3	Photograph of elastic interface between booster and orbiter fuselages.	54
4	Schematic of fuselage-wing interface.	55
5	Schematic of booster delta wing.	56
6	Schematic of orbiter delta wing.	57
7	Geometry for multipoint constraint equations.	58
8	Schematic of booster fuselage-wing interface geometry.	59
9	Schematic of orbiter fuselage-wing interface geometry.	60
10	Schematic of booster airplane idealization.	61
11	Schematic of orbiter airplane idealization.	62
12	Bending modes of booster fuselage.	63
13	Bending modes of orbiter fuselage.	64
14	Plotter orientation for delta wing mode shape plots.	65
15	Mode shapes of booster delta wing.	66
16	Mode shapes of orbiter delta wing.	69
17	Mode shapes of elastically connected fuselages. Liftoff weight distribution. 10^2 lb/in nominal springs.	72
18	Mode shapes of elastically connected fuselages. Liftoff weight distribution. 10^5 lb/in nominal springs.	73
19	Variation of NASTRAN and rigid body analyses frequencies with nominal spring constant.	74

Figure	Title	Page
20	Comparison of NASTRAN and rigid body analyses modes. 10^2 lb/in nominal spring.	75
21	Plotter view of elastically connected fuselages.	76
22	Mode shapes of elastically connectef fuselages. Theoretical flexibility matrix. Nominal 10^3lb/in.	77
23	Frequency spectrums for elastically connected fuselages.	81
24	Variation of NASTRAN and rigid body analyses frequencies. Elastically connected fuselages. Theoretical flexibility matrix.	82
25	Plotter orientation for complete model mode shape plots.	83
26	Mode shapes of booster airplane. Liftoff weight distribution.	84
27	Mode shapes of orbiter airplane. Liftoff weight distribution.	86
28	Mode shapes of complete model. 10^3 lb/in theoretical flexibility matrix. Liftoff weight distribution.	88
29	Frequency spectrums for booster and orbiter airplanes and complete model. 10^3 lb/in theoretical flexibility matrix. Liftoff weight distribution.	93
A-1	Schematic of elastic interface.	94
A-2	Displacement components of elastic interface.	95
A-3	Elements of matrix $[K_Z]$.	96
A-4	Elements of matrix $[K_{XZ}]$.	96
B-1	Plane motion rigid body model.	97
B-2	General motion rigid body model.	97
B-3	Stiffness matrix in interface coordinates.	98
B-4	Stiffness matrix $[K_1]$ in attachment coordinates.	99
B-5	Elements of $[K_1]$ in generalized coordinates.	100

List of Tables

Table	Title	Page
I	Booster and orbiter simulated propellent weights.	102
II	Booster fuselage element properties.	103
III	Booster fuselage concentrated mass properties.	104
IV	Orbiter fuselage element properties.	105
V	Orbiter fuselage concentrated mass properties.	106
VI	Booster wing grid point coordinates.	107
VII	Booster wing element properties.	109
VIII	Orbiter wing grid point coordinates.	110
IX	Orbiter wing element properties.	111
X	Theoretical and Experimental flexibility. Matrices for elastic interface.	111
XI	Resequencing of grid points for complete model.	112
XII	Natural frequencies of booster and orbiter fuselages.	113
XIII	Natural frequencies of free-free booster and orbiter wings.	114
XIV	Frequencies of elastically connected fuselages. Nominal springs. Liftoff weight distribution.	19
XV	Frequencies of elastically connected fuselages. Theoretical flexibility matrix. Liftoff weight distribution.	115
XVI	Comparison of frequencies for elastically connected fuselages. Nominal 10^3/in interface. Liftoff weight distribution.	116
XVII	Frequencies of booster and orbiter airplanes.	117
XVIII	Frequencies of complete model.	118
AI	Spring interface dimensions.	119
AII	Spring interface flexibility matrix.	120
AIII	Spring interface stiffness matrices.	128
BI	Mass properties of booster and orbiter rigid body models.	136

NOMENCLATURE

a	height of orbiter attachment bracket, see Figure A-1.
[a]	flexibility matrix.
A	cross-sectional area.
A_p	cross-sectional area of one pitch leaf.
A_j	coefficient in equation of constraint, see equation 4.
C	width of booster attachment bracket, see Figure A-1.
d	distance from top of booster attachment bracket to orbiter centerline.
E	modulus of elasticity.
f_i	forces applied at grid point i, see equation (1).
G	modulus of rigidity.
h	vertical distance between pitch leafs, see Figure A-1.
I, I1, I2	area moments of inertia for CBAR elements.
I12	product of inertia for CBAR elements.
I_{BX}, I_{BY}	area moments of inertia of booster attachment bracket
I_{PX}, I_{PZ}	area moments of inertia of pitch leafs.
I_{YWX}, I_{YWY}	area moments of inertia of yaw leafs.
I_1, I_2	mass moments of inertia of plane rigid body model, see equation (B-3).
I_{xx}	mass moment of inertia of concentrated masses representing fuselage roll inertia.
I_{XO}, I_{YO}, I_{ZO}	mass moments of inertia of rigid body model of orbiter.
I_{XB}, I_{YB}, I_{ZB}	mass moments of inertia of rigid body model of booster.

J	polar moment of inertia.
K	spring constant.
$[K]$	stiffness matrix.
ℓ_P	length of pitch spring, see Figure A-1.
L	total height of interface, see Figure A-4.
ℓ_Y	length of yaw spring, see Figure A-1.
L_1, L_2	effective lengths of booster attachment bracket arms for bending in XZ and YZ planes, respectively.
M	concentrated mass.
$[M]$	mass matrix.
M_1, M_2	masses of plane rigid body model, see equation (B-3).
$[M_O]$	rigid body mass matrix of orbiter, see equation (B-8b).
$[M_B]$	rigid body mass matrix of booster, see equation (B-8c).
$\{q\}$	generalized displacement coordinates.
R1, R2, R3	rotational displacement components in mode shapes.
$[S]$	rigid body transformation matrix, see equation (1).
t_P	thickness of pitch leaf, see Figure A-1.
t_Y	thickness of yaw leaf, see Figure A-1.
T1, T2, T3	translational displacement components in mode shapes.
$\{u\}$	displacement vector.
V_1	strain energy of elastic interface.
X,Y,Z	coordinate axes.
X_0, Y_0, Z_0	coordinates of dependent grid point in equations of constraint, see equation (5) and Figure 7.

$[Z]$	NASTRAN flexibility matrix.
Z, Z_2	dimensions of wing attachment brackets, see Figure 4.
$[\beta_a], [\beta_b]$	transformation matrices.
$\delta_1, \delta_2 \ldots$	deflection components.
$\Theta_1, \Theta_2, \ldots$	rotation components about X or Y axes.
ρ	mass density.
$\theta_1, \theta_2, \ldots$	rotation components about Z axis.
ω	circular frequency.

NASTRAN notation:

CBAR	beam element connecting two grid points.
CELAS2	scalar spring element connecting two grid points.
CONM2	concentrated mass at a grid point.
CORD2R	rectangular coordinate system defined by three points.
GENEL	general element connecting two grid points; defined in terms of flexibility matrix [Z] and transformation matrix [S].
MPC	multipoint constraint; used to define rigid connections.
OMIT1	defines degrees of freedom to be deleted from problem through matrix partitioning; used to remove mass singularities.
NSM	nonstructural mass.
PBAR	specifies properties of CBAR element.
SEQGP	used to reidentify the sequence of grid points such as to optimize bandwidth of matrices.

INTRODUCTION

The determination of the dynamic characteristics of a spacecraft structure is an important step in the development of the overall spacecraft systém. This is particularly true for the Space Shuttle since a new concept in space vehicle design is being used. The Space Shuttle will be comprised of a parallel arrangement of the launch vehicle and space vehicle during the launch phase. This arrangement raises the possibility of dynamic effects which have not previously been encountered.

To initiate the dynamic studies of the Space Shuttle configuration, an unpublished analysis was made at LRC of a proposed design supplied by the NASA Manned Spacecraft Center. This analysis, for a straight-wing configuration of the Shuttle, represented the vehicles by an assembly of finite beam elements and lumped masses. Each of the two elastic connections between the vehicles was represented by a single translational spring. Pitch motions of the fuselages and flapping motions of the wings were permitted. Normal mode calculations were made for six different values of the connecting springs. The results of this exploratory study showed that, in general, the modes were significantly controlled by the spring rates of the vehicle connections.

As the next phase in the study of the Space Shuttle dynamic behavior, Langley Research Center designed and procured a 1/15 scale model of proposed straight wing and delta wing configurations of the Shuttle. The vibration characteristics of this model are being analytically and experimentally investigated.

During an 11 week period at Langley Research Center in the summer of 1970, the principal investigator, under the NASA-ASEE Summer Faculty Fellowship program, was involved in computations to establish pre-test frequencies and mode shapes for the straight wing configuration of this model. These computations made use of the finite element modeling technique as implemented in the NASTRAN (NASA Structural Analysis) computer program. Some of the results of this work and some preliminary experimental results were presented at the NASA Space Shuttle Technology Conference held at LRC in March, 1971, (reference 1).

The present study is an extension of this work and is concerned with an analytical investigation of the delta wing configuration of this model.

The objectives of this study were to:

(a) Use the NASTRAN finite element computer program to compute the natural frequencies and mode shapes for the 1/15 scale dynamic model of the Space Shuttle with delta wings.

(b) Study the effect of connection spring rates on frequencies, mode shapes, and the coupling between vehicle motion.

(c) Formulate and analyze a rigid body representation of the 1/15 scale model to determine the feasibility of neglecting elastic deformations in the calculation of the lower modes of the system.

DESCRIPTION OF MODEL

In this section a brief description of the delta wing configuration of the 1/15 scale shuttle model will be given. The complete model will be described first, and then the important characteristics of each component will be reviewed.

Complete Model

The complete delta wing model is shown suspended by cables in Figure 1. This figure shows the booster component supporting the orbiter component through two elastic interfaces in a forward mounting position. It is also possible to support the orbiter through a rear mounting position which is not shown. A schematic with the orbiter mounted in the forward position is given in Figure 2. This figure also gives some of the general dimensions and defines the overall coordinate system used to describe the model.

The stiffness and mass properties of the model are based upon the 12,500 lb. payload version of the MSC Space Shuttle Configuration. Each component was designed to closely approximate scaled stiffness and mass distribution curves of the MSC design.

Fuselage Components

The booster fuselage spar was fabricated from thin walled, tapered aluminum cylindrical sections reinforced by internal bulkheads. The orbiter fuselage spar is similar except that over a major portion of its length the diameter is constant. Each fuselage component has foam ballast weight holders used to support lead weights which simulate the propellant. The orbiter fuselage includes a lead nose mass to simulate the payload. The locations of the weights are shown in Figure 2, and the values of the added weights are tabulated in Table I.

Wing Components

Each wing has three spars which were designed to give the proper bending stiffness distribution for the wing. The wings are clamped to the fuselages at three locations through mounting brackets welded to each spar. Over the length of each spar where the mounting bracket is attached the cross section of the spar is constant and has the form of an H. Slightly outboard of the mounting bracket the cross changes to a form obtained by welding two angle bars together. This cross section tapers linearly from the fuselage to the wing tip. The three spars are connected by forward-aft members of constant cross section. The forward-aft members are generally angle bars except at the wing tips where flat bars were used.

Elastic Interface

The details of one of the elastic interfaces are shown in a photograph in Figure 3. Each of the interfaces was designed to permit varying the nominal spring rates in the pitch and yaw directions. This was accomplished by incorporating removable pitch and yaw leaves. Four sets of spring leaves with nominal spring constants 10^2, 10^3, 10^4, and 10^5 lb/in. were designed for each of the pitch and yaw directions. No scaling considerations were involved in selecting the nominal spring constant values. The values were selected from the results of preliminary calculations made at LRC. The dimensions of these leaves and other interface dimensions are given in Table A-I of Appendix A.

Fuselage-Wing Interface

Some of the details of a typical booster and orbiter fuselage-wing interface are shown in Figure 4. The interface consists of two parts: (1) a top semi-circular bracket welded to the fuselage, and (2) a larger bottom bracket welded to the wing spar. The two brackets are joined by two bolts per side. The overall dimensions of the interfaces for the two fuselage are also shown in Figure 4.

In this section a description of the model has been given. *In the next section the idealizations and properties of the* mathematical model will be described.

ANALYSIS

The analysis of the natural frequencies and mode shapes of the 1/15 scale model was made using a NASTRAN idealization and a rigid body idealization.

In the NASTRAN analysis, each component was first analyzed in a free-free condition. As the second step, the fuselage components were connected by the elastic interfaces. As the third step, the wings were attached to each fuselage component, and the booster and orbiter were analyzed as separate airplanes. In the final step, the two airplanes were connected through the elastic interface to represent the complete model.

In the rigid body idealization the plane motion of the two elastically connected fuselages was analyzed first. Then a three-dimensional analysis of the complete model was made.

NASTRAN Analysis

In this section the NASTRAN idealization of the model will be described. The idealization of each component will be described first. Then two methods of representing the elastic interfaces will be described. Finally, a description of the method of representing the fuselage-wing interfaces will be discussed.

Fuselage Components.- The booster fuselage was idealized by an assembly of ten concentrated masses and nine beam elements. The concentrated masses were represented in NASTRAN using the bulk data card CONM2, and the beam elements were represented by CBAR elements. The idealization and the associated mass and element properties of the booster fuselage are given in Tables II and III.

In NASTRAN, the beam element CBAR is assumed to have uniform properties. Because of this the cross-sectional properties tabulated in Table II are average values based on the diameter at the mid-point of each element.

Added weights 2 and 4 (See Figure 2) being distributed over relatively short lengths, were represented as concentrated masses at grid points 5 and 8, respectively. Added weights 1 and 3 were distributed uniformly over elements 2 and 3 and are shown as non-structural mass (NSM) in Table II. (Non-structural mass is a quantity of material which adds mass to a structural element but does not contribute to the stiffness.) The actual mass of each beam element is computed internally in the NASTRAN program from the input data shown in Table II. The NSM property is input on the PBAR beam property card.

Concentrated masses were also used to model local distributions of mass, such as the reinforcing bulkheads. The values of mass and mass moments of inertia shown in Table III for the Liftoff condition are listed as nominal values and test values. The nominal values were computed from the drawings of the model. The test values were obtained by adding laboratory weighed values of the elastic interfaces and rigging brackets to the nominal values.

The mass moment of inertia I_{xx} about the roll axis of the fuselage was represented by concentrations at each grid point. Included in each value of I_{xx} are the roll inertias of the bulkheads, the added weights, and each element of the fuselage. The inertia of each element was divided equally between adjacent grid points. In Table III for Liftoff, two values of the roll moments of inertia I_{xx} are shown. The nominal values are based upon the design dimensions of the model. The test values were calculated for slightly different radial locations of the weights used in the experimental vibration tests. The mass moments of inertia of the add-on weights and the fuselage itself about the other two axes, i.e., the "rotatory inertia", was neglected.

The orbiter fuselage was idealized in a manner similar to the booster fuselage. Seven beam elements and eight concentrated masses were used. The idealization and properties of the orbiter fuselage are shown in Tables IV and V.

The two added weights of this component were distributed over their supporting beam elements and modeled as NSM. The payload was modeled as a concentrated mass.

For all elements a modulus of elasticity $E = 10.1 \times 10^6$ lb/in^2 and a modulus of rigidity $G = 3.8 \times 10^6$ lb/in^2 were used. The mass density was taken as $\rho = 2.539 \times 10^{-4} lb\text{-}sec^2/in^4$. These values were also used for the wing components.

Wing Components.- The booster delta wing is shown schematically in Figure 5. Three coordinate systems were used to locate the grid points and are shown in this figure. The coordinates of the grid points in these coordinate systems are tabulated in Table VI. In NASTRAN, coordinate system 1 was used as the basic coordinate system, and coordinate systems 2 and 3 were referenced to the basic coordinate system by using the bulk data cards CORD2R.

The wing was idealized using 55 CBAR elements. For the spars which are tapered the average properties of the elements were used. The properties for all elements are tabulated in Table VII. All properties listed in this table are referred to the local beam element coordinate system. I1 represents the moment of inertia of the cross section associated with bending in a plane perpendicular to the plane of the wing; I2 represents the moment of inertia associated with bending in the plane of the wing. I12 represents the product of inertia in the local NASTRAN coordinate system. The sign was established according to the NASTRAN sign conventions given in paragraph 1.3.2 of Reference 2.

The lower half of the fuselage mounting brackets which are welded to the wing spars were represented as concentrated masses. Equal masses of 10.34-4 lb-sec^2/in were located at grid points 1-9. The bending stiffnesses of these brackets were neglected.

The orbiter delta wing is shown schematically in Figure 6. The grid points for this wing were located in one basic coordinate system, and these coordinates are tabulated in Table VIII.

The wing was idealized using 29 CBAR elements. As for the booster wing, average values were used for the tapered portions.

The element properties are tabulated in Table IX. The definitions for these quantities are similar to those for the booster wing.

Equal concentrated masses of 4.66-4 lb-sec^2/in were located at grid points 1-9 to represent the fuselage mounting brackets.

Elastic Interface.- The elastic interfaces were modeled in two ways. In the first model the interface was represented using simple linear springs with the nominal spring constants in the pitch and yaw planes. In NASTRAN these are called scalar elements and were input as bulk data through the use of the CELAS2 card.

In the second representation of the elastic interfaces the general structural element GENEL was used. The element describes the elastic interface through a six by six flexibility matrix [Z] and a six by six rigid body transformation matrix [S]. These matrices are defined by the equation, (See Reference 3, Section 5.7),

$$\{u_i\} = [Z]\{f_i\} + [S]\{u_d\} \tag{1}$$

where $\{u_i\}$ denotes the set of displacement components at grid point i;

$[Z]$ denotes the flexibility matrix;

$\{f_i\}$ denotes the forces at grid point i corresponding to the u_i displacements,

$[S]$ a rigid body matrix whose terms are the displacements $\{u_i\}$ due to unit motions of the coordinates $\{u_d\}$, when all $f_i = 0$.

$\{u_d\}$ denotes the set of displacement components at grid point j.

For example, the forward elastic interface connects grid point 3 on the booster fuselage and grid point 22 on the orbiter fuselage. In this case

$$\{u_i\} = \lfloor 22\text{-}1,\ 22\text{-}2,\ 22\text{-}3,\ 22\text{-}4,\ 22\text{-}5,\ 22\text{-}6 \rfloor^T,$$

and

$$\{u_d\} = \lfloor 3\text{-}1,\ 3\text{-}2,\ 3\text{-}3,\ 3\text{-}4,\ 3\text{-}5,\ 3\text{-}6 \rfloor^T, \tag{2}$$

where 22-1 denotes the displacement component 1 at grid point 22, 22-2 denotes the displacement component 2 at grid point 22, etc.

With no applied forces $\{f_i\}$ the displacements $\{u_i\}$ and $\{u_d\}$ are related by the transformation matrix [S]. For the geometry shown in Figure 2,

$$[S] = \begin{bmatrix} 1 & 0 & 0 & 0 & 15.6 & 0 \\ 0 & 1 & 0 & -15.6 & 0 & 0 \\ 0 & 0 & 1 & 0 & 0 & 0 \\ 0 & 0 & 0 & 1 & 0 & 0 \\ 0 & 0 & 0 & 0 & 1 & 0 \\ 0 & 0 & 0 & 0 & 0 & 1 \end{bmatrix} . \tag{3}$$

The flexibility matrix [Z] was determined for each of the nominal spring constants using the theory developed in Appendix A. The results of these calculations are tabulated there in Table A-II. In addition, for the nominal spring case of 10^3 lb/in, the flexibility coefficients were measured experimentally at Langley Research Center. The non-zero elements of the theoretical flexibility matrix for the nominal 10^3 lb/in case and the experimental values for this case are tabulated in Table X.

Fuselage-Wing Interfaces.- Each fuselage-wing interface was assumed to be rigid. In NASTRAN rigid connections are modeled by writing equations of constraint between the displacement components at the grid points of interest. These equations take the form

$$\sum_j A_j u_j = 0 \tag{4}$$

where A_j are coefficients determined from geometry and u_j are the displacement components. The first coordinate in the sequence is assumed to be the dependent coordinate. Equations of the form of (4) are called multipoint constraints and are input as bulk data using MPC cards.

For the fuselage-wing interfaces a general set of multipoint constraint equations were derived as follows. Consider grid points A and B shown in Figure 7. For convenience, the origin of the coordinate system is located at grid point A. Grid point A and B are connected by a fictitious rigid link. The displacements at point B are then related to the displacements at A by the equation

$$\begin{bmatrix} u_1 \\ u_2 \\ u_3 \\ u_4 \\ u_5 \\ u_6 \end{bmatrix}_B - \begin{array}{c} \begin{bmatrix} 1 & 0 & 0 & 0 & Z_0 & -Y_0 \\ 0 & 1 & 0 & -Z_0 & 0 & X_0 \\ 0 & 0 & 1 & Y_0 & -X_0 & 0 \\ 0 & 0 & 0 & 1 & 0 & 0 \\ 0 & 0 & 0 & 0 & 1 & 0 \\ 0 & 0 & 0 & 0 & 0 & 1 \end{bmatrix} \\ \begin{matrix} u_1 & u_2 & u_3 & u_4 & u_5 & u_6 \end{matrix} \end{array} \begin{bmatrix} u_1 \\ u_2 \\ u_3 \\ u_4 \\ u_5 \\ u_6 \end{bmatrix}_A = 0. \qquad (5)$$

Equation (5) represents 6 equations of constraint each of the form of equation (4). The multipoint equations of constraint for NASTRAN were written by substituting appropriate values of x_0, y_0, z_0 in these equations.

The wings were attached to the fuselage by assuming a rigid connection between six grid points at the outboard edge of the mounting brackets on the wing spars and the nearest grid points on the fuselage. Thus the wings were "cantilevered" from the fuselage with the cantilever points below and outboard of the fuselage centerline.

For the booster fuselage-wing interface grid points 6, 8, 9 on the booster fuselage were connected to grid points 34-39 on the booster wing. These connections are shown schematically in Figure 8. The values of x_0, y_0, z_0 used in equations (5) are tabulated in this figure. A total of 36 equations of constraint were written for the booster fuselage-wing interface.

The orbiter fuselage-wing interface was modeled in a similar way and is shown schematically in Figure 9. For this interface, 36 equations of constraint were also written.

Booster and Orbiter Airplanes.- The booster fuselage and delta wing components were connected using the multipoint equations of constraint to give a complete airplane. The same grid point numbers were used for the fuselage; new grid points for the wings were obtained by adding a double zero suffix. A plan view of the booster airplane idealization is shown schematically in Figure 10. The interface masses were equally distributed at grid points 34-39 of this idealization.

The orbiter fuselage and delta wing components were connected in a similar way to yield a complete airplane as shown in Figure 11. New wing grid point numbers were obtained by adding a zero one suffix to the original numbers. The interface masses were equally distributed at grid points 44-49 of this model.

Complete Model.- Using two GENEL elements, the booster and orbiter airplanes were elastically connected to represent the complete model. The forward GENEL element connected grid point 3 on the booster fuselage to grid point 22 on the orbiter fuselage.

The aft GENEL element connected grid point 4 on the booster fuselage to grid point 26 on the orbiter fuselage.

To reduce the band width of the stiffness matrix for the complete model the grid points were renumbered. This grid point resequencing was input to NASTRAN through the SEQGP bulk data cards. The resequencing of grid points is tabulated in Table XI.

Rigid Body Analysis

Two mathematical idealizations were used for the rigid body vibration analysis. In the first idealization the motion was assumed to be restrained to the pitch plane with longitudinal displacements prohibited. This gave a simple four degree of freedom model. The elastic interface for this case was represented as a scalar spring. In the second idealization, general three dimensional motion was permitted. The booster and orbiter were each allowed to have three displacements and three rotations so that the system possessed twelve degrees of freedom. The elastic interfaces in this case were represented by twelve by twelve stiffness matrices.

The details of these analyses are presented in Appendix B.

RESULTS AND DISCUSSION

In this section the results of the analysis will be presented and discussed beginning first with frequencies and mode shapes of each component. Then the results for the elastically connected fuselages will be described. Next the modes of the booster and orbiter airplanes will be discussed, and finally, the frequencies and mode shapes for the complete model will be given.

Component Modes

Fuselages.- The natural frequencies of the booster and orbiter fuselages were calculated using the properties given in Tables II-V for the nominal masses and moments of inertia. The booster fuselage has 60 degrees of freedom (DOF) with all displacements permitted; the orbiter has 54 DOF permitting all displacements. The consistent mass matrix option was specified, and the eigenvalue problems were solved by the inverse power method. The natural frequencies of the booster and orbiter fuselages are tabulated in Table XII. For comparison, some preliminary experimental frequencies obtained at LRC are also listed.

For the nominal weights these results show for the booster there are one to three bending modes in the frequency range below 200 HZ depending on the weight condition. For the cases where the weights were added, a torsional mode was also predicted at about 114 HZ. The axial modes were found to be outside of the frequency range of interest. For the orbiter fuselage, the frequencies tended to be substantially higher than the booster fuselage with only the fundamental bending mode below 200 Hz.

The experimental frequencies tend to generally confirm the predicted values particularly in the lower modes. The agreement becomes poorer with an increase in modal number. Better agreement with the experimental values for the higher modes could possibly be found by including the rotatory inertia of the added weights and by further subdivision of the fuselages using more beam elements. Because of the reasonable agreement of the lower modes these steps were not pursued.

The mode shapes of the bending modes of each fuselage are shown in Figures 12 and 13 for the liftoff and burnout weight distributions. These modes correspond to either pitch or yaw bending due to symmetry.

Wings.- In the "free-free" condition with all grid points having 6 displacement components the booster delta wing has 198 DOF, and the orbiter delta has 162 DOF. To reduce the size of the eigenvalue problems the lumped mass option was selected for each wing, and the rotational displacement components were deleted from the eigenvalue problem through the use of the bulk data card OMIT1. This reduced the size of the eigenvalue problems for the booster and orbiter wings to 99 and 81 DOF, respectively. Both of these eigenvalue problems were solved using the Givens method. The natural frequencies for the two wing components are listed in Table XIII. Some preliminary experimental frequencies are also listed.

The frequency tabulations show that the wings have relatively dense frequency spectrums compared to the fuselage components. The booster wing has 20 frequencies below 200 HZ, and the orbiter wing has 16 frequencies in this range.

The experimental frequencies show reasonable agreement with the predicted values; however, a large number of the theoretical modes were not detected in the vibration tests. This may be due to a number of reasons including the fact that a number of the frequencies tend to be very closely spaced. Also, it is likely that the higher modes of the analytical model are somewhat in error because of the crudeness of the finite element model.

There are at least two ways in which the mathematical model could have been improved. In the central region of each wing the mounting brackets are welded to the spars. Although the mass of these brackets was included, the stiffening effect of these brackets was neglected. No further attention was given to improving the finite element model of the wing in this region, however, because for the assembled components the fuselage-wing interface was assumed to be rigid. The second way of improving the finite element model concerns the tapered spars. Outboard of the fuselage brackets the wing spars taper to give a relatively rapid variation of EI. For simplicity, one finite element of constant cross section was used to represent each spar between junctions with the fore-aft wing members. For better agreement in the higher modes these sections of the wing should be represented with more elements. Since this would have roughly doubled the DOF for each wing further subdivision of the elements was not attempted.

The NASTRAN structural plotting capability was used to generate plots for the wing components. Figure 14 shows the plotter view of a typical delta wing. In the plots, each wing is viewed from an aft position at an angle of about 23° above the X axis. The first nine modes of the booster wing viewed in this manner are shown in Figure 15; the first nine modes of the orbiter wing are shown in Figure 16.

Each wing is symmetrical about the centerline of the fuselage, and the modes are therefore either symmetrical or antisymmetrical about this axis. Most of the modes are characterized by flapping motions, i.e. displacements which are primarily perpendicular to the plane of the wing. For the booster wing, of the mode shapes shown, all modes except 3 and 5 illustrate this type of deformation. Modes 3 and 5 consist of fore and aft deformations in the plane of the wing. For the orbiter wing, all modes shown, except for modes 4 and 7, have primarily out-of-plane displacements. Mode 4 has mainly in-plane displacements, and mode 7 has a large in-plane displacement at the centerline but the wing tips move perpendicular to the plane.

Although most wing modes are characterized by a large displacement component in one direction, the modes are generally three dimensional. For this reason, it should be observed that plots of the mode shapes from a single view such as used in Figures 15 and 16 do not show the general complexity of the motion.

Elastically Connected Fuselages

<u>Nominal springs</u>.- The frequencies of the elastically connected fuselages were first calculated with NASTRAN assuming plane motion with axial displacements prohibited. A consistent mass matrix was specified, and the inverse power method was used to solve the eigenvalue problem. The frequencies of the first six modes for the nominal weight condition and the four nominal spring cases are tabulated in Table XIV.

Table XIV Frequencies of elastically connected fuselages. Nominal springs. Liftoff weight distribution.

Frequencies, HZ

	K lb/in			
Mode	10^2	10^3	10^4	10^5
1	3.53	10.96	27.50	32.21
2	10.16	30.15	41.24	57.60
3	36.90	38.61	77.89	117.1
4	103.9	107.3	117.1	156.0
5	117.3	117.4	147.3	196.9
6	198.8	199.0	201.5	223.5

The mode shapes for the nominal 10^2 lb/in spring are shown in Figure 17, and the mode shapes for the 10^5 lb/in in spring are shown in Figure 18.

For the 10^2 lb/in spring, Figure 17 shows the fuselages move as rigid bodies in modes 1 and 2. Moreover, modes 3, 4, and 5 are essentially uncoupled fuselage bending modes for this spring constant. However, as the nominal spring constant is increased the fuselages have coupled deformations in all modes.

This is clearly shown in Figure 18.

The plane motion rigid body analysis was used to predict the frequencies for these spring and weight conditions, and the results are compared with the NASTRAN frequencies in Figure 19. This figure shows the rigid body analysis gives good agreement with the NASTRAN results for the first two modes for spring constants less than 10^3 lb/in. For spring constants greater than 10^3 lb/in., the rigid body analysis diverges rapidly from the NASTRAN results. Thus for $K > 10^3$ lb/in., the flexibility of the fuselage components play an important role and cannot be neglected. The mode shapes for the 10^2 lb/in case are compared in Figure 20.

Interface matrix representation.- The frequencies for the elastically connected fuselages were also calculated with NASTRAN by representing the elastic interface by its theoretical flexibility matrix. The lumped mass approach was taken and rotational components of displacement in the XZ and YZ planes were omitted. Each grid point was thus permitted to have all three translational components of displacement and a rotational component of displacement about the X axis. The resulting eigenvalue problem involved 72 DOF and was solved by the Givens method. The test weights were used for these calculations. The frequencies for the first fourteen modes for the four nominal spring cases are tabulated in Table XV.

The predominate motion associated with each frequency is also specified in this table.

With three dimensional motions permitted, the modes become more complex. Generally, the modes may be identified with motion in either the XZ (pitch) plane or YZ (yaw) plane. However, as Table XV shows, combined pitch-axial modes and roll modes also exist.

Computer plots of these modes were made for the 10^3 lb/in case. The plotter view of the elastically connected fuselages is shown in Figure 21a. Significant displacement components of each end of the fuselages are given in each plot. The positive conventions of the displacement components are shown in Figure 21b. The first nine modes for the 10^3 lb/in case are plotted in Figure 22.

Modes 1-6, 8, 9, and 11 of Figure 22 have essentially uncoupled motion in either the yaw or pitch planes. Mode 7, however, illustrates a strong coupling between axial and pitch plane displacements while mode 10 is characterized by coupling between yaw displacements and roll of the orbiter fuselage.

For the nominal 10^3 lb/in case, the frequencies were also calculated using the experimentally determined flexibility matrix. These results are compared with the frequencies for the nominal spring constants and the theoretical flexibility matrix in Table XVI. The agreement between the frequencies predicted by the two different flexibility matrices was reasonably close. The only significant difference occurs for the frequency of the combined pitch-axial mode which the theoretical interface matrix predicts to be 75.2 HZ, and the experimental interface matrix predicts as 64.3 HZ.

As Table XVI indicates, the nominal interface predicts the frequencies of the pitch and yaw modes to be identical. The pitch frequencies for the first four modes were predicted fairly well, but the yaw modes and the combined pitch-axial modes were poorly predicted.

Analysis of the elastically connected fuselages shows the connection of the two fuselages produces significantly more frequencies with more complex mode shapes than the individual components possess. This is illustrated in a frequency spectrum plot in Figure 23a where the number of frequencies for the connected fuselages and the fuselage components are presented. The connected fuselages have thirteen frequencies less than 150 HZ while the individual components possess only four frequencies in this range.

Some preliminary experimental data obtained at LRC are plotted in Figure 23b for comparison with the predicted values. The experimental data also shows rather dense frequency spectra at two widely separated frequency bands. Although some experimental and theoretical frequencies appear to be in agreement, a comparison of mode shapes will be necessary before further conclusions can be reached concerning the theoretical-experimental correlation.

The first six modes of the elastically connected fuselages were also calculated using the rigid body analysis and a stiffness matrix representation of the interface. Some of these results are compared with NASTRAN calculated frequencies in Figure 24. Up to $K = 10^3$ lb/in, the rigid body analysis predicts the frequencies of the first four modes reasonably well.

Frequencies of the fifth and sixth modes, however, are predicted with considerable error and are not shown. Above 10^3 lb/in the rigid body analysis results in considerable error even for the first or second modes. These observations are in agreement with the mode shapes shown in Figure 22 where it may be seen that the fuselages undergo significant deformation after the fourth mode.

Booster and Orbiter Airplanes

The booster and orbiter airplanes were both analyzed using the lumped mass approach. To avoid a singular mass matrix all rotational coordinates on the wings were omitted on both airplanes. On the fuselages, the rotations in the XZ and the YZ planes were omitted at all grid points except the wing attachment points. Initially it appeared necessary that rotational components in the XZ and YZ planes at the wing attachment points should also be omitted. This was attempted and resulted in an ill-conditioned mass matrix. Subsequent investigation showed that the multipoint constraint equations removed the apparent mass singularity, and the rotational components at these points should not be omitted. Roll rotations were permitted on both fuselages. The booster airplane was described by 136 DOF, and the orbiter airplane had 110 DOF. Both eigenvalue problems were solved by the Givens method.

The first thirteen frequencies of the booster airplane and orbiter airplane are tabulated in Table XVII. Computer plots of the mode shapes were used to classify the modes according to two types of predominant motion. The plotter orientation for the airplane components and complete model is shown in Figure 25. Plots of six booster airplane modes are shown in Figure 26, and similar plots for the orbiter are shown in Figure 27.

Both the booster and orbiter were characterized by the fact that only a few modes represented coupling between fuselage and wing displacements. The majority of the modes consisted only of wing motions with little or no fuselage deformation. The wing-type modes were either symmetric or anti-symmetric about the XZ plane.

For the booster, modes 1 and 2 in Figure 26 illustrate coupled motions between the fuselage and wings. The next four modes shown consist solely of either symmetric or anti-symmetric wing deformations. Similar behavior for the orbiter modes is shown in Figure 27. In this case, however, the first four modes consist of only wing deformations and the fifth and sixth modes show fuselage-wing coupling.

Complete Model

The final representation of the complete model was obtained by joining the two airplane models with the matrix representation for the elastic interfaces. The lumped mass approach was taken with the same rotations deleted as in the airplane analyses. Using the Givens method a matrix eigenvalue problem with 246 DOF was solved. The total computational time (CPU) on a LRC CDC-6600 computer was 2900 seconds.

The frequencies for the nominal 10^3 lb/in interface are tabulated in Table XVIII. There were forty modes less than 200 HZ, and the frequencies of thirty-two of these are tabulated. Computer plots of the mode shapes were used to classify the modes according to their predominant motion. The plotter view of the undeformed complete model is shown in Figure 25b, and plots of ten selected mode shapes are shown in Figure 28.

Of the thirty two modes tabulated, eight modes involve coupled motions between the fuselages and twenty-four modes involve uncpupled wing motions. Mode 2 (Figure 28b) is a good example of a coupled fuselage-wing mode. The uncoupled wing modes occur with either the booster wing vibrating, the orbiter wing vibrating, or both wings vibrating simultaneously. Mode 13 (Figure 28h) shows the booster wing vibrating separately, mode 5 (Figure 28e) shows both orbiter wing vibrating separately, and mode 6 (Figure 28f) shows both wings vibrating in phase in a symmetric mode. Wing modes also occur in which one wing is vibrating symmetrically, and the other is vibrating anti-symmetrically. These are designated as combined wing modes in Table XVIII. Mode 14 (Figure 28i) is an example of this type mode.

The complete model was also analyzed for the nominal 10^3 lb/in case using the experimental flexibility matrix to represent the interface. The agreement between the results was good with all frequencies and mode shapes matching very closely except for one mode. The experimental flexibility matrix introduced a mode at 59.7 HZ not predicted by the theoretical interface. The mode consisted of coupled fuselage-wing deformations.

The connection of the booster and orbiter airplanes gives a relatively dense frequency spectrum. The theoretical frequency spectrums for the two airplanes and the complete model are compared in Figure 29a-29c.

Connecting the two airplanes introduces a number of new modes into the frequency spectrum. Examples are the coupled fuselage modes which occur at about 11, 14, 21 and 24 HZ. However, a number of modes in the complete model may be identified with matching modes in the airplane components. For example, the booster wing mode at 65.6 HZ (Figure 28h) for the complete model can be identified as the booster airplane wing mode at 65.2 HZ shown in Figure 26f. A number of other modes also can be matched. However, it should be observed that earlier calculations for the fuselage components have shown that the spring interface stiffness plays an important role in the coupling of motions between individual components. Thus it can be reasonably expected that higher spring rates would give a considerably larger proportion of modes with coupled motions between the two components.

Some preliminary vibration test data for the complete model are shown in Figure 29d. As with the fuselage components a number of frequencies tend to be in agreement, but a comparison of mode shapes will be necessary to establish definite correlations.

The rigid body analysis was also performed for the complete model. For the 10^3 lb/in^2 interface the rigid body analysis predicted the first mode frequency to be 12.1 HZ which is 11% higher than the NASTRAN value. The frequencies of the higher modes were in considerable error. This result was to be expected since Figure 28 from the NASTRAN analysis showed significant deformations in all modes.

CONCLUSIONS

On the basis of the vibration analysis of the 1/15 scale dynamic model of the Space Shuttle with delta wings the following conclusions were reached:

1. The model has a relatively dense frequency spectrum with about forty modes less than 200 HZ. The mode shapes are generally three-dimensional with coupled fuselage-wing deformations. However, numerous uncoupled wing modes were present.

2. The coupling of the booster and orbiter motions is affected very significantly by the spring interface stiffnesses. A good analytical representation of the interface is necessary. The representation of the interface by its flexibility matrix through the NASTRAN general element appears to be a satisfactory approach.

3. The correlation of the predicted frequencies and preliminary LRC experimental frequency data was generally fair. A final conclusion on this correlation can be reached only after detailed comparison of the mode shapes. Some regions of the analytical model may require further refinements in the finite element representation.

4. It is feasible to use a rigid body analysis to predict the lower modes only for very weak spring interfaces. Generally, for a nominal spring of less than 10^3 lb/in., a rigid body analysis is satisfactory for predicting only the first mode.

REFERENCES

1. Leadbetter, S. A. and Kiefling, L. A., "Recent Studies of Space Shuttle Multibody Dynamics", NASA Space Shuttle Technology Conference, NASA TM X-2274, Vol. III, pp. 3-25, (April 1971).

2. McCormick, C. W., Editor, "The NASTRAN User's Manual", NASA SP-222, September 1970.

3. MacNeal, R. H., Editor, "The NASTRAN Theoretical Manual", NASA SP-221, September 1970.

APPENDIX A

Calculation of Elastic Interface Flexibility and Stiffness Matrices

In this appendix the analytical determination of the flexibility and stiffness matrices of the elastic interface will be described. The elements of the flexibility matrix were determined for use in the general structural element GENEL in the NASTRAN program. The stiffness matrices were developed for use in the FORTRAN program for the rigid body vibration analysis. In the first part of this appendix the determination of the flexibility matrices will be described. Next the form of the stiffness matrix will be described in terms of its submatrices. Finally, relations between the stiffness and flexibility coefficients will be derived.

Flexibility Matrix

A schematic of the elastic interface is shown in Figure A-1, and the positive conventions for the displacements and rotations are shown in Figure A-2.

The flexibility matrix will be defined in terms of the displacements and rotations at the orbiter centerline. For calculating the flexibility matrix, the interface will be assumed rigidly clamped at the booster fuselage. The flexibility matrix then will take the form

$$[a] = \begin{array}{c} \begin{array}{cccccc} u_1 & u_5 & u_3 & u_9 & u_7 & u_{11} \end{array} \\ \left[\begin{array}{cccccc} a_Z & & & & & \\ & a_{55} & a_{53} & & & \\ & a_{35} & a_{33} & & & \\ & & & a_{99} & a_{97} & \\ & & & a_{79} & a_{77} & \\ & & & & & a_T \end{array}\right] \end{array} \begin{array}{c} \\ u_1 \\ u_5 \\ u_3 \\ u_9 \\ u_7 \\ u_{11} \end{array} \qquad \text{(AI-1)}$$

where all terms not shown are zero. The flexibility coefficients may be identified as follows:

> The coefficient a_Z may be identified with the axial displacment of the interface, i.e., the displacement in the Z direction;
>
> The two by two matrix with subscripts 5 and 3 is associated with displacements in the XZ plane;
>
> The two by two matrix with subscripts 9 and 7 is associated with displacements in the YZ plane, and
>
> The coefficient a_T is associated with torsional deformation of the interface, i.e., with the rotation about the Z axis.

Equations for each of these coefficients will now be derived.

Axial Displacement:

The coefficient a_Z may be calculated by applying a unit force to the interface at the orbiter attachment point and computing the displacement u_Z (See Figures A1 and A2). For this calculation it is reasonable to assume the axial displacement of the yaw spring is negligible as well as the axial displacements of the booster and orbiter brackets. Then the only displacement contributing to a_Z is due to the bending of the four pitch leaves in the YZ plane. Thus

$$a_Z = \frac{\ell^3 P}{48EI_{PX}} \qquad \text{(A-2)}$$

where I_{PX} represents the moment of inertia of one pitch leaf about an X axis through its centroid.

Displacements in the XZ Plane:

The flexibility coefficients a_{55} and a_{35} are found by applying a unit force at the orbiter centerline in the X direction and calculating the u_5 displacement and the u_3 rotation.

In calculating the u_5 displacement the following contributions were considered:

(1) Bending deflection of the yaw leaves as cantilever beams,

$$\delta_1 = \frac{\ell_Y^3}{6EI_{YWY}} + \frac{(a+h)\,\ell_Y^2}{4EI_{YWY}} \qquad \text{(A-3a)}$$

where I_{YWY} represents the moment of inertia of one yaw leaf about a Y axis through its centroid.

(2) Deflection at orbiter centerline due to end rotation of the yaw leaves as cantilevers,

$$\delta_2 = a\Theta_1 = \frac{(a+h)\,\ell^2{}_Y}{4EI_{YWY}} + \frac{(a+h)^2\,\ell_Y}{2EI_{YWY}} \qquad \text{(A-3b)}$$

where Θ_1 is the end rotation at the yaw leaves as cantilevers.

(3) Deflection at orbiter centerline due to rotation of pitch leaves about a local Y axis, midway between the upper and lower pitch leaves,

$$\delta_3 = a\Theta_2 = \frac{1}{12}\,\frac{(a+\frac{h}{2})^2}{h^2}\,\frac{\ell^3 P}{EI_{PZ}} \qquad \text{(A-3c)}$$

where I_{PZ} represents the moment of inertia of one pitch leaf about a Z axis through its centroid.

(4) Bending deflection of booster bracket. For this calculation the bracket was assumed to act as a cantilever beam with an effective length L_1 for bending in XZ plane.

$$\delta_4 = \frac{L_1^{\,3}}{6EI_{BY}} + \frac{dL_1^{\,2}}{4EI_{BY}} \qquad \text{(A-3d)}$$

where I_{BY} denotes the moment of inertia of one arm of the bracket about a Y axis through its centroid. The quantity d is the distance from the top of the bracket to the orbiter centerline.

(5) Deflection at orbiter centerline due to end slope of booster bracket.

$$\delta_5 = d\Theta_3 = \frac{L_1^{\,2}d}{4EI_{BY}} + \frac{d^2L_1}{2EI_{BY}}\,. \qquad \text{(A-3e)}$$

The total deflection due to a unit force is

$$a_{55} = \delta_1 + \delta_2 + \delta_3 + \delta_4 + \delta_5. \qquad \text{(A-3f)}$$

The rotation u_3 due to this unit load is assumed to be made up of the following components:

(1) The end rotation of the yaw springs as cantilever beams,

$$\Theta_1 = \frac{\ell_Y^{\,2}}{4EI_{YWY}} + \frac{(a+h)\,\ell_Y}{2EI_{YWY}}\,. \qquad \text{(A-4a)}$$

(2) The rotation of the pitch springs about the local Y axis,

$$\Theta_2 = \frac{(a+\frac{h}{2})\,\ell^3{}_P}{12h^2EI_{PZ}} \tag{A-4b}$$

(3) The end rotation of the bracket arms as cantilever beams,

$$\Theta_3 = \frac{L_1{}^2}{4EI_{BY}} + \frac{dL_1}{2EI_{BY}}\ . \tag{A-4c}$$

The total rotation due to a unit force is

$$a_{35} = \Theta_1 + \Theta_2 + \Theta_3\ . \tag{A-4d}$$

The flexibility coefficients a_{53} and a_{55} are found by applying a unit moment about a Y axis through the orbiter attachment point. By symmetry,

$$a_{53} = a_{35}\ . \tag{A-5}$$

The rotation u_3 due to a unit moment has three components similar to the rotation components considered in a_{35}. Thus

$$a_{33} = \frac{\ell_Y}{2EI_{YWY}} + \frac{\ell_P{}^3}{12h^2EI_{PZ}} + \frac{L_1}{2EI_{BY}}\ . \tag{A-6}$$

Displacements in the YZ plane:

The flexibility coefficients a_{99} and a_{79} are found by applying a unit force in the Y direction and calculating the u_9 displacement and the u_7 rotation.

In calculating the displacement u_9 the following contributions were considered:

(1) Bending deflection of the yaw leaves as "guided" (i.e. having zero slope at the top of the yaw leaves) cantilever beams,

$$\delta_6 = \frac{\ell_Y{}^3}{24EI_{YWX}} \tag{A-7a}$$

where I_{YWX} represents the moment of one yaw leaf about a X axis through its centroid.

(2) Deflection at orbiter centerline due to axial deformation of the pitch springs. The axial deformations of the pitch springs permits a rotation of the orbiter bracket about a local X axis. The deflection at the orbiter centerline due to this rotation is

$$\delta_7 = \frac{(a+\frac{h}{2})^2 \ell_P}{A_P E h^2} \qquad \text{(A-7b)}$$

where A_P is the cross sectional area of one pitch leaf.

(3) Bending deflection of booster bracket. Each arm of the bracket was assumed to act as a cantilever beam with an effective length L_2 for bending in the YZ plane,

$$\delta_8 = \frac{L_2^{\,3}}{6EI_{BX}} + \frac{dL_2^{\,2}}{4EI_{BX}} \qquad \text{(A-7c)}$$

where I_{BX} represents the moment of inertia of one bracket arm about an X axis through its centroid.

(4) The deflection at the orbiter centerline due to end slope of booster bracket,

$$\delta_9 = \frac{L_2^{\,2} d}{4EI_{BX}} + \frac{dL_2^{\,2}}{2EI_{BX}} \ . \qquad \text{(A-7d)}$$

The total deflection due to a unit force is

$$a_{99} = \delta_6 + \delta_7 + \delta_8 + \delta_9 \ . \qquad \text{(A-7e)}$$

The rotation considered due to the unit force is assumed to have two components:

(1) The rotation introduced by the axial deformation of the pitch leaves,

$$\Theta_4 = -\frac{(a+\frac{h}{2})\ell_P}{A_P E h^2} \ . \qquad \text{(A-8a)}$$

(2) The end rotation of the booster bracket arms bending as cantilever beams,

$$\Theta_5 = -\frac{L_2^{\,2}}{4EI_{BX}} - \frac{dL_2}{2EI_{BX}} \ . \qquad \text{(A-8b)}$$

The total rotation is

$$a_{79} = \theta_4 + \theta_5 \qquad \text{(A-8c)}$$

The flexibility coefficients a_{97} and a_{77} are found by applying a unit moment about an X axis through the orbiter attachment point and calculating the displacement u_9 and rotation u_7. By symmetry,

$$a_{97} = a_{79} \; . \qquad \text{(A-9)}$$

The rotation a_{77} due to the unit moment has two components similar to the rotations considered in calculating a_{79}. Thus

$$a_{77} = \frac{\ell_P}{A_P E h^2} + \frac{L_2}{2EI_{BX}} \; . \qquad \text{(A-10)}$$

Torsion about Z axis:

The flexibility coefficient a_T is the rotation about the Z axis due to a unit moment about this axis. Four rotations were assumed to contribute to a_T:

(1) The rotation of the pitchleaves about a Z axis through the mounting brackets. The pitchleaves are assumed to be clamped at their outer ends,

$$\phi_1 = \frac{\ell_P}{16EI_{PZ}} \; . \qquad \text{(A-11)}$$

(2) The rotation introduced at the top of the yaw springs due to the yaw springs bending in the XZ plane as cantilever beams,

$$\phi_2 = \frac{2\ell_Y{}^3}{3C^2 EI_{YWY}} \qquad \text{(A-11b)}$$

where C is the distance between the yaw leaves as shown in Figure A-1.

(3) The rotation introduced at the top of the yaw springs due to the slope of the arms of the booster bracket bending as cantilever beams,

$$\phi_3 = \frac{2}{C^2}\left[\frac{L_1{}^2 \ell_Y}{2EI_{BY}} + \frac{\ell_Y{}^2 L_1}{EI_{BY}}\right] . \qquad \text{(A-11c)}$$

(4) The rotation introduced at the top of the brackets due to the bending deflections of the arms as cantilever beams.

$$\phi_4 = \frac{2}{C^2}\left[\frac{L_1{}^3}{3EI_{BY}} + \frac{\ell_P L_1{}^2}{2EI_{BY}}\right] . \qquad \text{(A-11d)}$$

The total rotation is

$$a_T = \phi_1 + \phi_2 + \phi_3 + \phi_4 . \qquad \text{(A-11e)}$$

Using the equations derived above, all of the elements in the flexibility matrix for the elastic interface were evaluated. The values of the various dimensions used in the calculations are tabulated in Table A-I. For the pitch and yaw leavesa modulus of elasticity, $E = 3 \times 10^7 \text{lb/in}^2$ was used, and for the booster bracket, $E = 10^7 \text{lb/in}^2$. The results of these calculations are tabulated in Table A-II. For each nominal spring constant the results of two calculations are shown. The first calculation in each case was made for effective lengths $L_1 = 5.5$ in. and $L_2 = 2.0$ in. which were found by approximately matching the bracket arm bending deflections to the experimentally measured deflection of the arms. The second calculation neglects the bending of the bracket arms, i.e., the effective lengths are taken as zero.

Stiffness Matrix

The stiffness matrix for the elastic interface in the coordinates shown in Figure A-2 may be written as

(A-12)

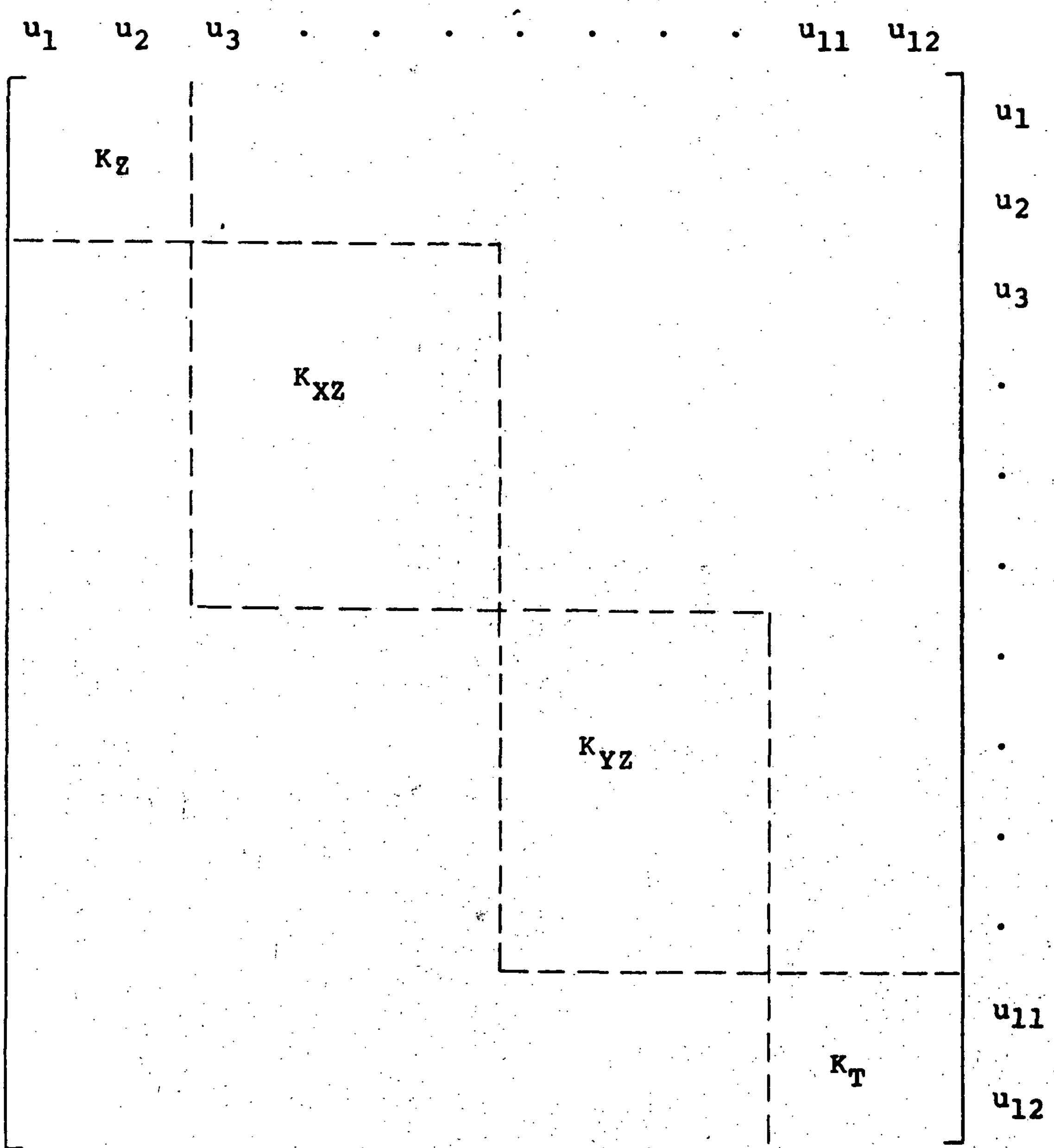

where all elements outside of the dashed lines are zero. The submatrix K_Z represents the axial stiffness matrix for Z displacements; K_{XZ} represents the stiffness due to bending in the XZ plane; K_{YZ} represents the bending in the stiffness YZ plane;

and K_T represents the rotational stiffness about the Z axis.

Not all of the elements of this matrix are independent. By symmetry, of course, $K_{ij} = K_{ji}$. In addition, equilibrium requirements may also be used to establish other relations between the elements in each submatrix.

Axial and Torsional Stiffness Submatrices:

The axial and torsional problems are similar for analytical purposes. For simplicity, only the axial problem will be considered; the conclusions reached can be applied to both problems. The axial stiffness matrix K_Z has the form

$$[K_Z] = \begin{bmatrix} K_{11} & K_{12} \\ K_{21} & K_{22} \end{bmatrix} .$$

The four elements are related as will now be shown. Applying the definition of K_{ij} as the force at i due to a unit displacement at j with all other displacements zero, the elements of K_Z are as shown in Figure A-3. Then equilibrium of forces, requires

$$K_{21} = -K_{11}$$
$$K_{12} = -K_{22} .$$

Since, $K_{21} = -K_{11}$, these equations show there is actually only one independent element of the axial stiffness matrix. Let this be K_Z, then in general,

$$[K_Z] = \begin{bmatrix} K_Z & -K_Z \\ -K_Z & K_Z \end{bmatrix} . \qquad \text{(A-13)}$$

Similarly, the torsional stiffness matrix is

$$[K_T] = \begin{bmatrix} K_T & -K_T \\ -K_T & K_T \end{bmatrix} . \qquad \text{(A-14)}$$

Bending Stiffness Matrices:

The bending stiffness submatrices $[K_{XZ}]$ and $[K_{YZ}]$ are similar and only one matrix will be considered. The matrix $[K_{XZ}]$ is defined, from equation (A-12), as

$$[K_{XZ}] = \begin{bmatrix} K_{33} & K_{34} & K_{35} & K_{36} \\ K_{43} & K_{44} & K_{45} & K_{46} \\ K_{53} & K_{54} & K_{55} & K_{56} \\ K_{63} & K_{64} & K_{65} & K_{66} \end{bmatrix} . \qquad \text{(A-15)}$$

Because of symmetry there are 10 unknown values in the array. When equilibrium requirements are considered it turns out that only three of the values are independent. This follows from applying the definition of K_{ij} as shown in Figure A-4. Equilibrium of forces and moments gives the following eight relations,

$$\sum \text{Forces} = 0$$

$$\sum \text{Moments} = 0$$

$$\left.\begin{aligned} K_{53} + K_{63} &= 0 \\ K_{33} + K_{43} + LK_{53} &= 0 \end{aligned}\right\} \quad \text{(Figure A4-a)}$$

$$\left.\begin{aligned} K_{54} + K_{64} &= 0 \\ K_{34} + K_{44} + LK_{54} &= 0 \end{aligned}\right\} \quad \text{(Figure A4-b)}$$

$$\text{(A-16)}$$

$$\left.\begin{aligned} K_{55} + K_{65} &= 0 \\ K_{35} + K_{45} + LK_{55} &= 0 \end{aligned}\right\} \quad \text{(Figure A4-c)}$$

$$\left.\begin{aligned} K_{56} + K_{66} &= 0 \\ K_{36} + K_{46} + LK_{56} &= 0. \end{aligned}\right\} \quad \text{(Figure A4-d)}$$

With these eight relations and taking symmetry into account, the matrix above in equation (A-14) can be written as

$$[K_{XZ}] = \begin{bmatrix} K_{33} & K_{34} & -\dfrac{K_{33}+K_{34}}{L} & \dfrac{K_{33}+K_{34}}{L} \\ K_{34} & K_{44} & -\dfrac{K_{34}+K_{44}}{L} & \dfrac{K_{34}+K_{44}}{L} \\ -\dfrac{K_{33}+K_{34}}{L} & -\dfrac{K_{34}+K_{44}}{L} & \dfrac{K_{33}+2K_{34}+K_{44}}{L^2} & -\dfrac{K_{33}+2K_{34}+K_{44}}{L^2} \\ \dfrac{K_{33}+K_{34}}{L} & \dfrac{K_{34}+K_{44}}{L} & -\dfrac{K_{33}+2K_{34}+K_{44}}{L^2} & \dfrac{K_{33}+2K_{34}+K_{44}}{L^2} \end{bmatrix} \qquad \text{(A-17)}$$

The matrix $[K_{YZ}]$ may be found in the same form by changing subscripts appropriately.

As a result of symmetry and equilibrium requirements it has been shown that there are only 8 independent stiffness coefficients: K_Z and K_T and 3 elements each from the submatrices K_{XZ} and K_{YZ}.

Relations between the Stiffness and Flexibility Coefficients

To determine the stiffness coefficients in terms of the flexibility coefficients the definition of a_{ij} is used. For the interface in extension and torsion this means simply that

$$K_Z = \frac{1}{a_Z} \qquad \text{(A-18)}$$

and

$$K_T = \frac{1}{a_T} \quad . \qquad \text{(A-19)}$$

For the interface in bending this means that one end is rigidly fixed and a unit force and a unit moment are applied at the free end. The flexibility coefficients can then be used to write, assuming symmetry,

$$\begin{bmatrix} u_3 \\ u_5 \end{bmatrix} = \begin{bmatrix} a_{33} & a_{35} \\ a_{35} & a_{55} \end{bmatrix} \begin{bmatrix} P_3 \\ P_5 \end{bmatrix}$$

where P's denote the applied forces. In terms of the stiffness matrix of the interface in bending

$$\begin{bmatrix} P_3 \\ P_5 \end{bmatrix} = \begin{bmatrix} K_{33} & K_{35} \\ K_{35} & K_{55} \end{bmatrix} \begin{bmatrix} u_3 \\ u_5 \end{bmatrix}$$

Thus if the flexibility coefficients are known,

$$\begin{bmatrix} K_{33} & K_{35} \\ K_{35} & K_{55} \end{bmatrix} = \begin{bmatrix} a_{33} & a_{35} \\ a_{35} & a_{55} \end{bmatrix}^{-1} = \frac{1}{a_{33}\, a_{55} - a_{35}^2} \begin{bmatrix} a_{55} & -a_{35} \\ -a_{35} & a_{33} \end{bmatrix}$$

hence,

$$K_{33} = \frac{a_{55}}{a_{33}\, a_{55} - a_{35}^2}$$

$$K_{35} = \frac{-\ a_{35}}{a_{33}\, a_{55} - a_{35}^2} \qquad \text{(A-20)}$$

$$K_{55} = \frac{a_{33}}{a_{33}\, a_{55} - a_{35}^2}$$

Using these relations and the equations of equilibrium, (A-16) found above, the stiffness matrix $[K_{XZ}]$ can be found in terms of the flexibilities by: (A-21)

$$K_{XZ}] = \frac{1}{a_{33}a_{55}-a_{35}^2} \begin{bmatrix} a_{55} & La_{35}-a_{55} & -a_{35} & a_{35} \\ La_{35}-a_{55} & a_{55}-2La_{35}+L^2a_{33} & a_{35}-La_{33} & -a_{35}+La_{33} \\ -a_{35} & a_{35}-La_{33} & a_{33} & -a_{33} \\ a_{35} & -a_{35}+La_{33} & -a_{33} & a_{33} \end{bmatrix}.$$

A similar relation for $[K_{YZ}]$ can be found by appropriately changing the subscripts.

Equations (A-18), (A-19), and (A-21) were used to calculate the stiffness coefficients corresponding to the flexibility coefficients given in Table A-II. These stiffness coefficients are tabulated in Table A-III. As in Table A-II, for each nominal spring constant the stiffness coefficients were calculated for two cases of effective lengths of the booster bracket arms.

In this appendix, equations have been derived which may be used to calculate the flexibility matrix for the elastic interface. In addition explicit relations have been derived which may be used to calculate the elements of the corresponding interface stiffness matrix directly from the elements of the flexibility matrix. Numerical results for the flexibility and stiffness matrices for each nominal case of the elastic interface were presented.

APPENDIX B

Rigid Body Vibration Analysis

In this appendix a description of the rigid body vibration analysis will be given. Two analytical models were used for this analysis. In the first analysis, the motion was assumed to be restrained to the pitch plane with the longitudinal displacement prohibited. This gave a simple four degree of freedom model. In the second analysis, general three dimensional motion was permitted. The booster and orbiter each were allowed to have three translations and three rotations so that the system possessed twelve degrees of freedom.

Plane Motion

The mathematical model for the case of plane motion is shown in Figure B-1. The generalized coordinates are the vertical translations Z_1 and Z_2 of the mass center of each component and the rotations Θ_1 and Θ_2 about the mass center. Each elastic interface is represented as a scalar spring having a single spring constant.

For free vibrations, the equations of motion for small oscillations takes the form

$$[M]\ \{\ddot{q}\} + [K]\ \{q\} = 0 \qquad \text{(B-1)}$$

where [M] denotes the mass matrix and [K] denotes the stiffness matrix. For the present problem the generalized coordinates {q} are given by

$$\{q\} = \lfloor Z_1 \ Z_2 \ \Theta_1 \ \Theta_2 \rfloor^T. \qquad \text{(B-2)}$$

The mass and stiffness matrices were obtained by writing the kinetic and potential energies of the system. Since the generalized displacements are measured from the mass center of each body the mass matrix is diagonal and was found to be

$$[M] = \begin{bmatrix} M_1 & 0 & 0 & 0 \\ 0 & M_2 & 0 & 0 \\ 0 & 0 & I_1 & 0 \\ 0 & 0 & 0 & I_2 \end{bmatrix} \qquad \text{(B-3)}$$

From the geometry shown in Figure B-1, the relative displacement of each spring was written in terms of the generalized coordinates. With these displacements, the potential energy of the system was derived and written in matrix form to yield the stiffness matrix. For the present problem these calculations gave

$$[K] = \begin{bmatrix} (K_1+K_2) & -(K_1+K_2) & X_aK_1-X_cK_2 & -X_bK_1+X_dK_2 \\ -(K_1+K_2) & (K_1+K_2) & -X_aK_1+X_cK_2 & X_bK_1-X_dK_2 \\ X_aK_1-X_cK_2 & -X_aK_1+X_cK_2 & X_a{}^2K_1+X_c{}^2K_2 & -(X_aX_bK_1+X_cX_dK_2) \\ -X_bK_1+X_dK_2 & X_bK_1-X_dK_2 & -(X_aX_bK_1+X_cX_dK_2) & X_b{}^2K_1+X_d{}^2K_2 \end{bmatrix} \qquad \text{(B-4)}$$

Using the mass and stiffness matrices derived above the eigenvalue problem

$$[K]\ \{u\} = \omega^2\ [M]\ \{u\} \qquad \text{(B-5)}$$

was then solved to give the system's natural frequencies ω and mode shapes $\{u\}$. Since two "free-free" modes are possible, two zero frequencies were found as well as two frequencies corresponding to the system's modes of vibration.

General Motion

Figure B-2 shows the mathematical model for the general case of three dimensional motion. Each component was permitted to have six degrees of freedom: three translations of each mass center and three rotations about each mass center. The positive conventions for these coordinates are shown in Figure B-2. Each spring interface was represented by a twelve by twelve stiffness matrix.

The generalized coordinates in this case may be partitioned into orbiter and booster displacement sets as

$$\{q\} = \begin{bmatrix} u_O \\ u_B \end{bmatrix} \tag{B-6}$$

where the displacements of the orbiter are

$$\{u_O\} = \lfloor u_{1O}\ u_{2O}\ u_{3O}\ \Theta_{1O}\ \Theta_{2O}\ \Theta_{3O} \rfloor^T, \tag{B-7a}$$

and the displacements of the booster are

$$\{u_B\} = \lfloor u_{1B}\ u_{2B}\ u_{3B}\ \Theta_{1B}\ \Theta_{2B}\ \Theta_{3B} \rfloor^T. \tag{B-7b}$$

For the fuselages, the coordinate axes through the mass center are principal axes because of symmetry. With the wings attached, this is also a good approximation since the wing mass is relatively small. Thus the displacement coordinates will be assumed to be aligned and referenced to the principal axes. Then the mass matrix is

$$[M] = \left[\begin{array}{c|c} M_O & 0 \\ \hline 0 & M_B \end{array}\right] \tag{B-8a}$$

where the diagonal elements of $[M_O]$ are

$$M_{XO}\quad M_{YO}\quad M_{ZO}\quad I_{XO}\quad I_{YO}\quad I_{ZO}\ , \tag{B-8b}$$

and the diagonal elements of $[M_B]$ are

$$M_{XB} \quad M_{YB} \quad M_{ZB} \quad I_{XB} \quad I_{YB} \quad I_{ZB} \ . \qquad \text{(B-8c)}$$

All off-diagonal elements are zero. M_{XO} denotes the mass associated with the X displacement of the orbiter; I_{XO} denotes the mass moment of inertia of the orbiter about an X axis through the center of mass. The other terms associated with the Y and Z subscripts may be similarly interpreted. The analogous quantities for the booster are denoted with the B subscript.

The stiffness matrix for the system is the matrix sum of the stiffness matrices for each interface where each matrix is a twelve by twelve. Thus

$$[K] = [K_1] + [K_2] \qquad \text{(B-9)}$$

where $[K_1]$ represents the interface connecting points a and b, and $[K_2]$ represents the interface connecting points c and d in Figure B-2. For simplicity, the derivation of only the $[K_1]$ matrix will be given. It will be indicated later that the elements of the $[K_2]$ matrix may be obtained from $[K_1]$ by making appropriate substitutions.

To derive the stiffness matrix $[K_1]$ it is desirable to begin with the set of coordinates used in Appendix A to represent the interface. These coordinates, and the associated stiffness matrix for the interface in these coordinates are shown in Figure B-3. The sub-matrices in Figure B-3 may be identified as follows:

$[K_z]$ represents the axial stiffness of the interface to relative displacements in the z direction, two by two;

$[K_{xz}]$ represents the stiffness of the interface to relative displacements and rotations in the xz plane, four by four;

$[K_{yz}]$ represents the stiffness of the interface to relative displacements and rotations in the yz plane, four by four; and,

$[K_T]$ represents the torsional stiffness of the interface to relative rotations about the z axis, two by two.

It is desired to represent the stiffness of the interface in terms of the displacements at the center of mass. This will be done by writing the potential energy of the interface first in terms of the coordinates of points a and b, and then making a coordinate transformation. The potential energy may be written as

$$V_1 = \frac{1}{2} \begin{bmatrix} u_a \\ u_b \end{bmatrix}^T \begin{bmatrix} K_{aa} & K_{ab} \\ K_{ba} & K_{bb} \end{bmatrix} \begin{bmatrix} u_a \\ u_b \end{bmatrix} \qquad \text{(B-10)}$$

where

$$\{u_a\} = \lfloor u_{1a}\ u_{2a}\ u_{3a}\ \Theta_{1a}\ \Theta_{2a}\ \Theta_{3a} \rfloor^T, \qquad \text{(B-11a)}$$

and

$$\{u_b\} = \lfloor u_{1b}\ u_{2b}\ u_{3b}\ \Theta_{1b}\ \Theta_{2b}\ \Theta_{3b} \rfloor^T. \qquad \text{(B-11b)}$$

The submatrices in equation (B-10) are found by identifying the $\{u_a\}$ and $\{u_b\}$ displacement components with the displacement components shown in Figure B-3, and then appropriately reordering rows and columns in the stiffness matrix. The elements of the submatrices are defined in Figure B-4 where K_{ij} denotes an element in the matrix $[K_{XZ}]$ and K'_{ij} denotes an element in $[K_{YZ}]$.

Refering to Figure B-2 the transformation equations between the coordinates at points a and b and the generalized coordinates may be written. Assuming small rotations

$$\{u_a\} = [\beta_a]\ \{u_O\} \tag{B-12a}$$

where

$$[\beta_a] = \left[\begin{array}{ccc|ccc} 1 & 0 & 0 & 0 & -Z_a & 0 \\ 0 & 1 & 0 & Z_a & 0 & -X_a \\ 0 & 0 & 1 & 0 & X_a & 0 \\ \hline 0 & 0 & 0 & 1 & 0 & 0 \\ 0 & 0 & 0 & 0 & 1 & 0 \\ 0 & 0 & 0 & 0 & 0 & 1 \end{array}\right] . \tag{B-13}$$

Similarly,

$$\{u_b\} = [\beta_b]\ \{u_B\} \tag{B-14}$$

where

$$[\beta_b] = \left[\begin{array}{ccc|ccc} 1 & 0 & 0 & 0 & Z_b & 0 \\ 0 & 1 & 0 & -Z_b & 0 & -X_b \\ 0 & 0 & 1 & 0 & X_b & 0 \\ \hline 0 & 0 & 0 & 1 & 0 & 0 \\ 0 & 0 & 0 & 0 & 1 & 0 \\ 0 & 0 & 0 & 0 & 0 & 1 \end{array}\right] \tag{B-15}$$

Substituting equations (B-12) and (B-13) into equation (B-10) gives

$$V_1 = \frac{1}{2} \left[\begin{array}{c} u_O \\ \hline u_B \end{array}\right]^T \left[\begin{array}{c|c} \beta_a^T & 0 \\ \hline 0 & \beta_b^T \end{array}\right] \left[\begin{array}{c|c} K_{aa} & K_{ab} \\ \hline K_{ba} & K_{bb} \end{array}\right] \left[\begin{array}{c|c} \beta_a & 0 \\ \hline 0 & \beta_b \end{array}\right] \left[\begin{array}{c} u_O \\ \hline u_B \end{array}\right] .$$

From this, by inspection,

$$[K_1] = \left[\begin{array}{c|c} \beta_a^T & 0 \\ \hline 0 & \beta_b^T \end{array}\right] \left[\begin{array}{c|c} K_{aa} & K_{ab} \\ \hline K_{ba} & K_{bb} \end{array}\right] \left[\begin{array}{c|c} \beta_a & 0 \\ \hline 0 & \beta_b \end{array}\right] .$$

Finally, after performing the multiplications,

$$[K_1] = \left[\begin{array}{c|c} \beta_a^T \quad K_{aa} \quad \beta_a & \beta_a^T \quad K_{ab} \quad \beta_b \\ \hline \beta_b^T \quad K_{ba} \quad \beta_a & \beta_b^T \quad K_{bb} \quad \beta_b \end{array}\right] \tag{B-16}$$

Each of the submatrices is of order six by six. When these operations were carried out the final matrix was obtained. The non-zero elements of the upper triangle of this matrix are listed in Figure B-5. The elements of the lower triangle may be found by symmetry.

The elements of the $[K_2]$ stiffness matrix may be found from the $[K_1]$ matrix by replacing:

$$\begin{array}{ccc} X_a & \text{by} & -X_c \\ Z_a & \text{by} & Z_c \\ X_a & \text{by} & -X_d \\ Z_b & \text{by} & Z_d \end{array} .$$

These replacements were found by writing coordinate transformations similar to equations B-12 and B-14 for points c and d.

With the mass matrix and the stiffness matrix for the system as given in equations B-8 and Figure B-5, the free vibration modes were found by solving an eigenvalue problem of the type given in equation (B-5). In this case there are six "free-free" modes and six corresponding zero frequencies in addition to six natural modes of vibration.

The mass and inertia properties for the plane motion analysis and the general motion analysis are tabulated in Table BI. These values were found using the corresponding NASTRAN finite element model in each case. The rigid body mass and inertia properties are found in NASTRAN by requesting execution of the Grid Point Weight Generator. The Grid Point Weight Generator is requested by use of the bulk data PARAM card.

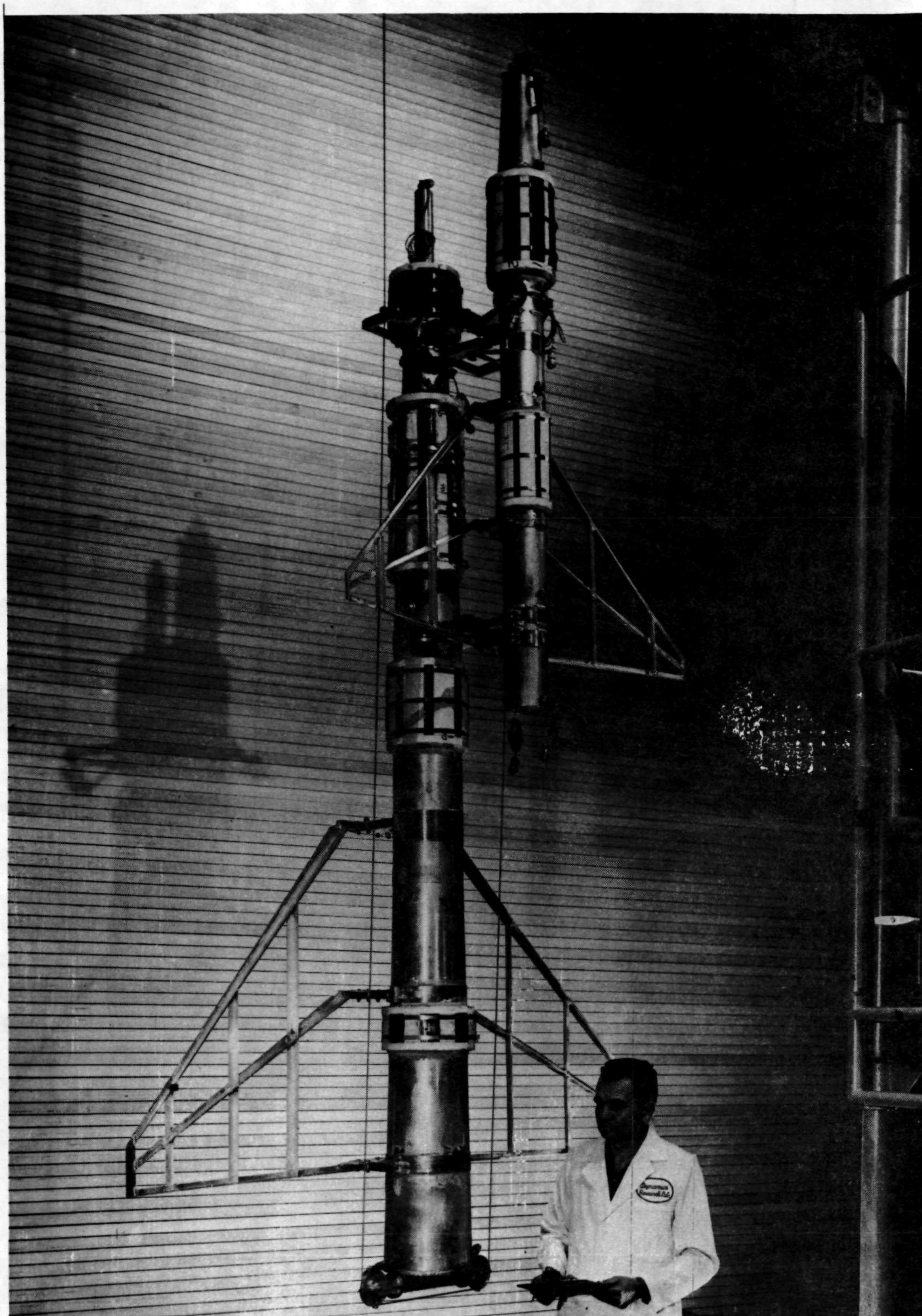

Figure 1.- Photograph of 1/15-scale space shuttle model.

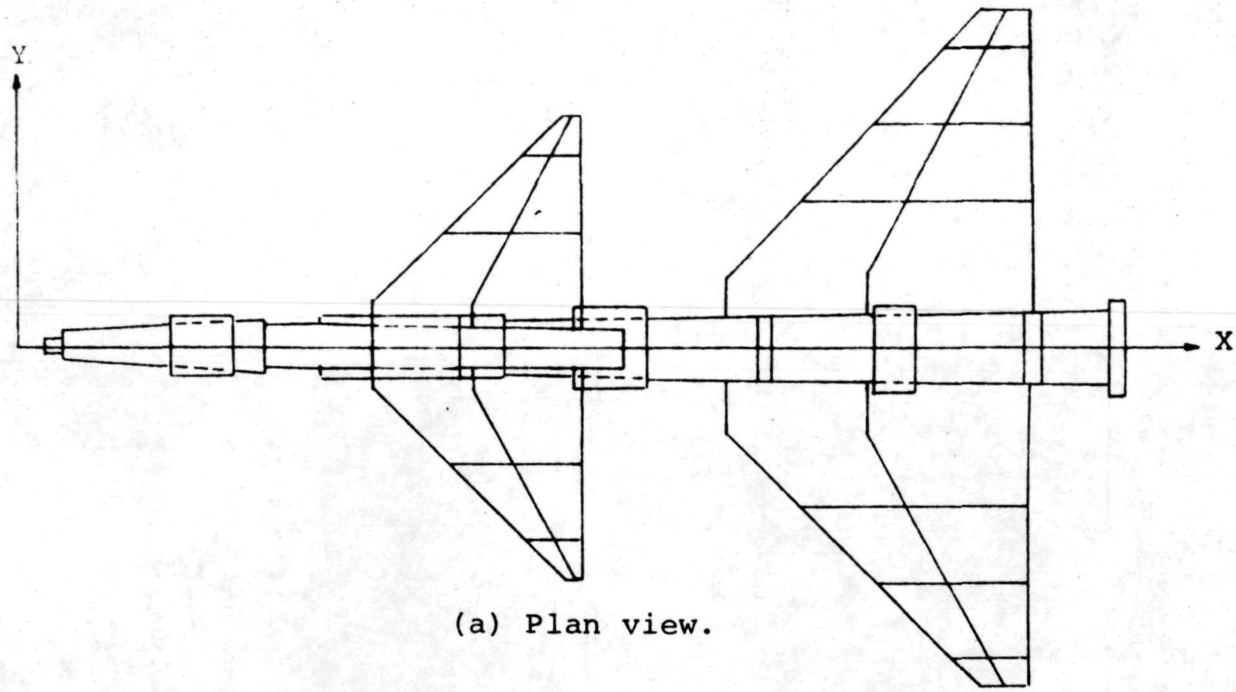

(a) Plan view.

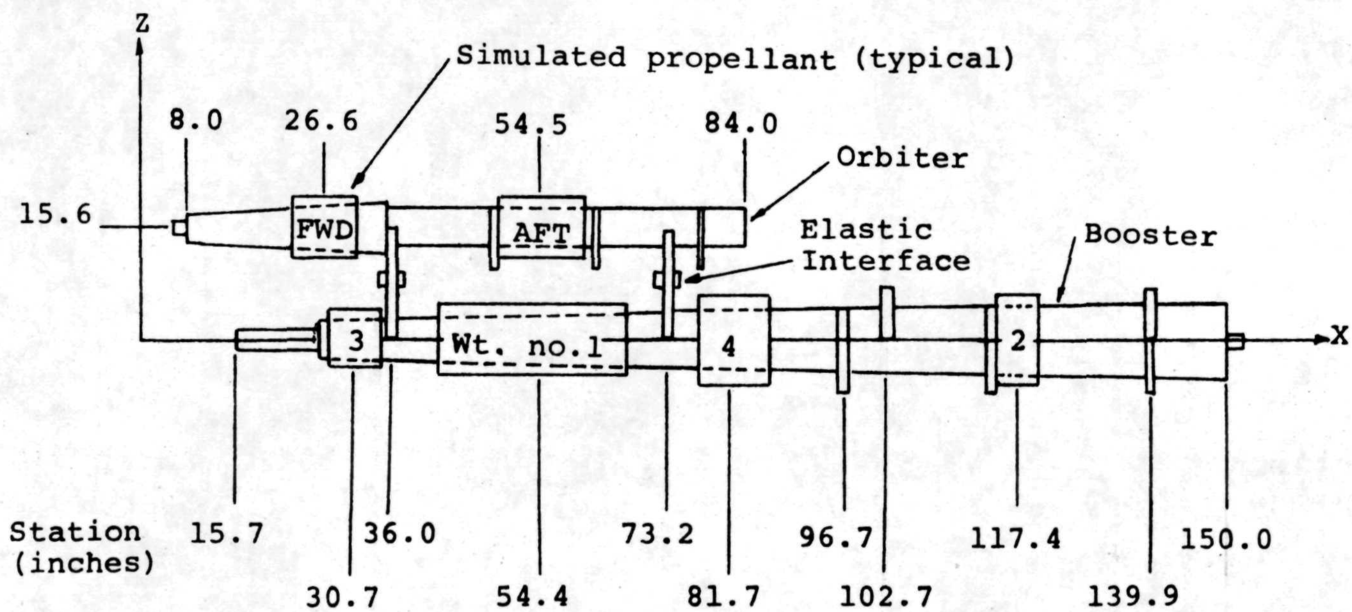

(b) Elevation view.

Figure 2.- Schematic of 1/15 scale space shuttle model.

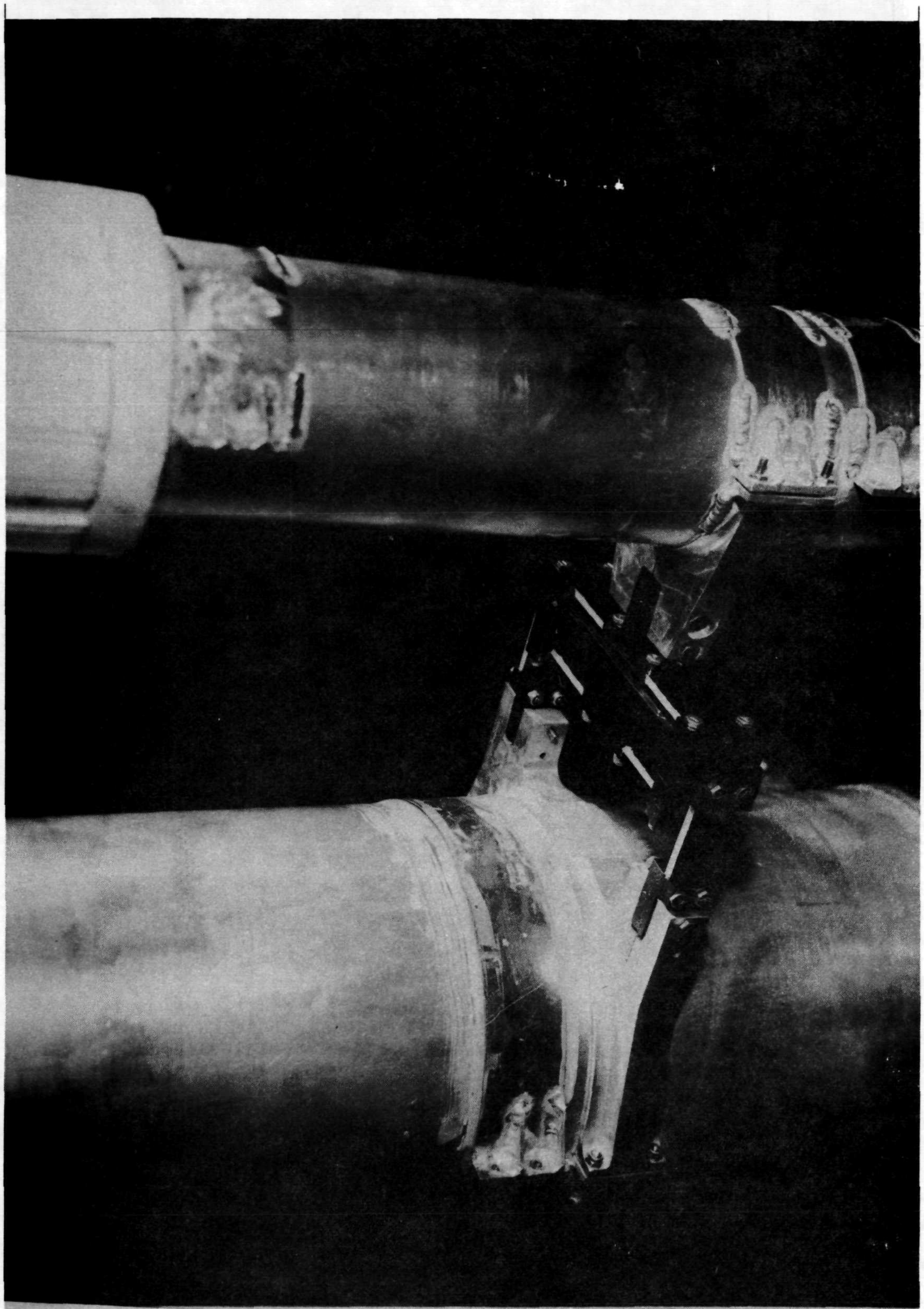

Figure 3.- Photograph of elastic interface between booster and orbiter fuselages.

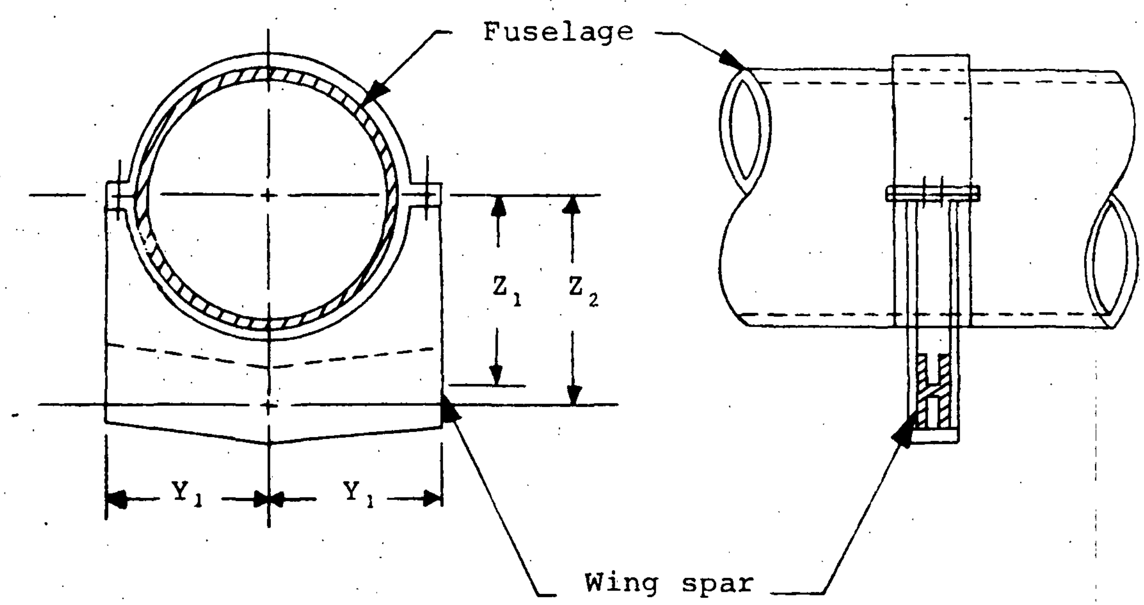

	Y_1 (in.)	Z_1 (in.)	Z_2 (in.)
Booster	5.82	5.88	6.88
Orbiter	3.94	3.38	4.06

Figure 4.- Schematic of fuselage-wing interface.

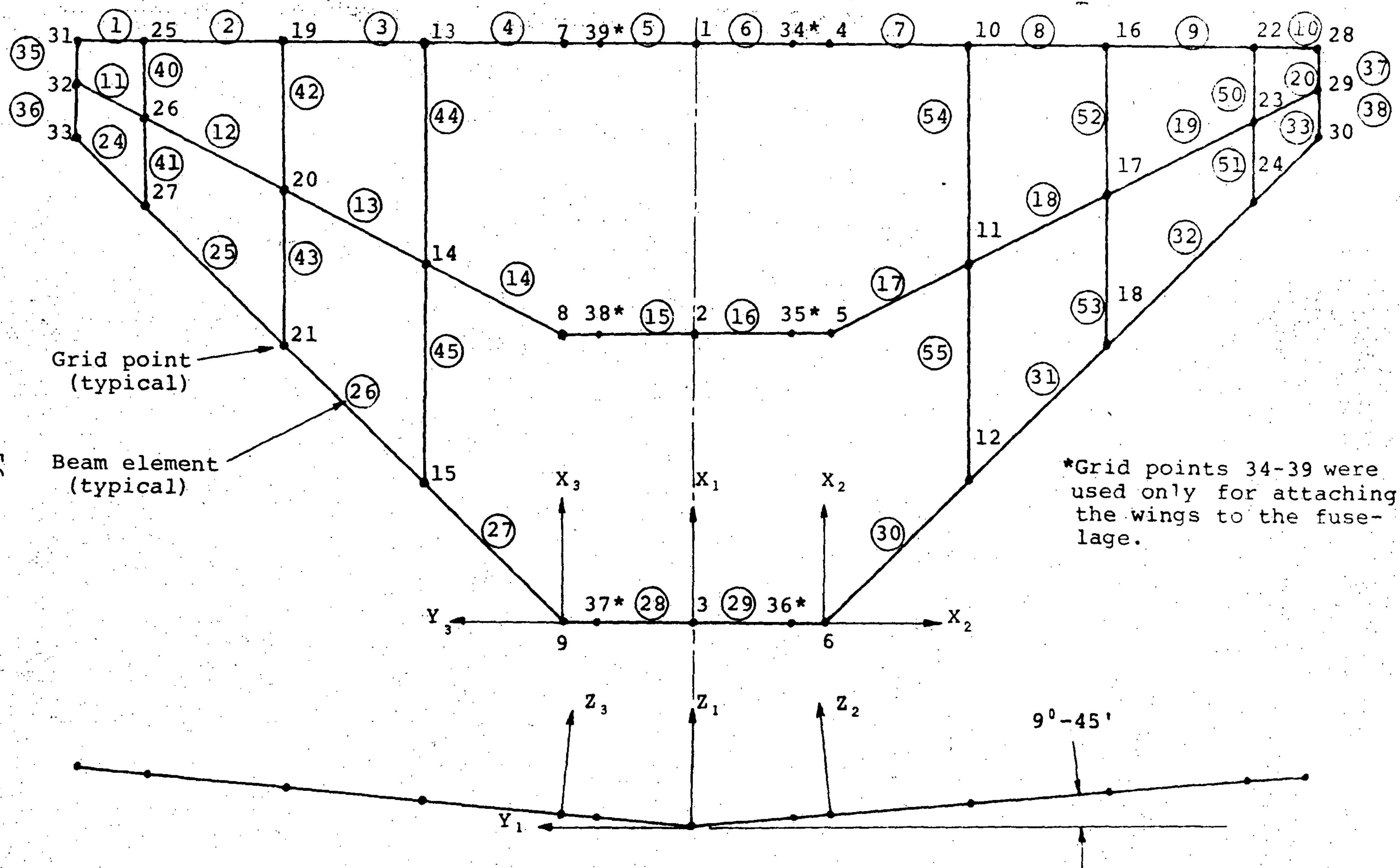

Figure 5.- Schematic of booster delta wing.

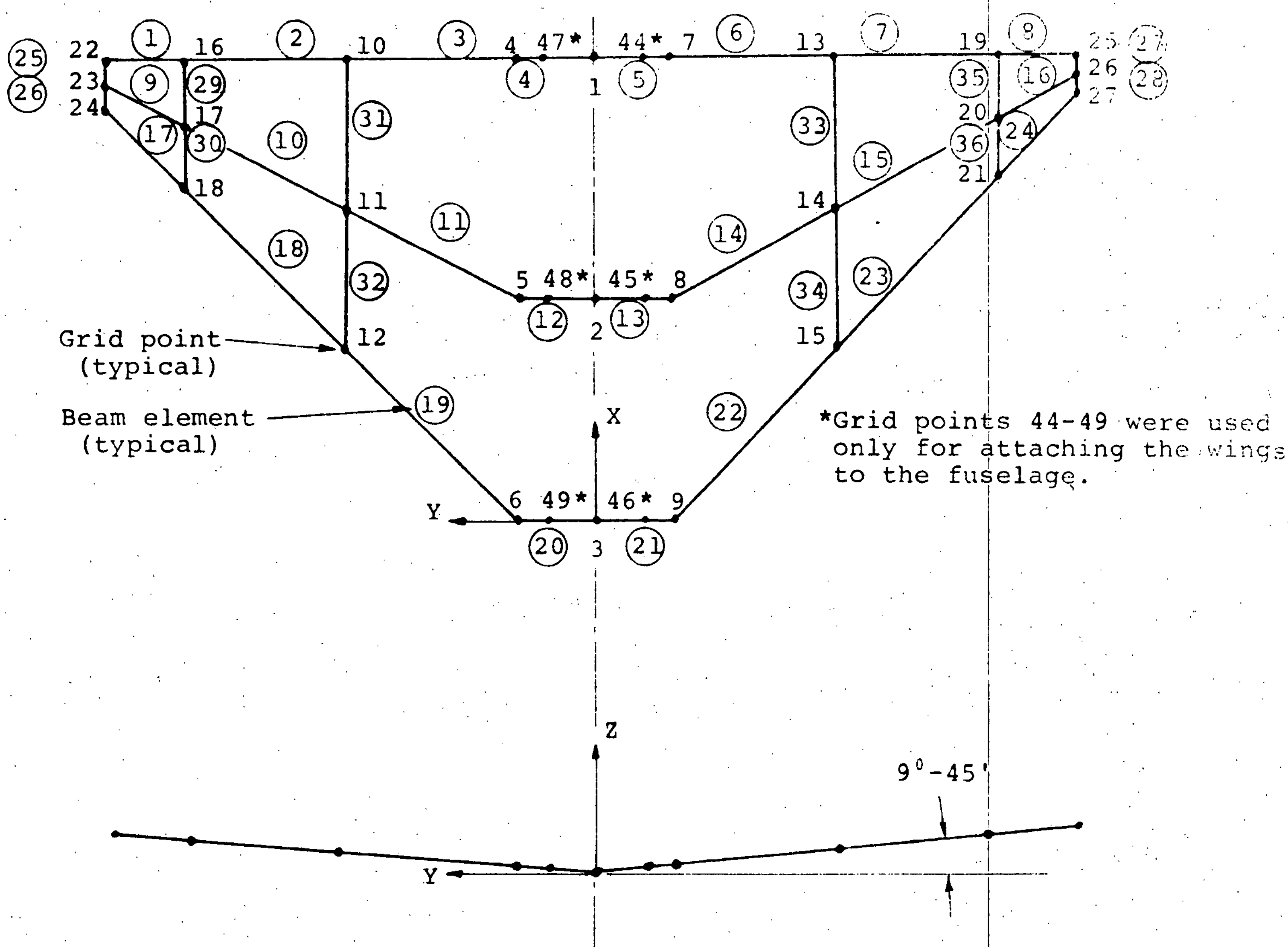

Figure 6.- Schematic of orbiter delta wing.

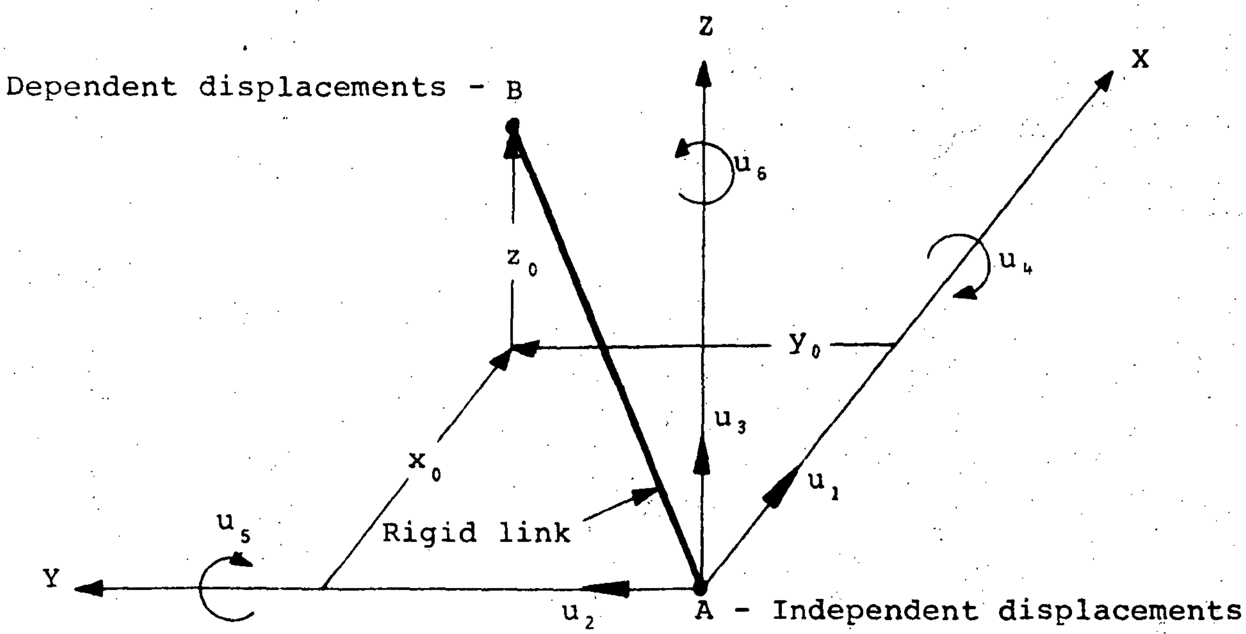

Figure 7.- Geometry for multipoint constraint equations.

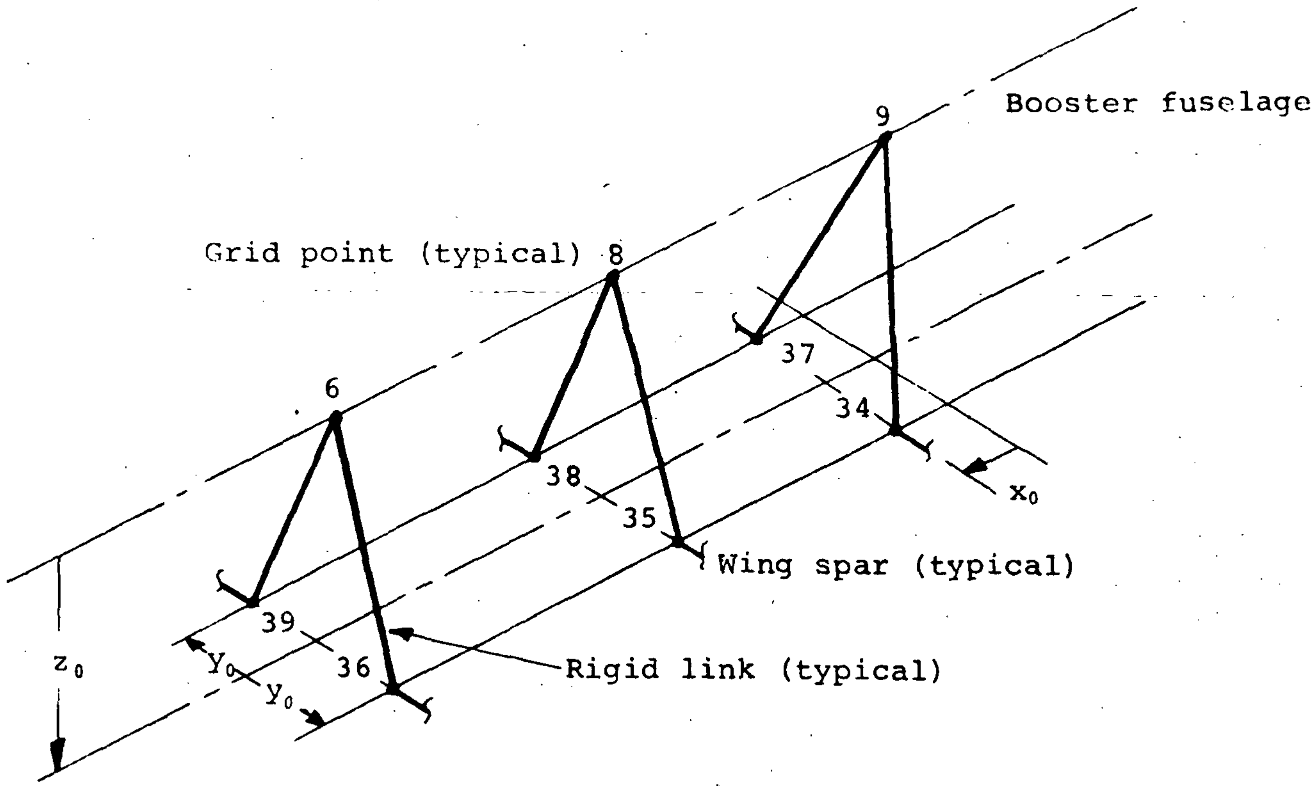

Grid Point	x_0 Inches	y_0 Inches	z_0 Inches
34	-1.90	-5.82	-5.88
35	0	-5.82	-5.88
36	0	-5.82	-5.88
37	-1.90	5.82	-5.88
38	0	5.82	-5.88
39	0	5.82	-5.88

Figure 8.- Schematic of booster fuselage-wing interface geometry.

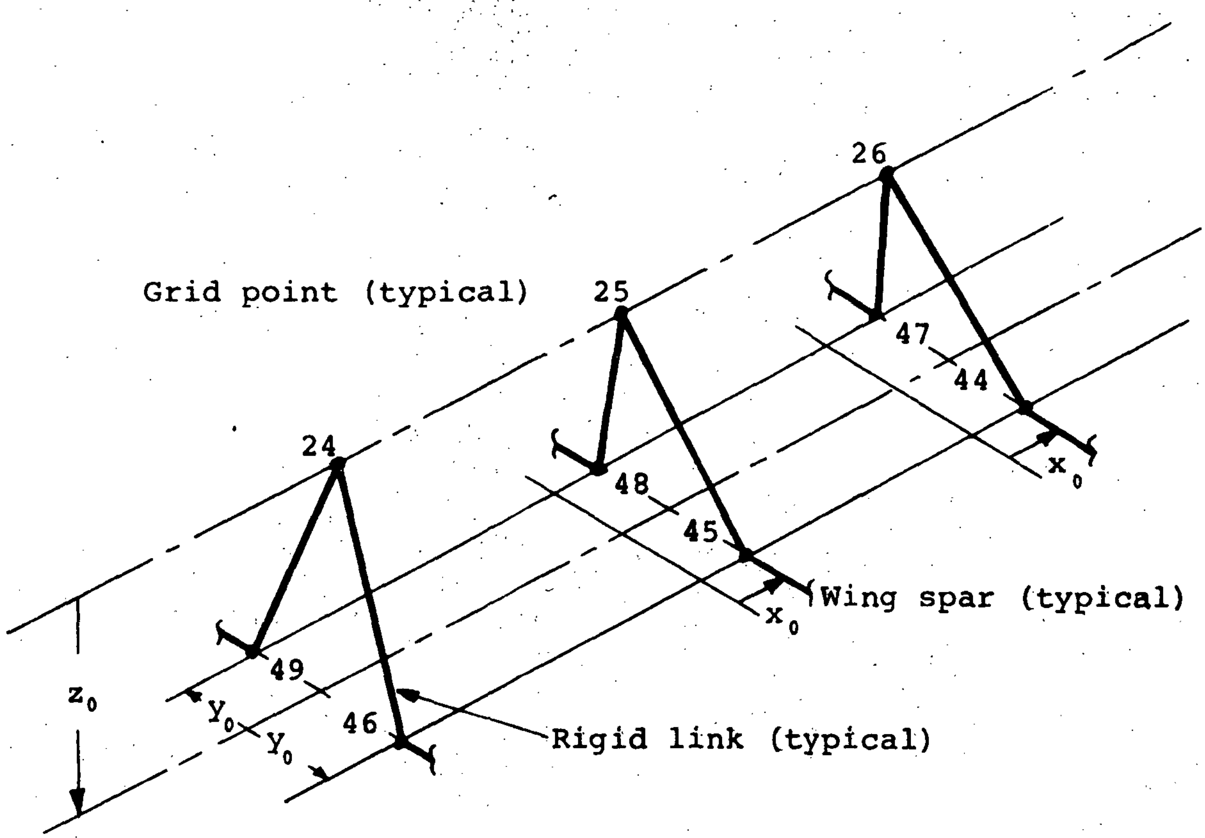

	x_0	y_0	z_0
Grid Point	Inches	Inches	Inches
44	3.62	-3.94	-3.384
45	2.18	-3.94	-3.384
46	0	-3.94	-3.384
47	3.62	3.94	-3.384
48	2.18	3.94	-3.384
49	0	3.94	-3.384

Figure 9.- Schematic of orbiter fuselage-wing interface geometry.

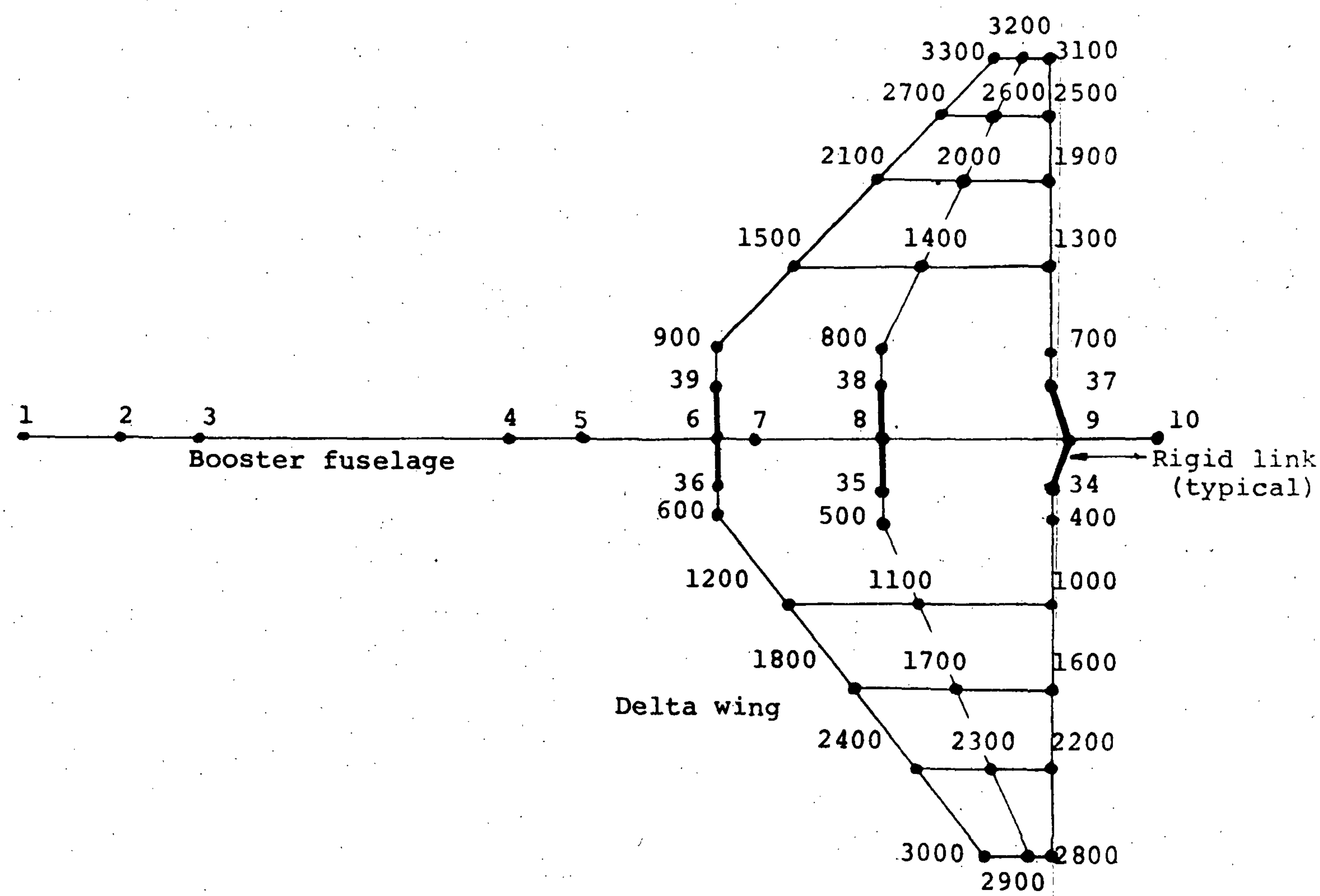

Figure 10.- Schematic of booster airplane idealization.

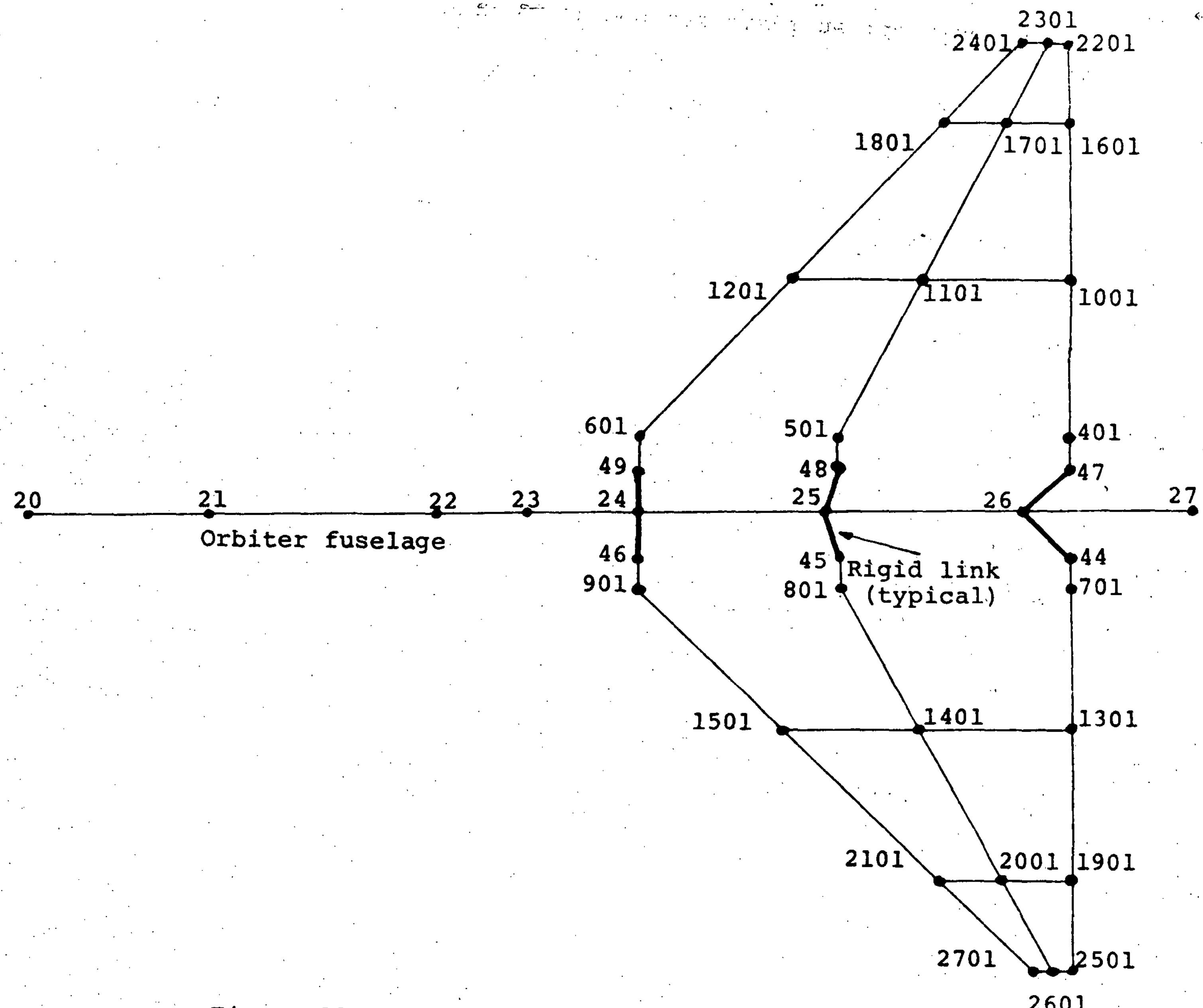

Figure 11.- Schematic of orbiter airplane idealization.

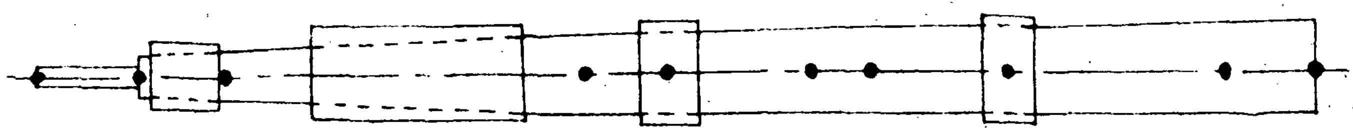

Frequency, HZ

Mode	Liftoff	Max Q	Burnout
1	36.8	53.7	83.9
2	117.2	137.9	243.7
3	198.7	252.3	464.1

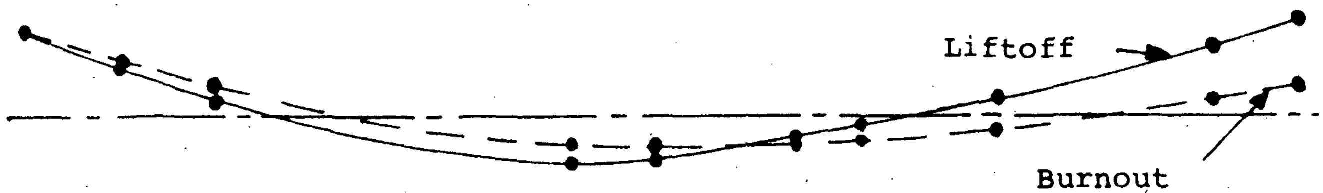

(a) Mode 1

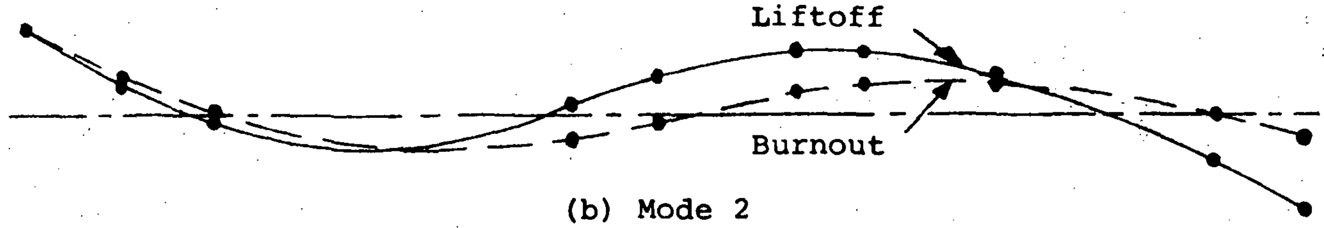

(b) Mode 2

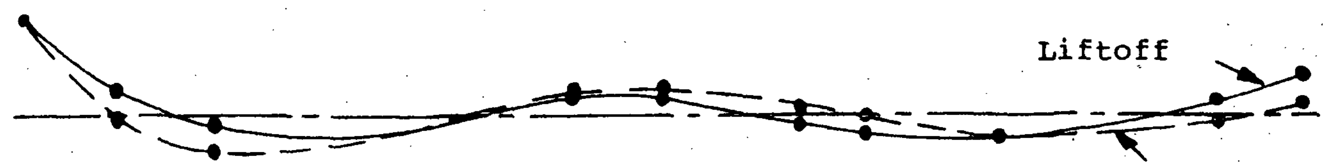

(c) Mode 3

Figure 12.- Bending modes of booster fuselage.

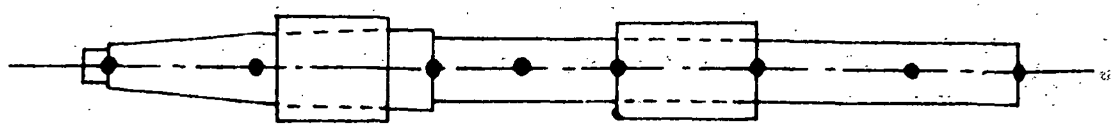

Frequency, HZ

Mode	Liftoff	Empty
1	103.5	141.5
2	229.7	451.6
3	460.3	

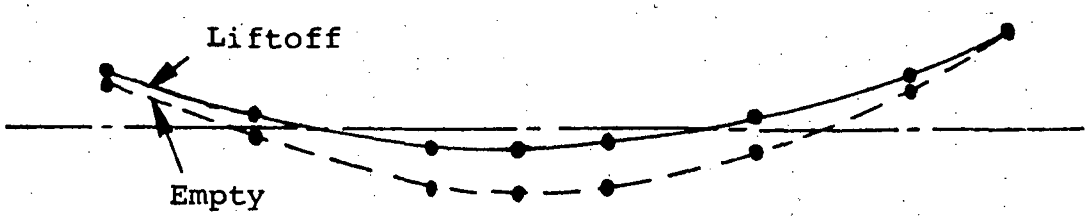

(a) Mode 1

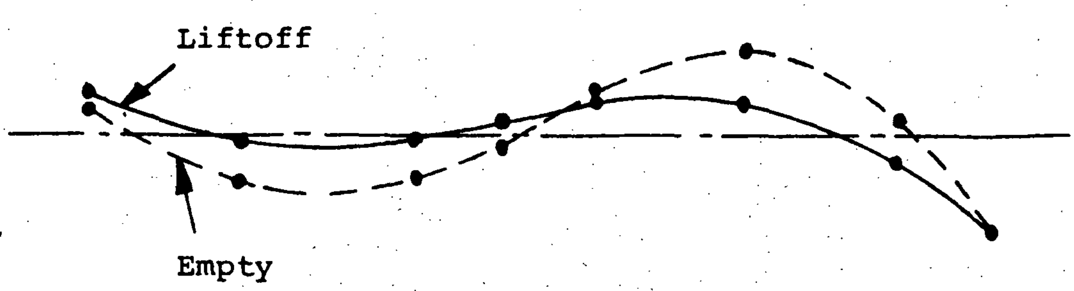

(b) Mode 2

Figure 13.- Bending modes of orbiter fuselage.

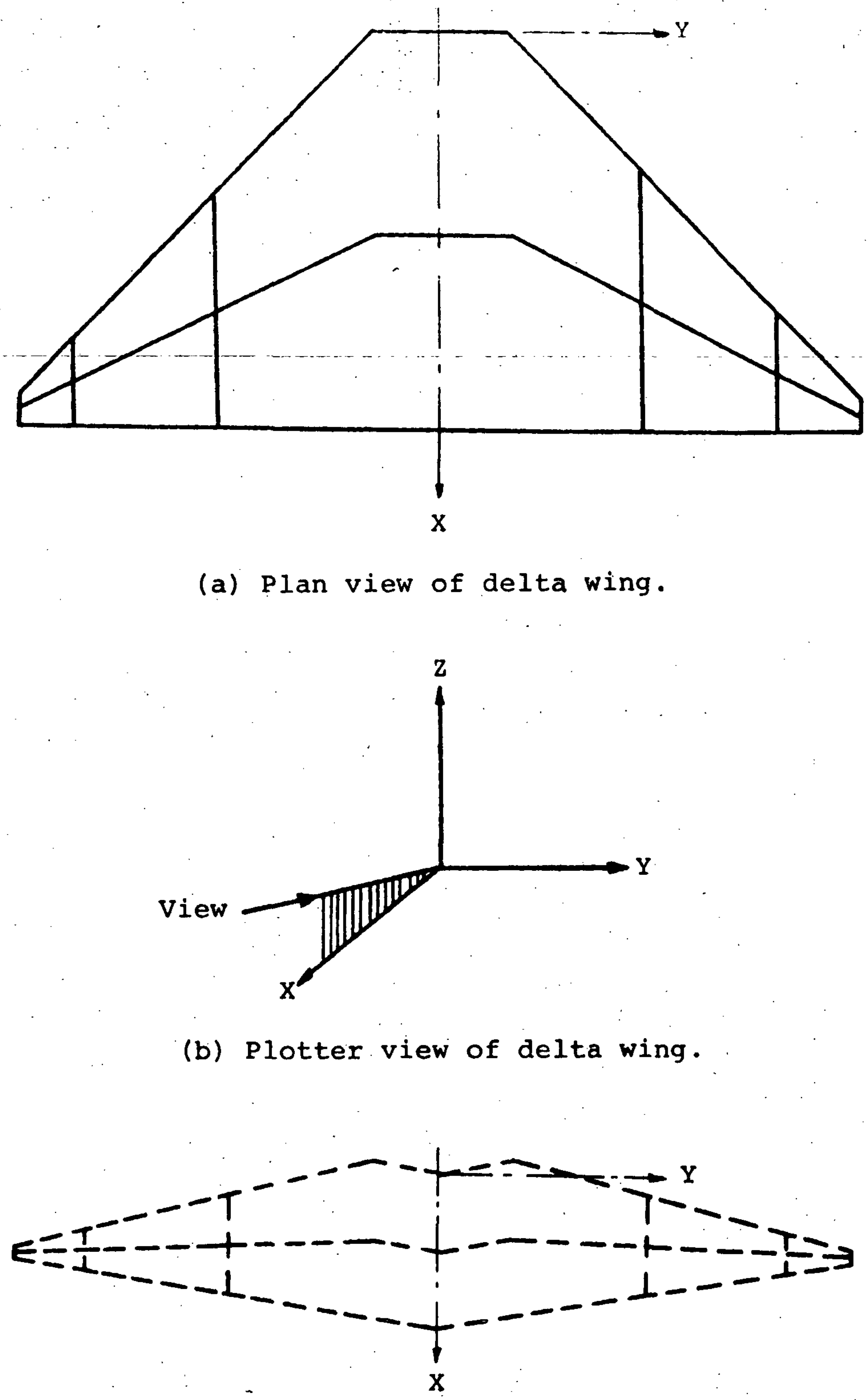

(a) Plan view of delta wing.

(b) Plotter view of delta wing.

(c) Undeformed wing as seen by plotter.

Figure 14.- Plotter orientation for delta wing mode shape plots.

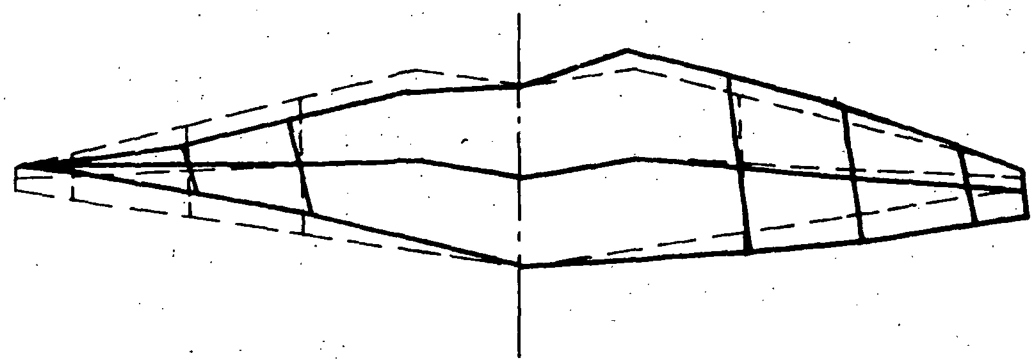

(a) Mode 1, 24.6 HZ.

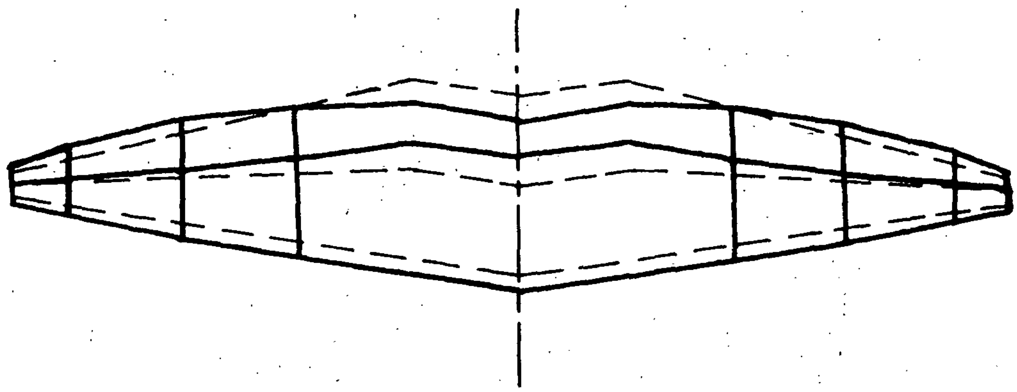

(b) Mode 2, 26.4 HZ.

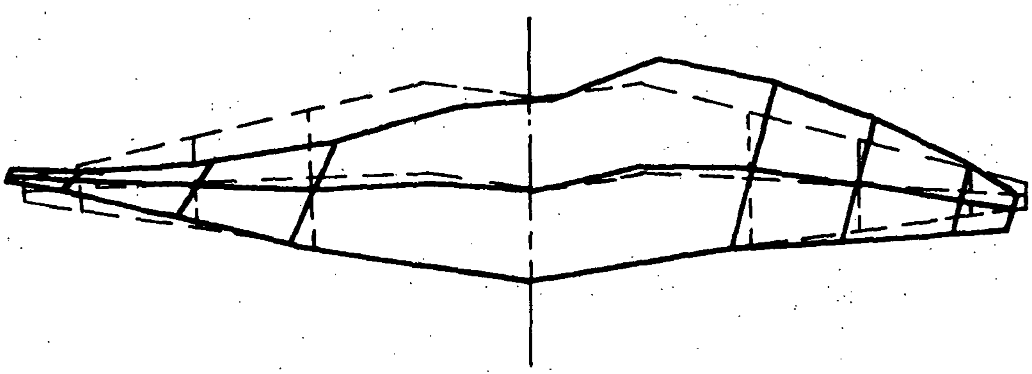

(c) Mode 3, 27.3 HZ.

Figure 15.- Mode shapes of booster delta wing.

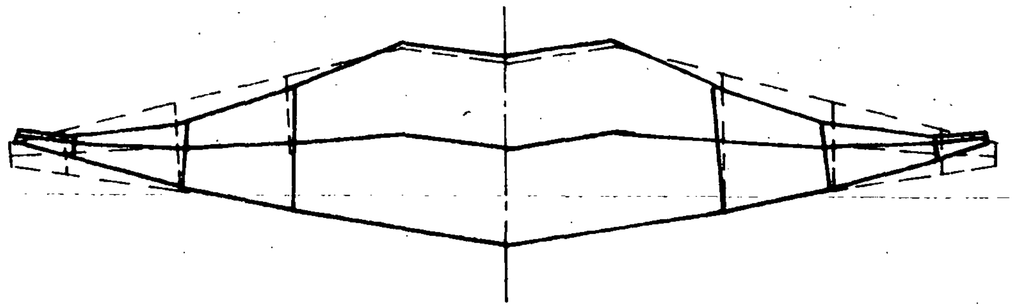

(d) Mode 4, 28.0 HZ.

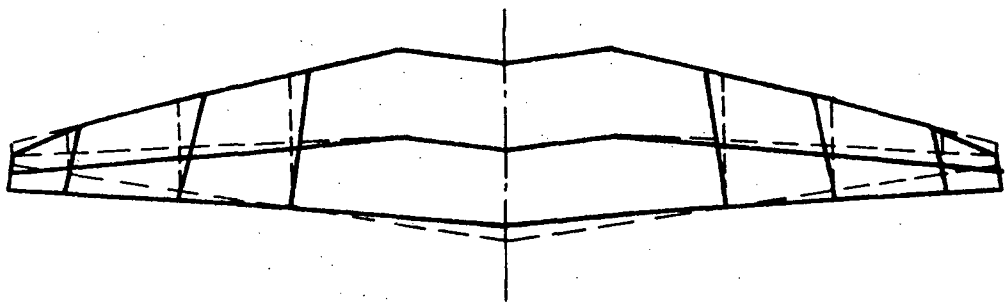

(e) Mode 5, 49.4 HZ.

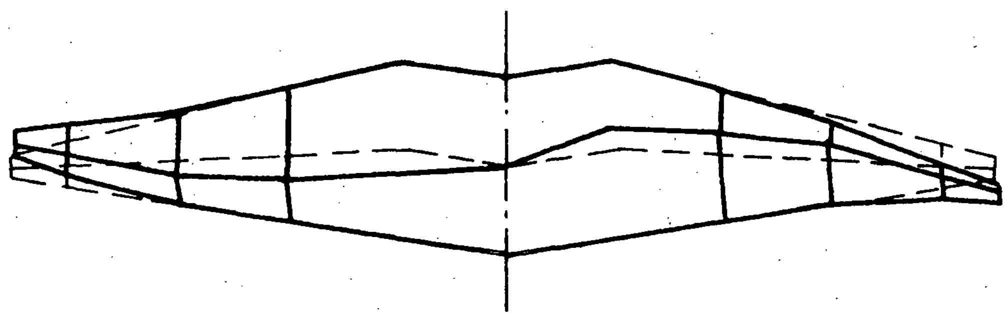

(f) Mode 6, 54.4 HZ.

Figure 15 (continued).- Mode shapes of booster delta wing.

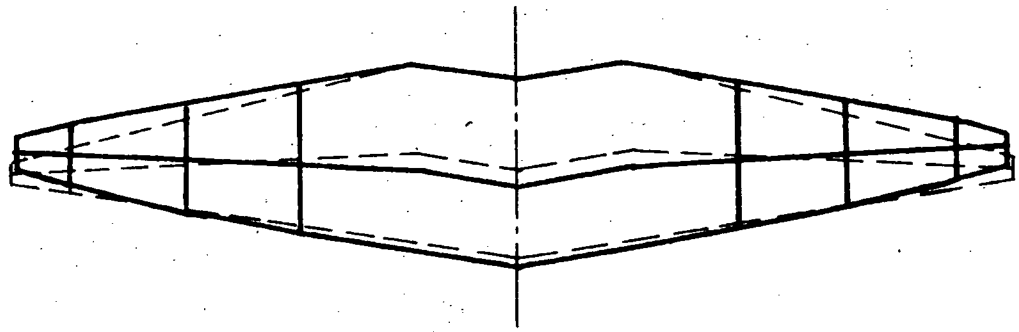

(g) Mode 7, 65.0 HZ.

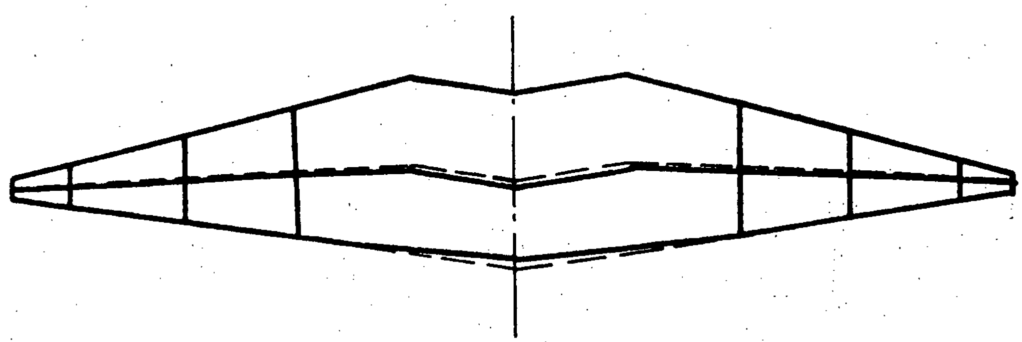

(h) Mode 8, 64.4 HZ.

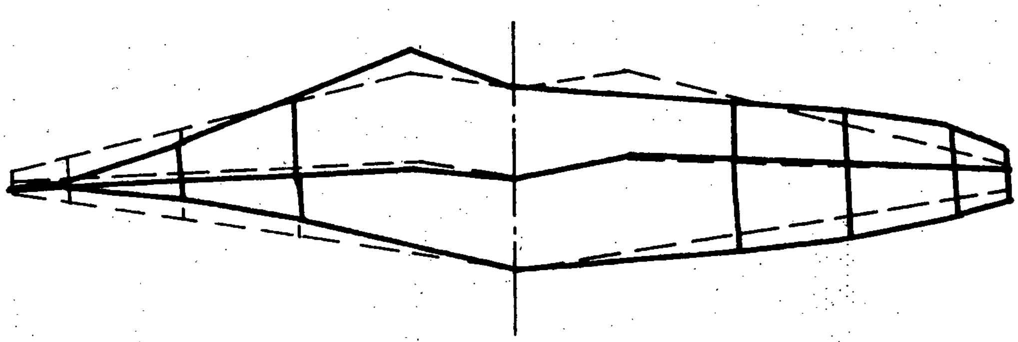

(i) Mode 9, 69.4 HZ.

Figure 15 (concluded).- Mode shapes of booster delta wing.

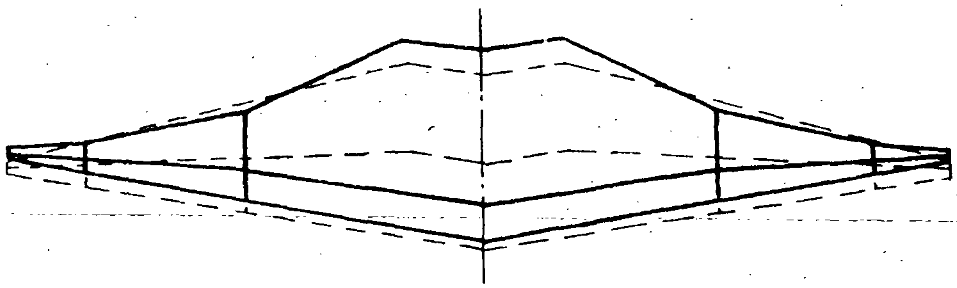

(a) Mode 1, 26.3 HZ.

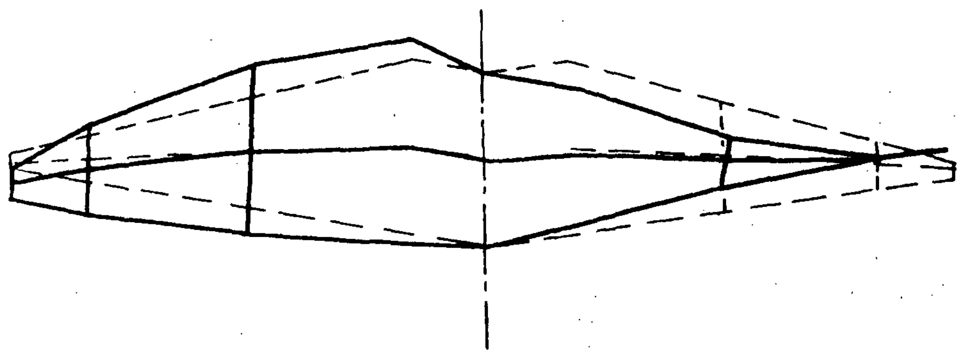

(b) Mode 2, 29.3 HZ.

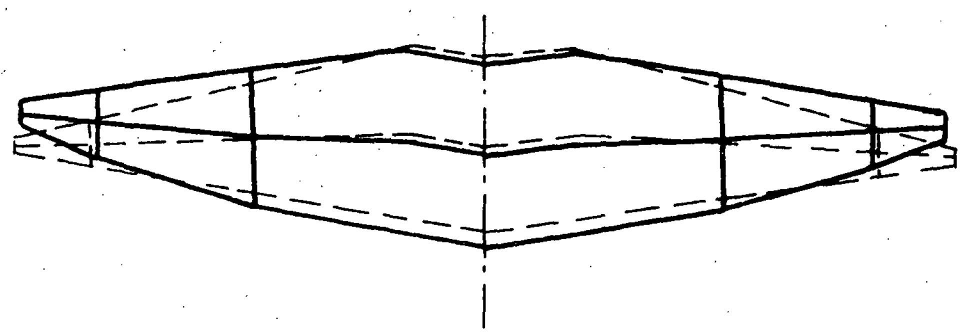

(c) Mode 3, 31.0 HZ.

Figure 16.- Mode shapes of orbiter delta wing.

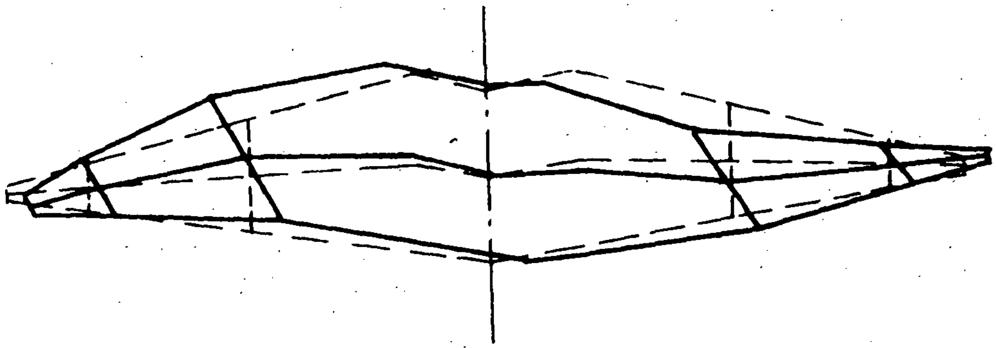

(d) Mode 4, 61.3 HZ.

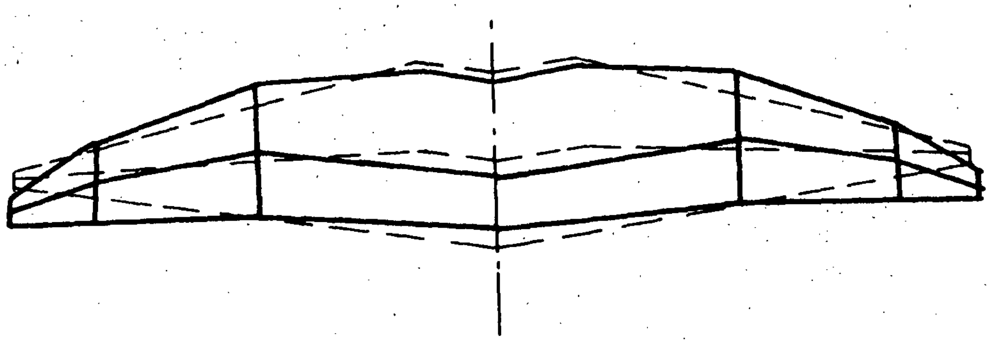

(e) Mode 5, 63.2 HZ.

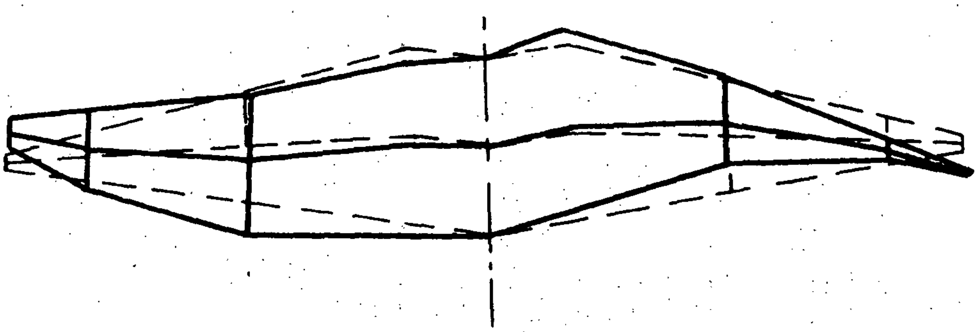

(f) Mode 6, 67.5 HZ.

Figure 16 (continued).- Mode shapes of orbiter delta wing.

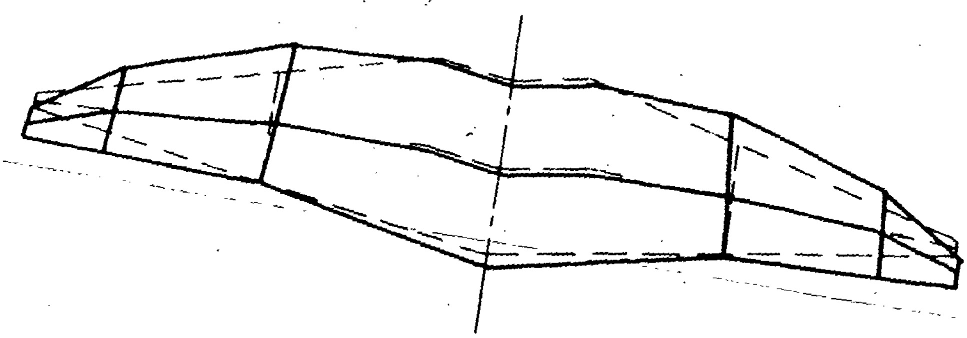

(g) Mode 7, 69.1 HZ.

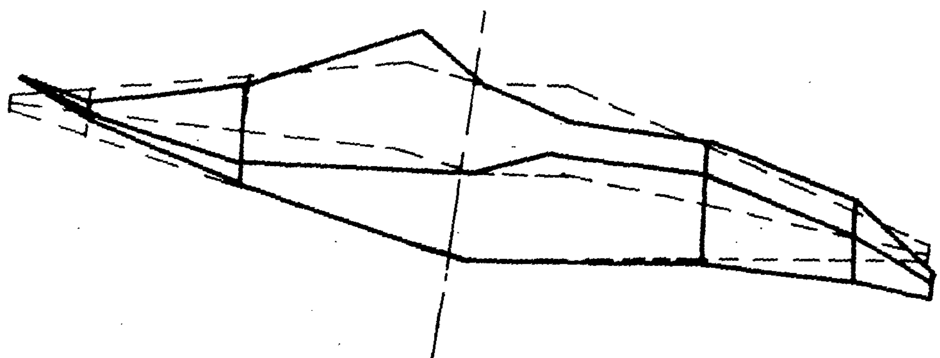

(h) Mode 8, 73.4 HZ.

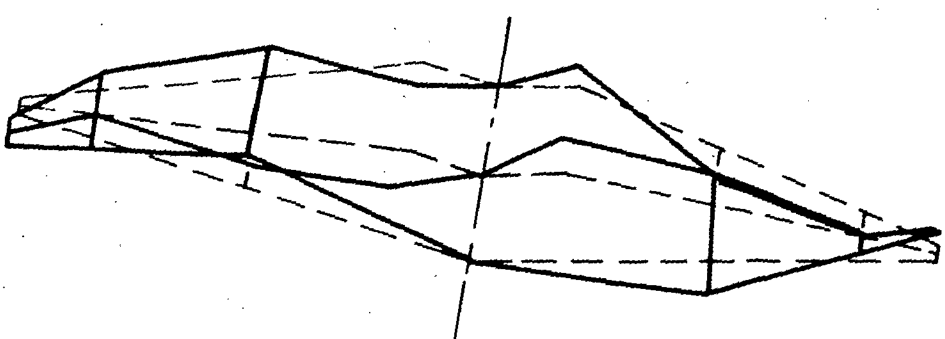

(i) Mode 9, 118.4 HZ.

Figure 16 (concluded).- Mode shapes of orbiter delta wing.

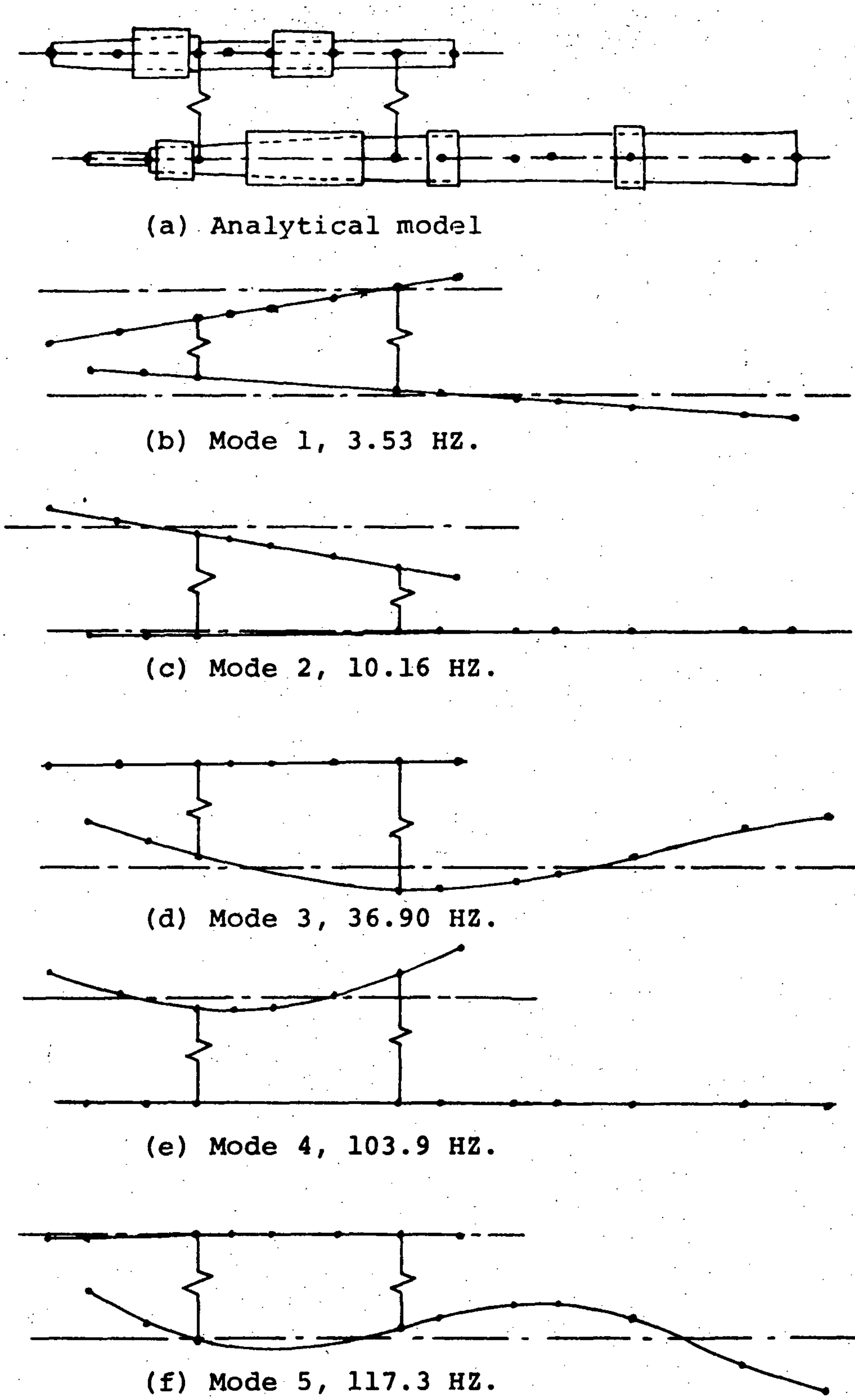

Figure 17.- Mode shapes of elastically connected fuselages.
Liftoff weight distribution.
10^2 lb/in nominal springs.

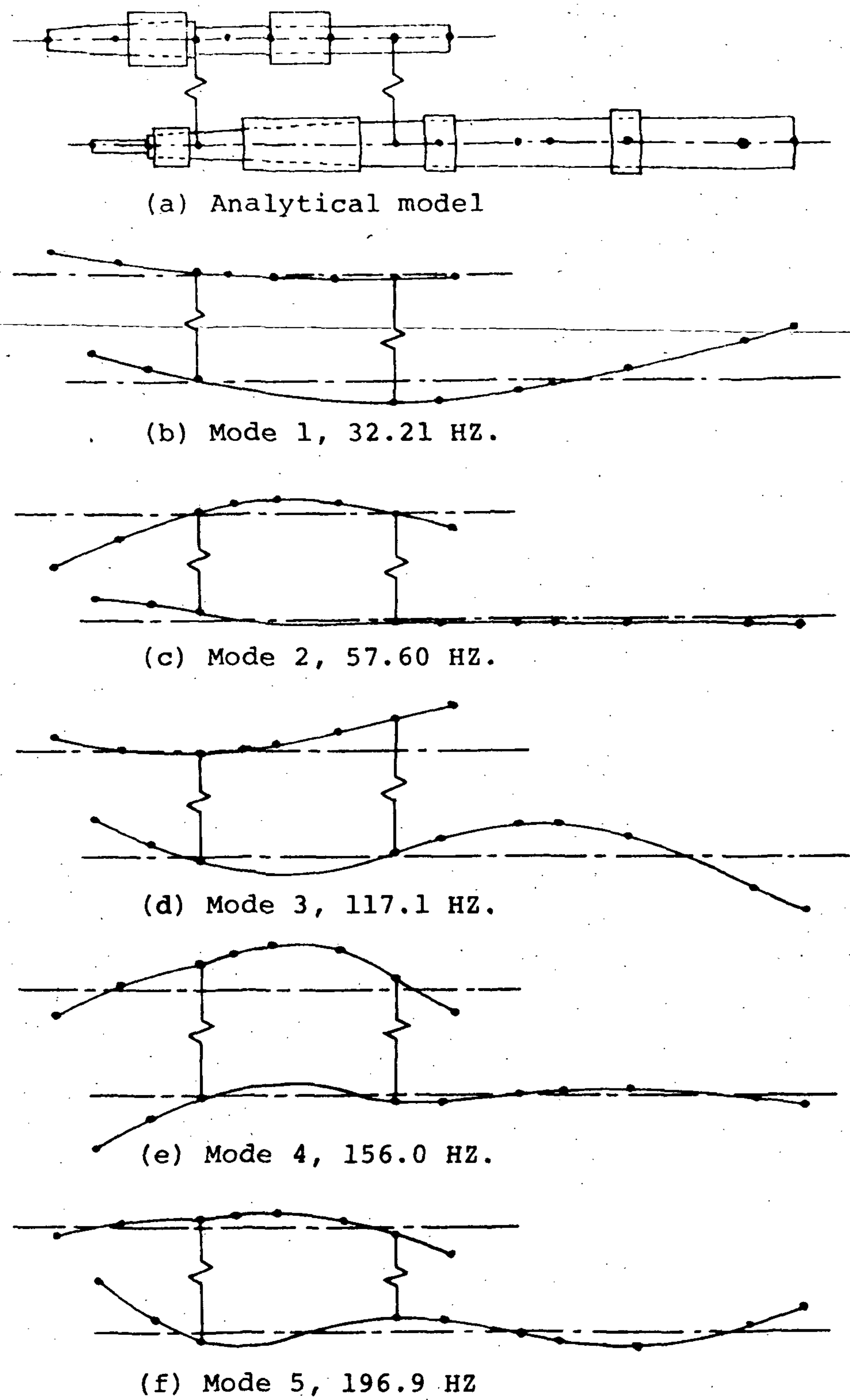

Figure 18.- Mode shapes of elastically connected fuselages.
Liftoff weight distribution.
10^5 lb/in nominal springs.

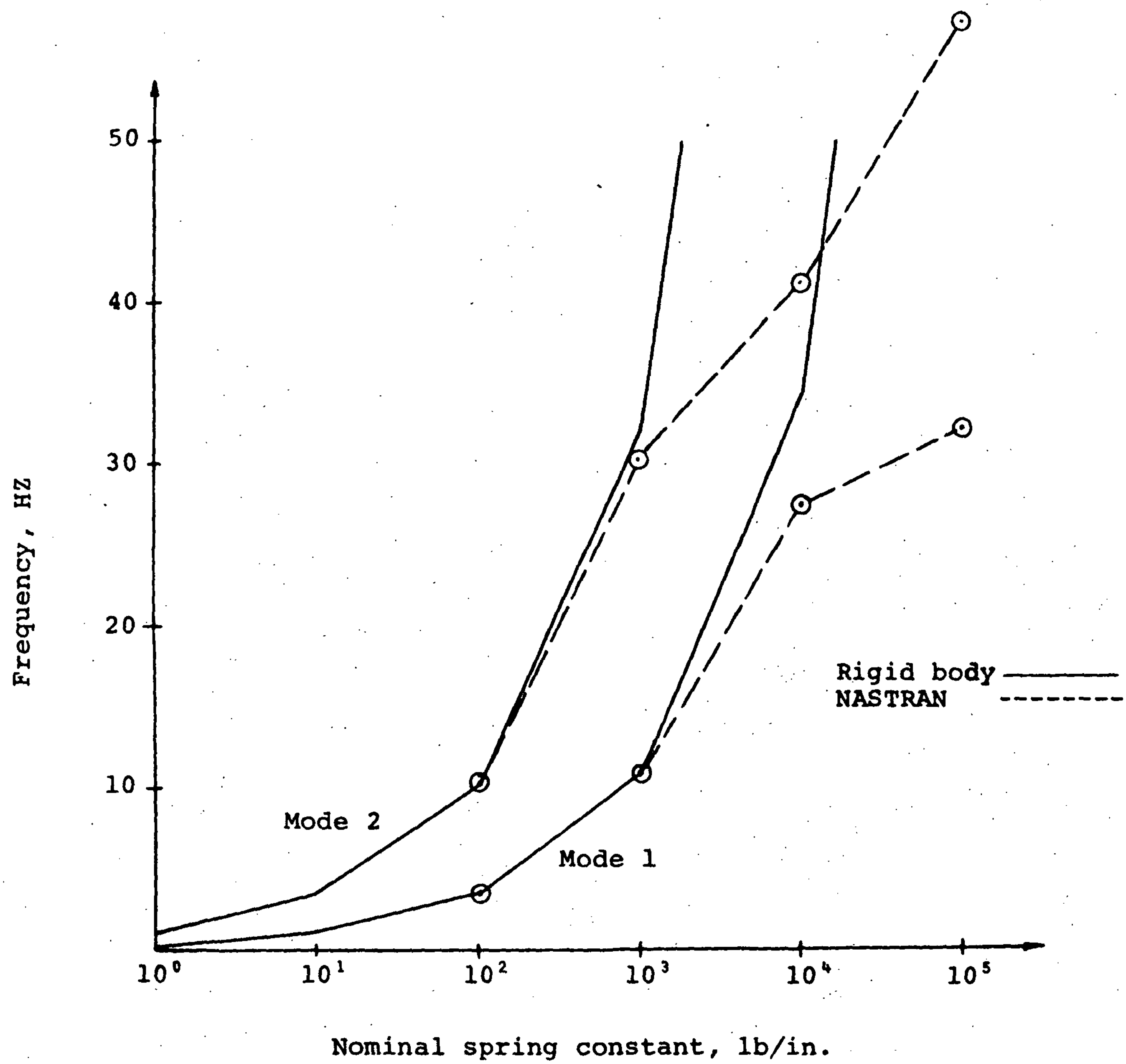

Figure 19.- Variation of NASTRAN and rigid body analyses frequencies with nominal spring constant.

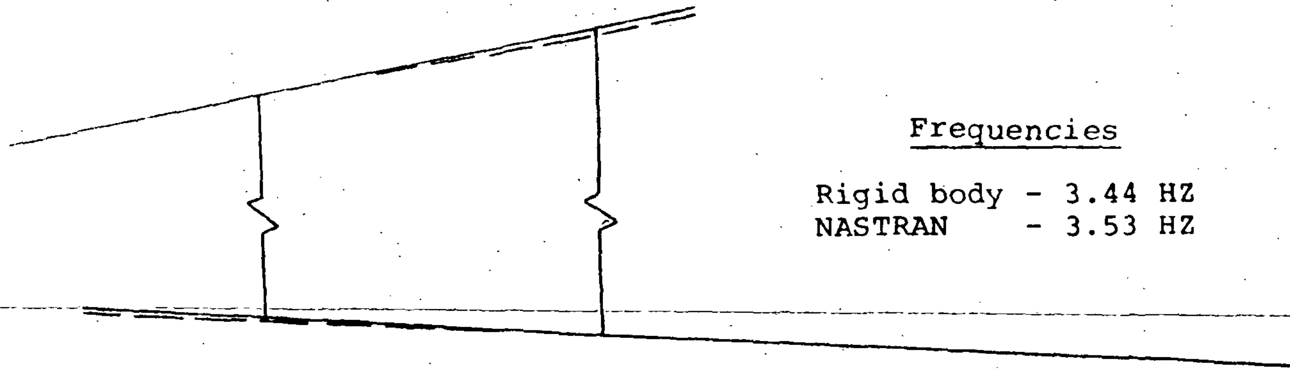

(a) First mode.

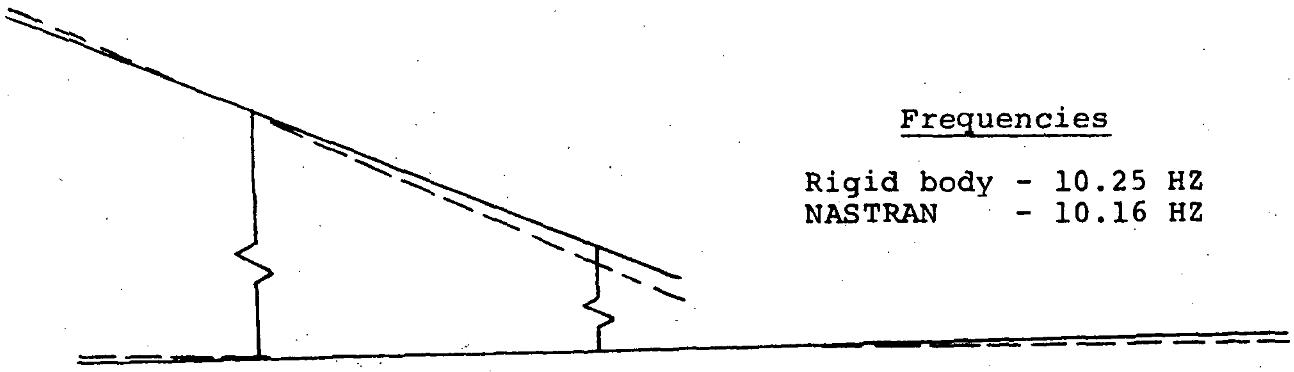

(b) Second mode.

Rigid Body ————

NASTRAN ----

Figure 20.- Comparison of NASTRAN and rigid body analysis modes. 10^2 lb/in nominal spring.

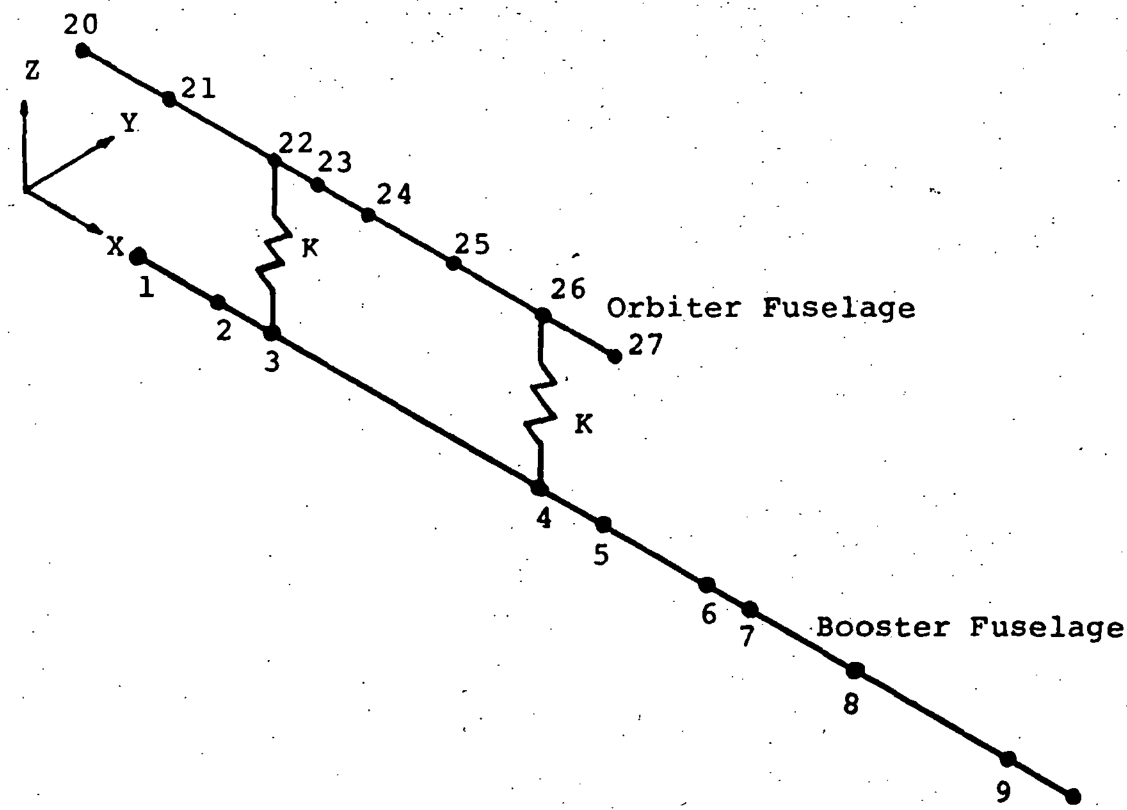

(a) Plotter view of elastically connected fuselages.

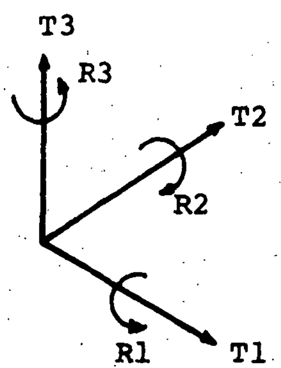

(b) Displacement components for mode shapes.

Figure 21.- Plotter view of elastically connected fuselages.

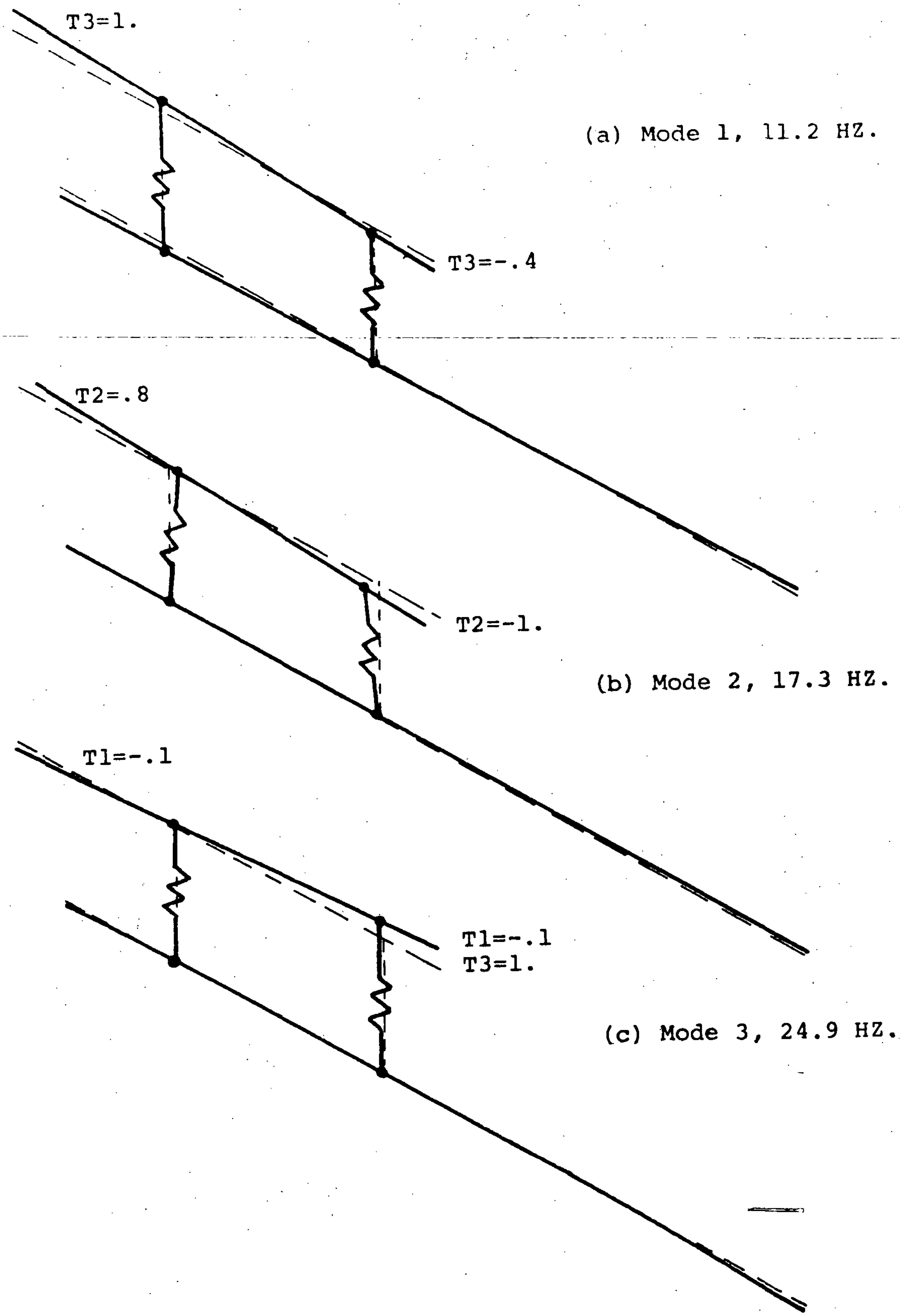

Figure 22.- Mode shapes of elastically connected fuselages. Theoretical flexibility matrix. Nominal 10^3 lb/in.

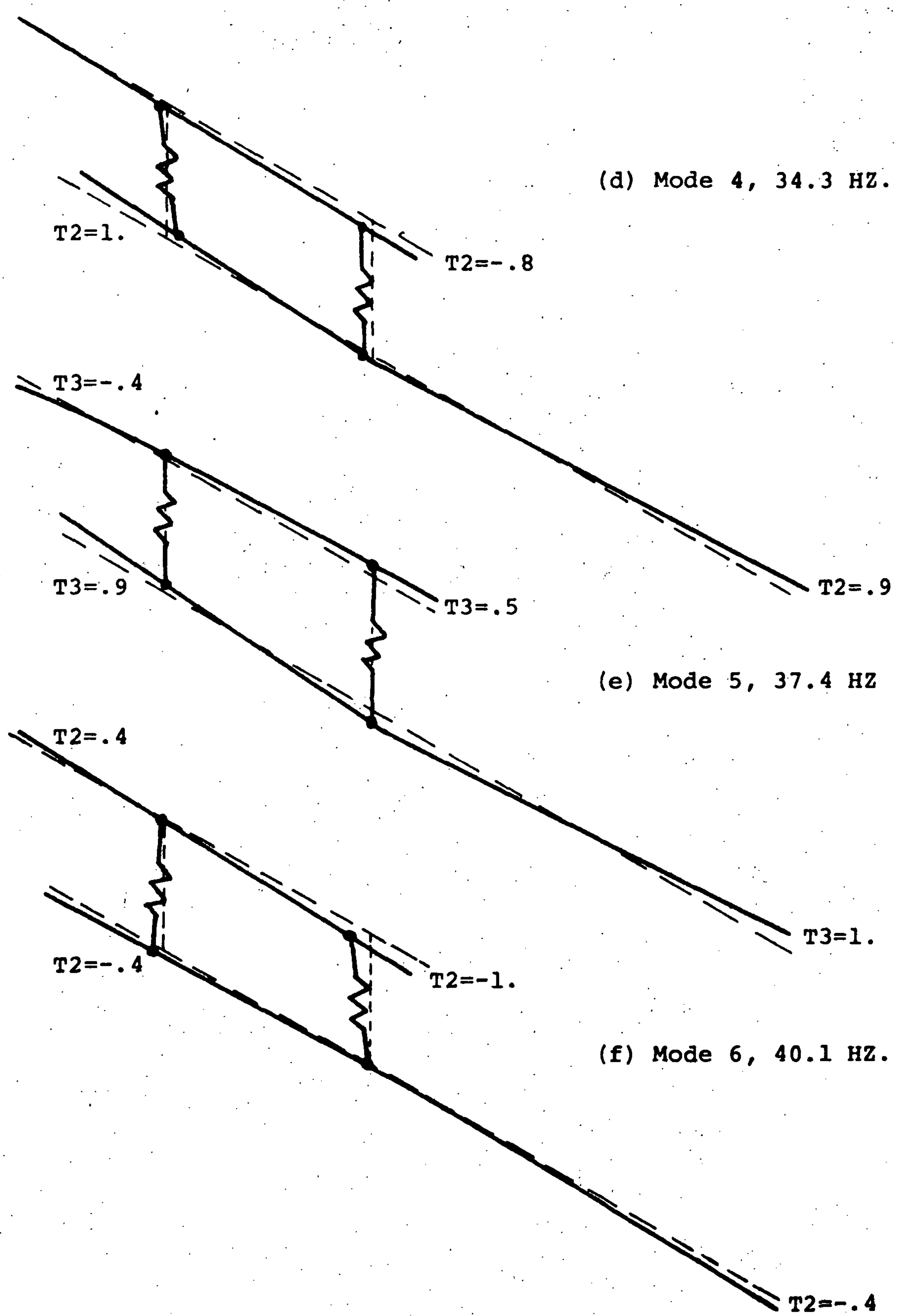

Figure 22 (continued).- Mode shapes of elastically connected fuselages. Theoretical flexibility matrix. Nominal 10^3 lb/in.

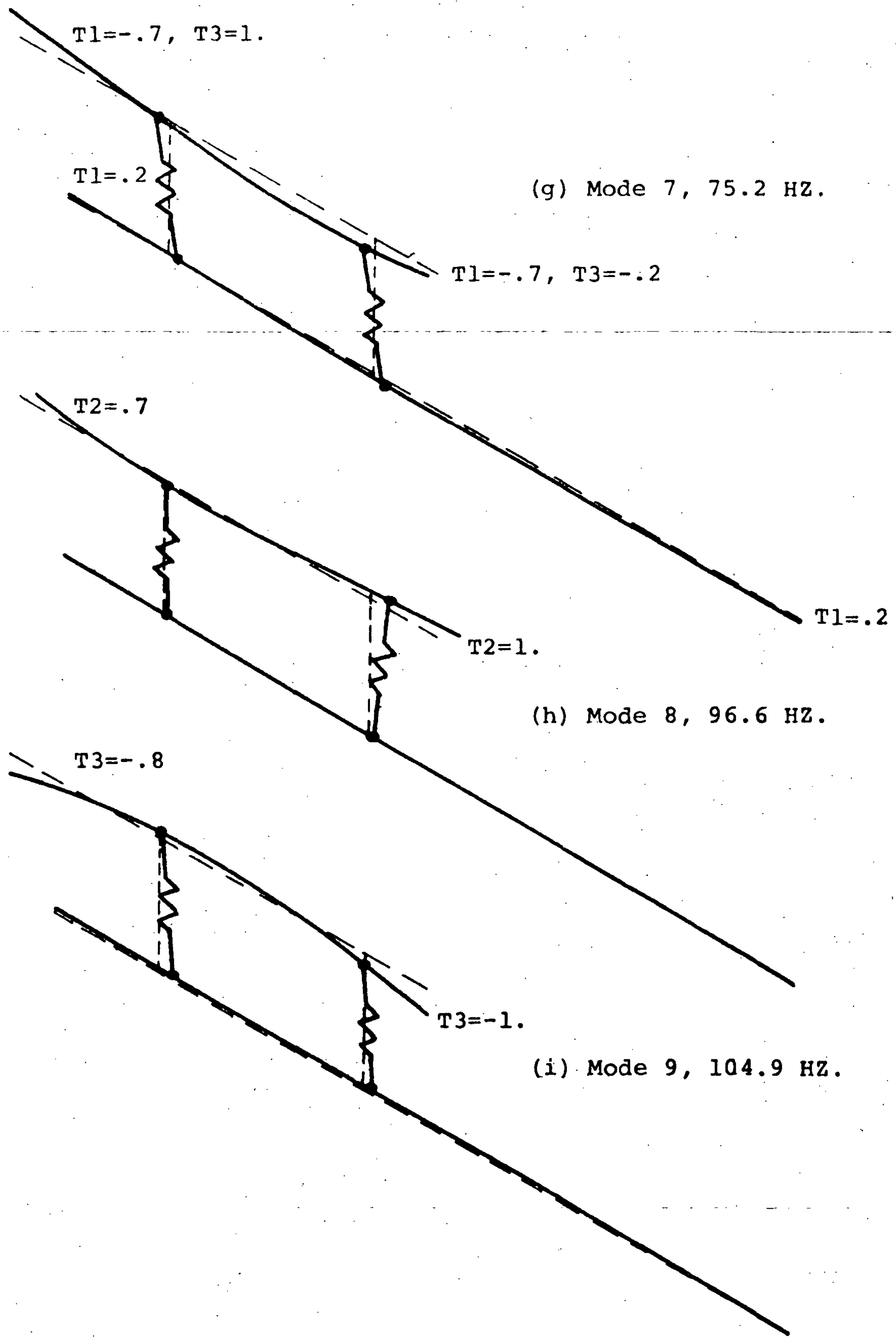

Figure 22 (continued).- Mode shapes of elastically connected fuselages. Theoretical flexibility matrix. Nominal 10^3 lb/in.

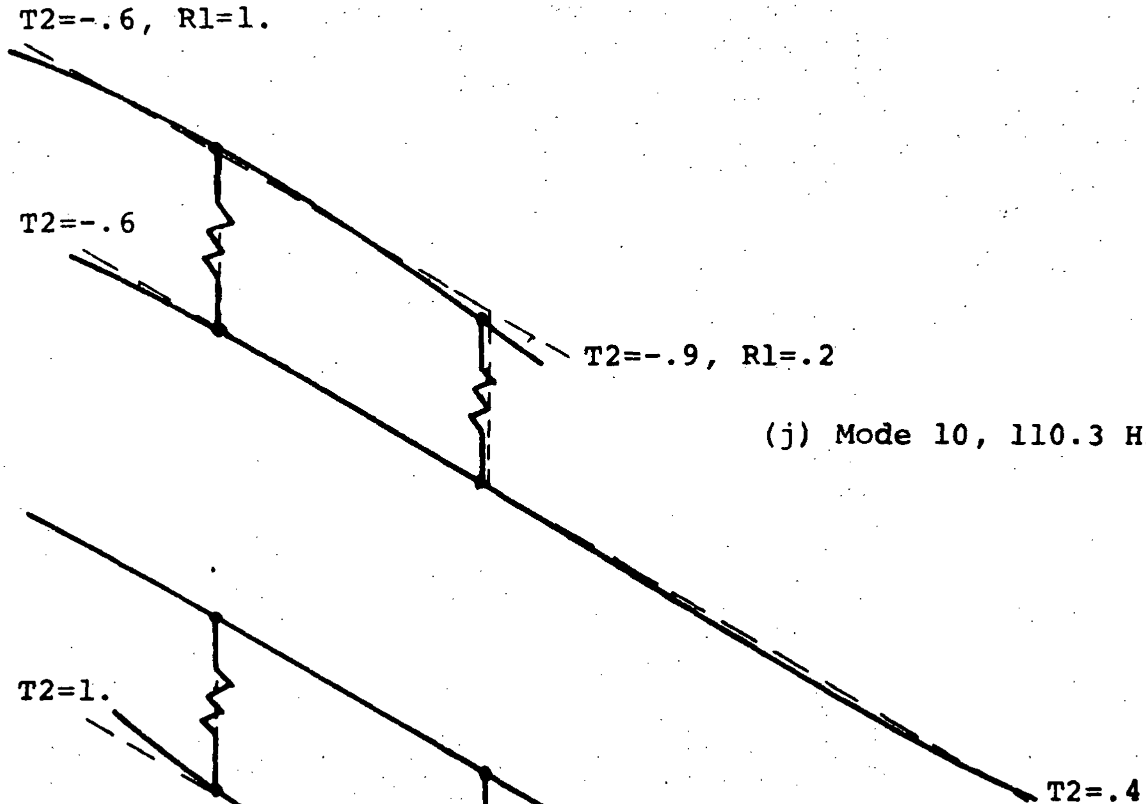

(j) Mode 10, 110.3 HZ.

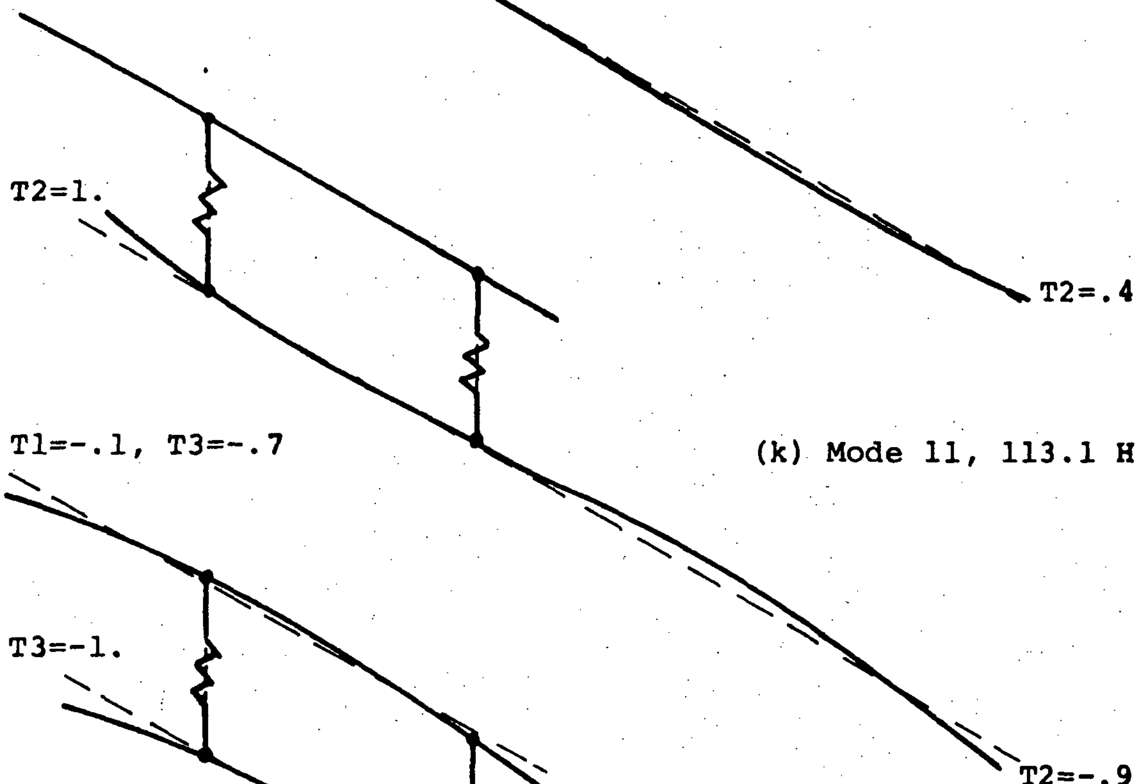

(k) Mode 11, 113.1 HZ.

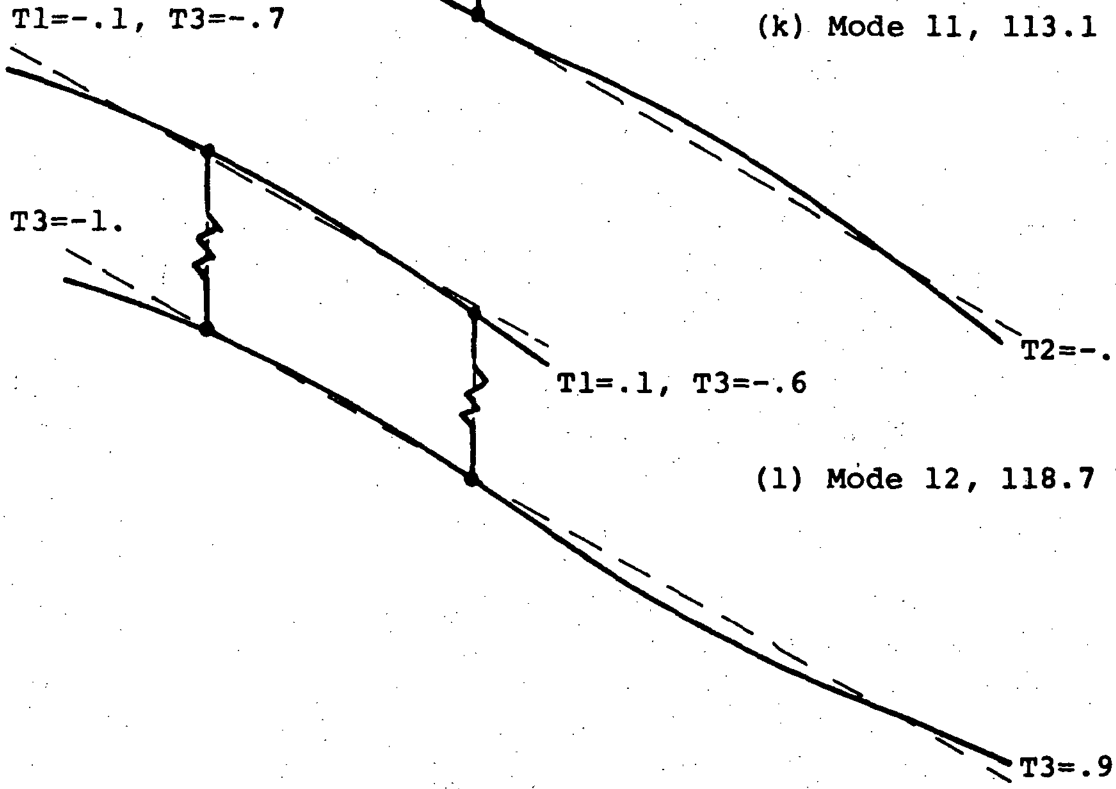

(l) Mode 12, 118.7 HZ.

Figure 22 (concluded).- Mode shapes of elastically connected fuselages. Theoretical flexibility matrix. Nominal 10^3 lb/in.

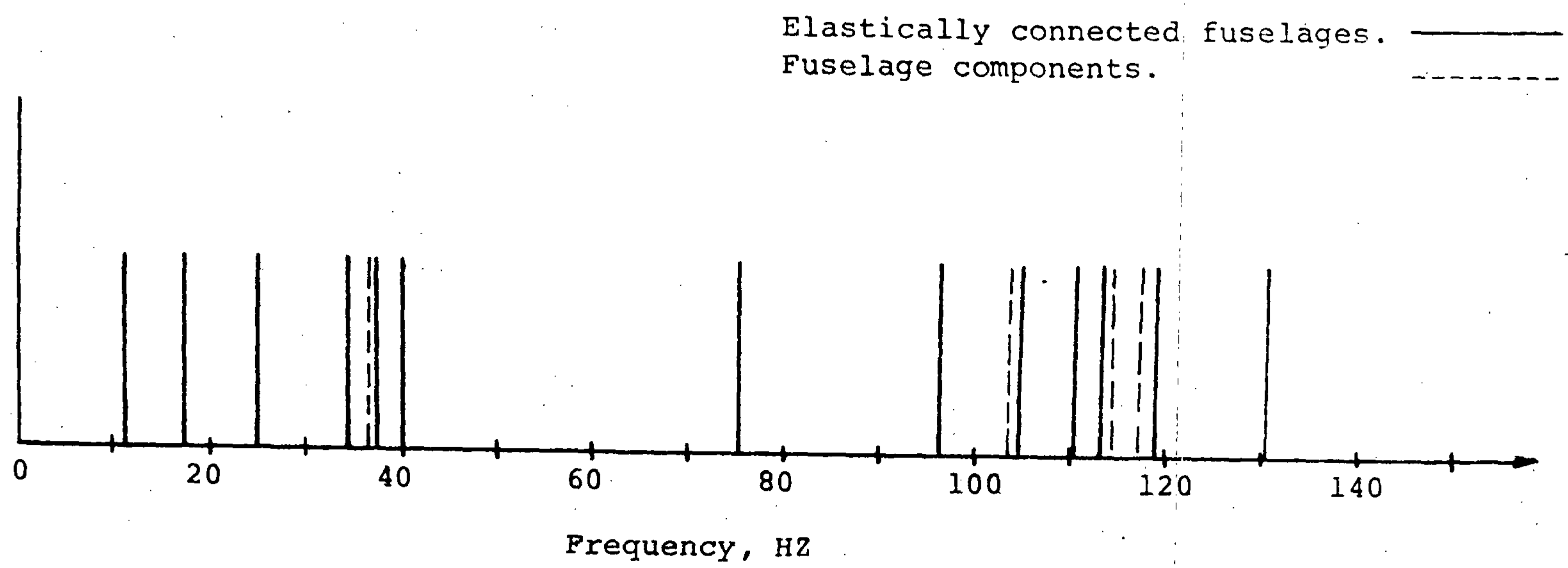

(a) Theoretical frequencies of elastically connected fuselages and fuselage components.

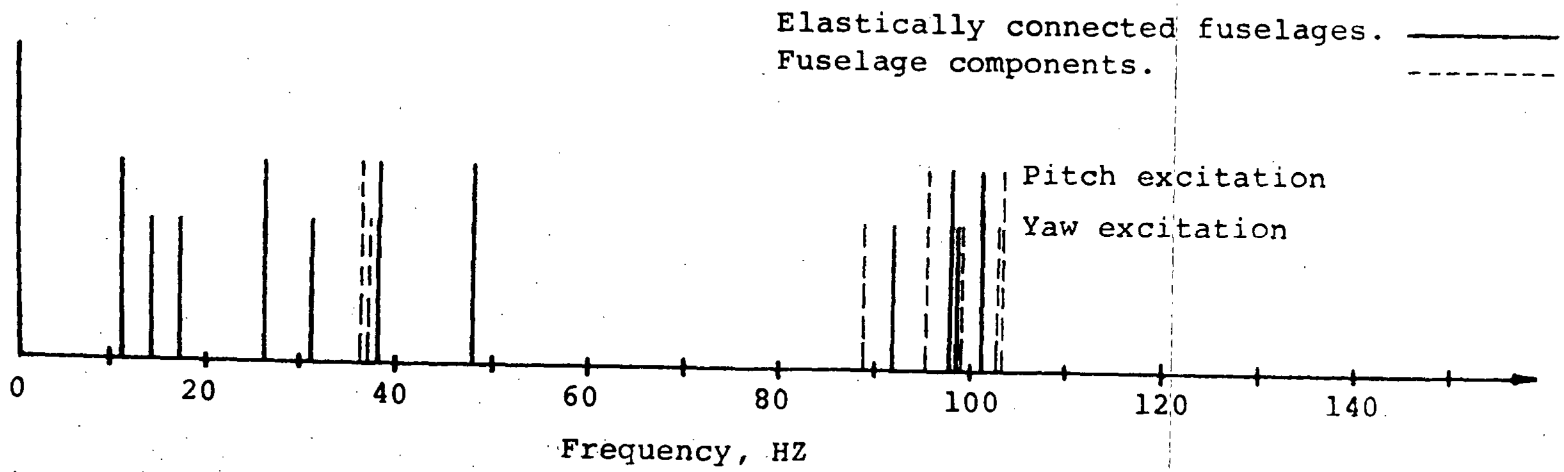

(b) Experimental frequencies of elastically connected fuselages and fuselage components.

Figure 23.- Frequency spectrums for elastically connected fuselages.

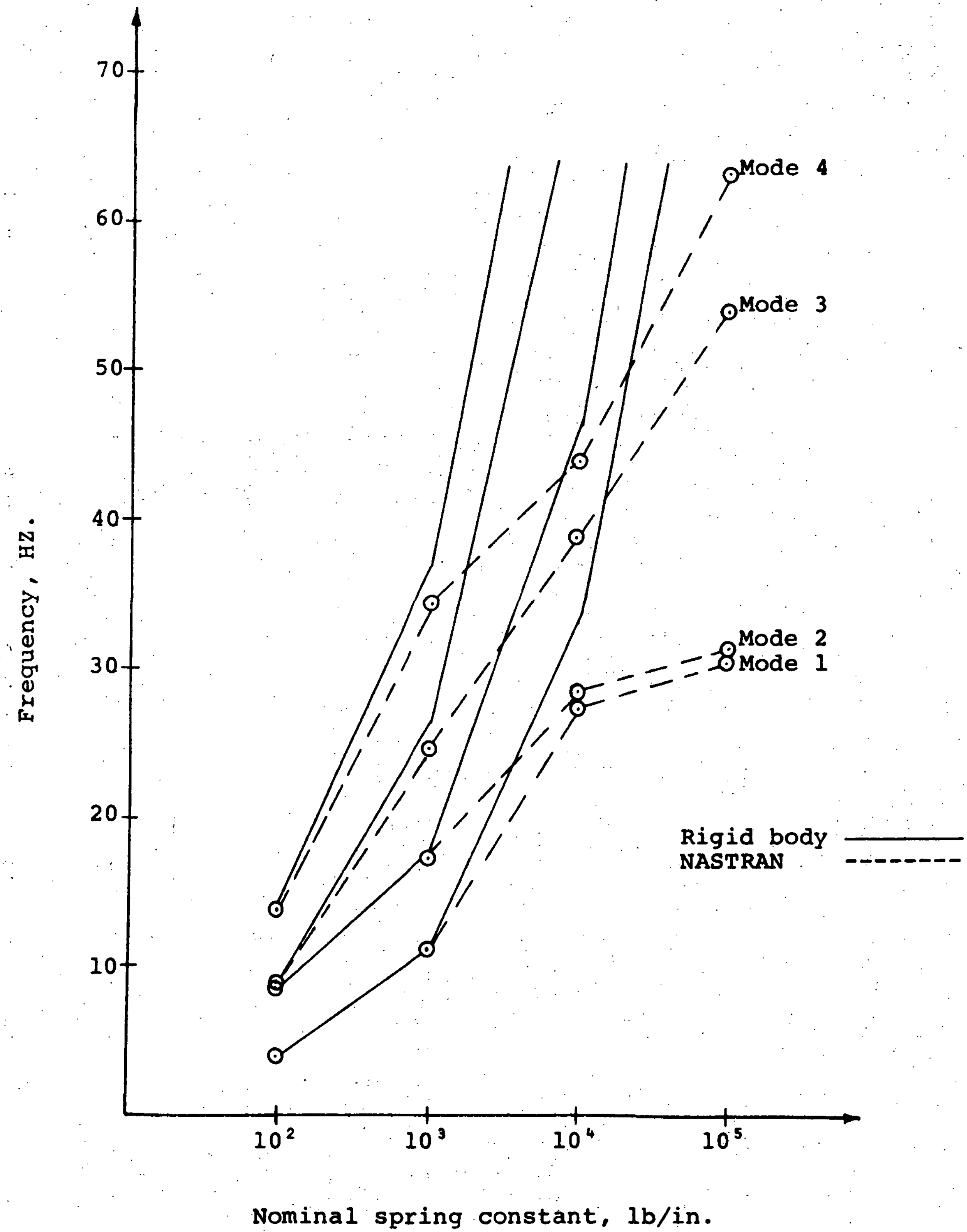

Figure 24.- Variation of NASTRAN and rigid body analyses frequencies. Elastically connected fuselages. Theoretical flexibility matrix.

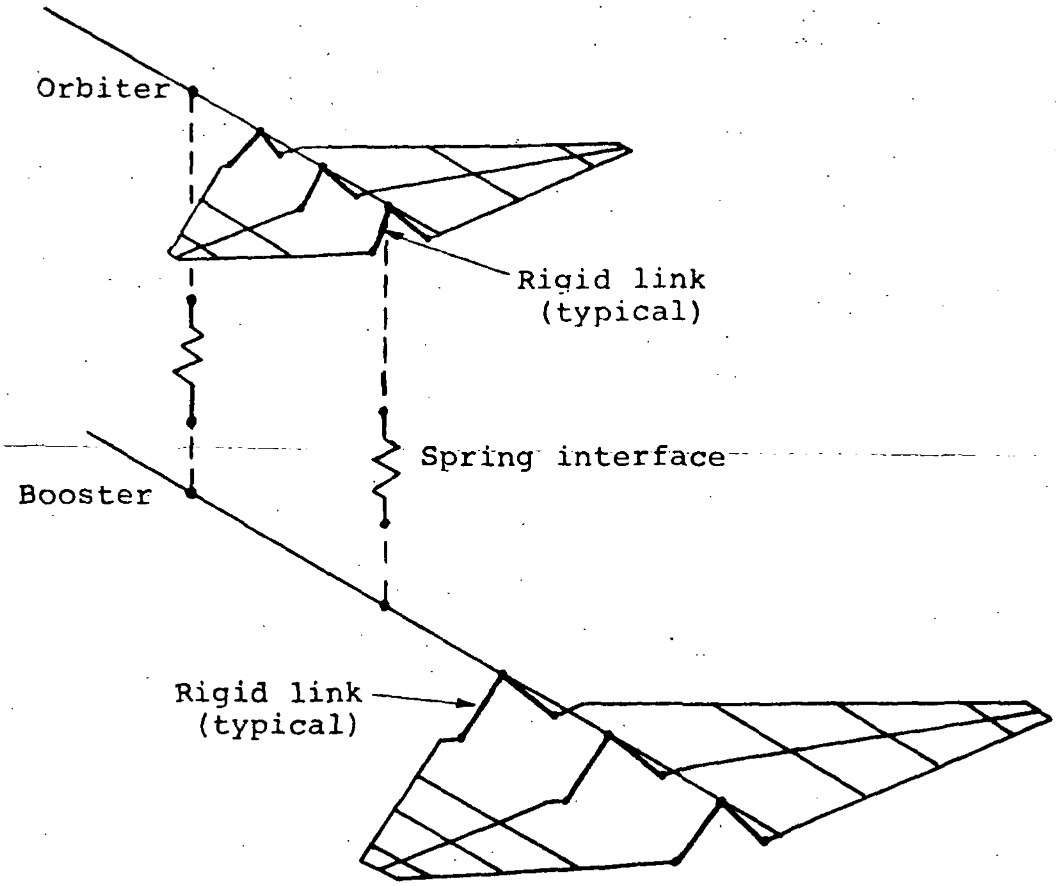

(a) Exploded view of complete model.

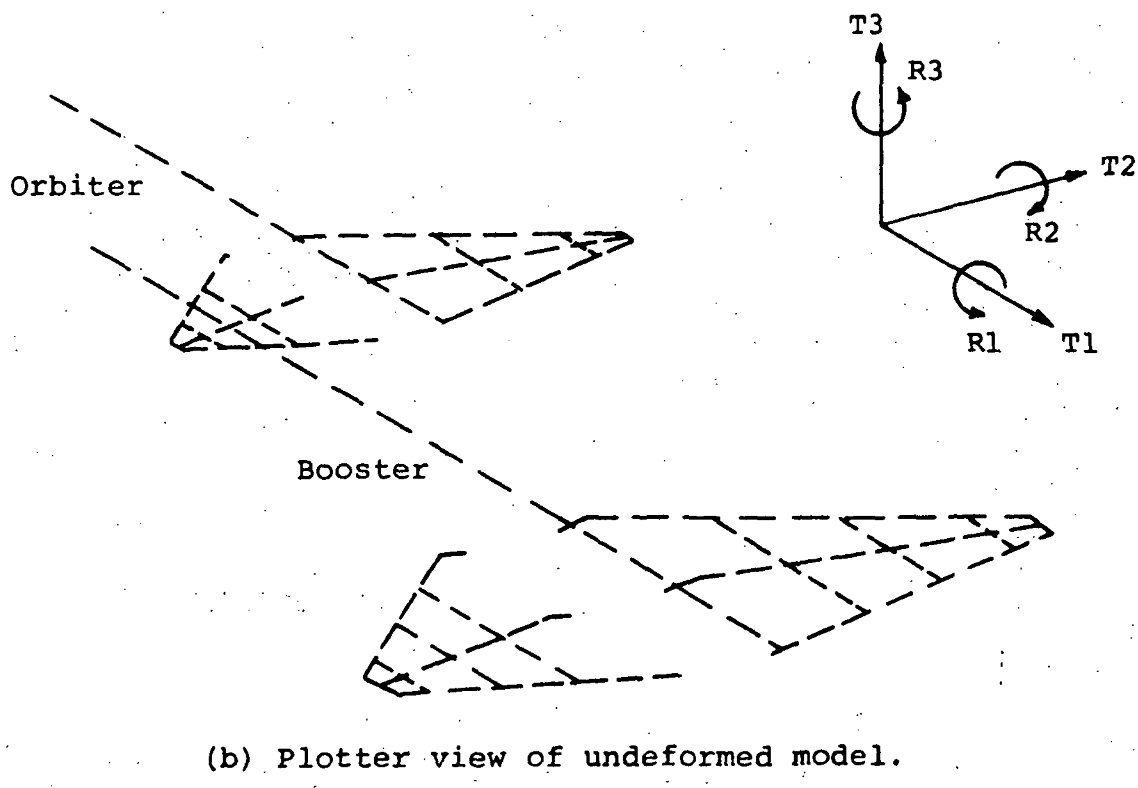

(b) Plotter view of undeformed model.

Figure 25.- Plotter orientation for complete model mode shape plots.

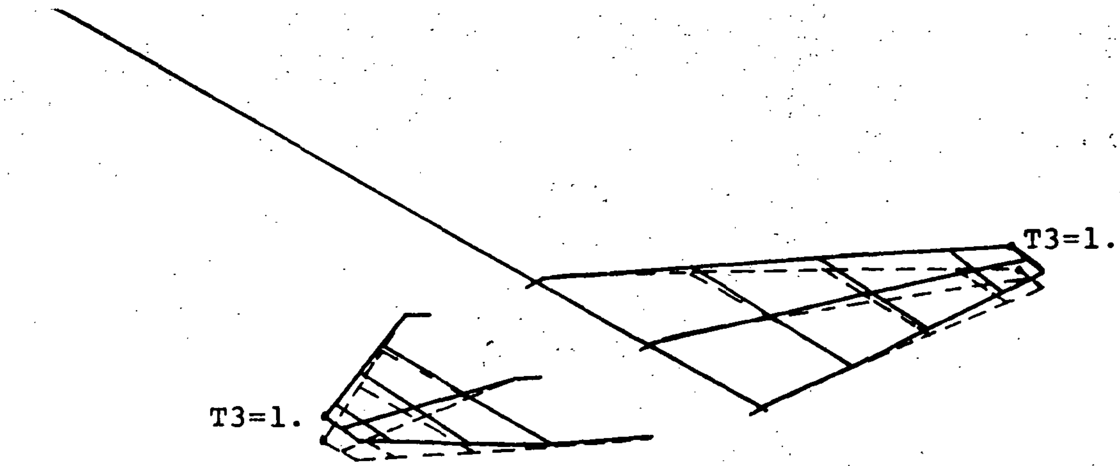

(a) Mode 1, 30.0 HZ.

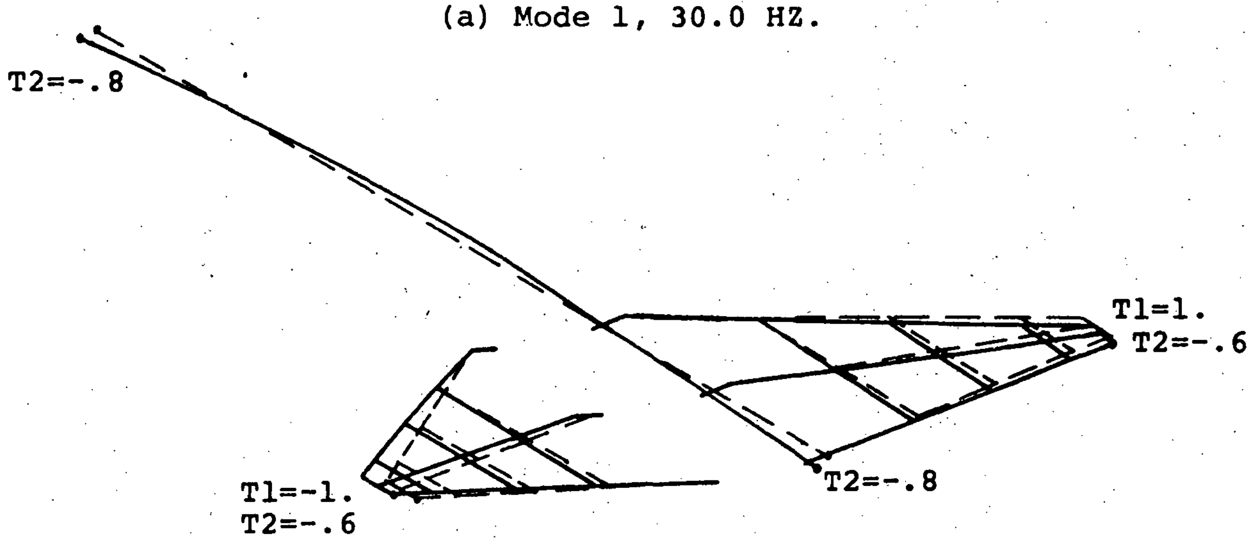

(b) Mode 2, 30.7 HZ.

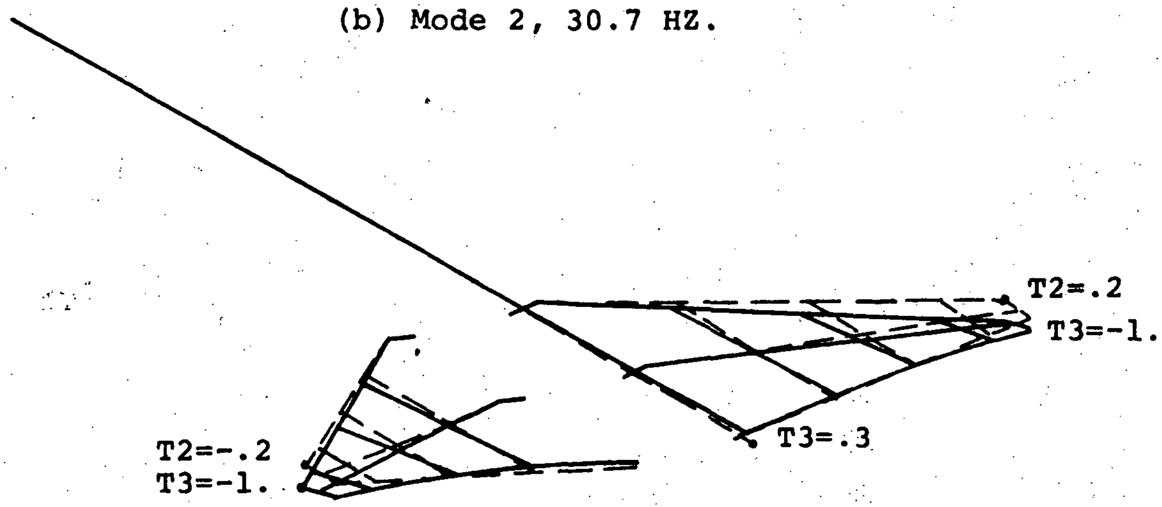

(c) Mode 3, 33.9 HZ.

Figure 26.- Mode shapes of booster airplane. Liftoff weight distribution.

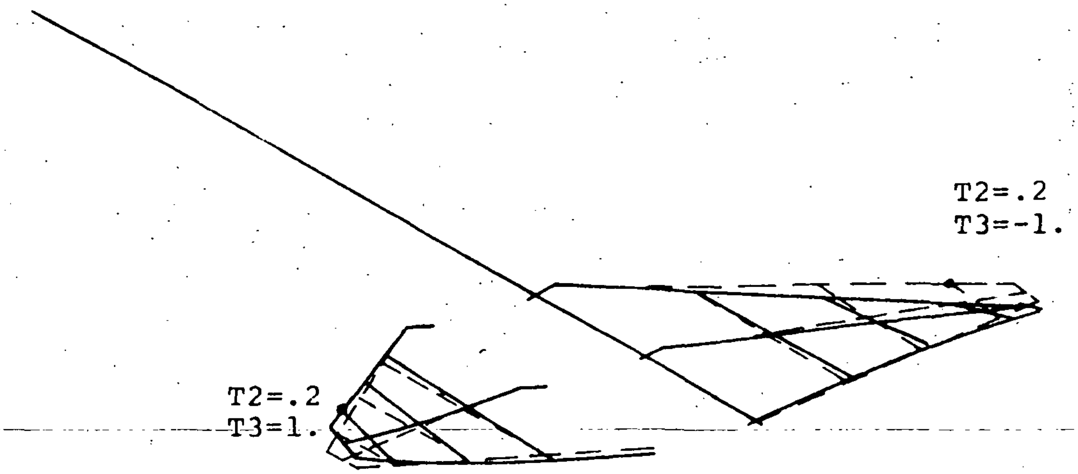

(d) Mode 4, 42.5 HZ.

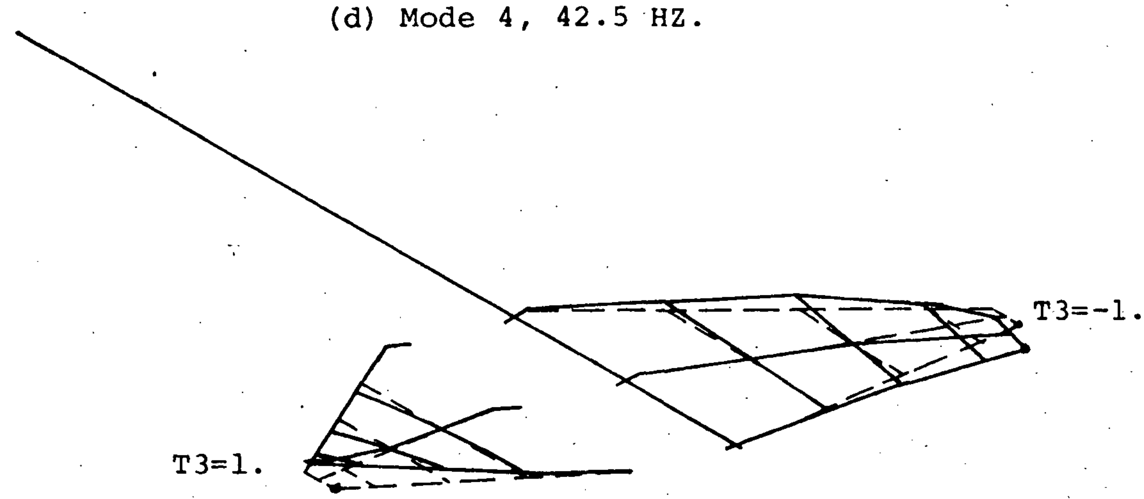

(e) Mode 5, 63.8 HZ.

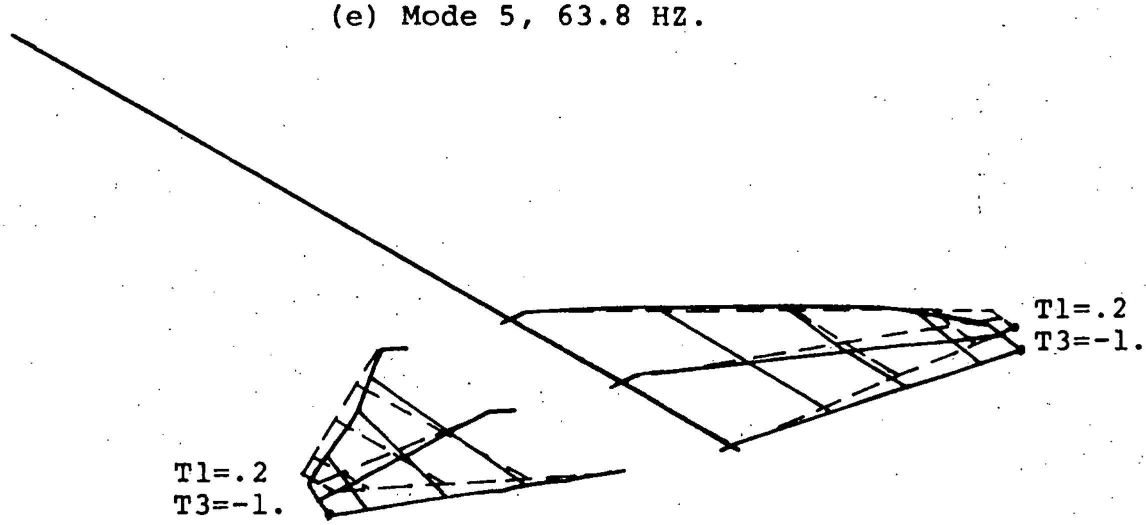

(f) Mode 6, 65.2 HZ

Figure 26 (concluded).- Mode shapes of booster airplane. Liftoff weight distribution.

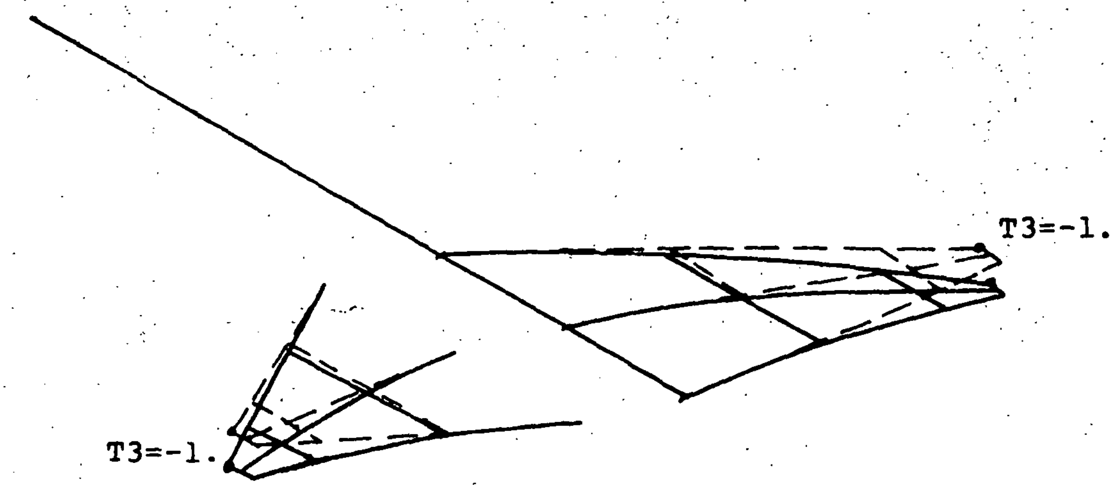

(a) Mode 1, 33.1 HZ.

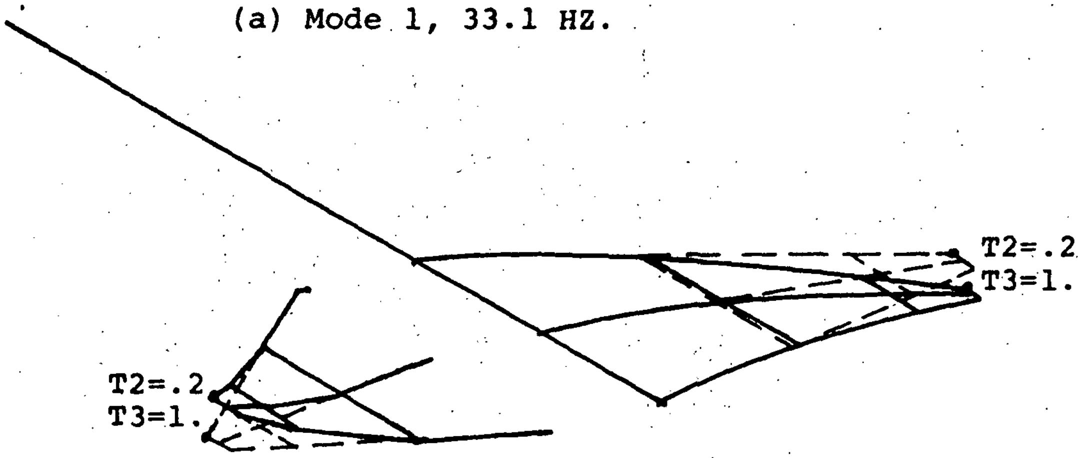

(b) Mode 2, 41.6 HZ.

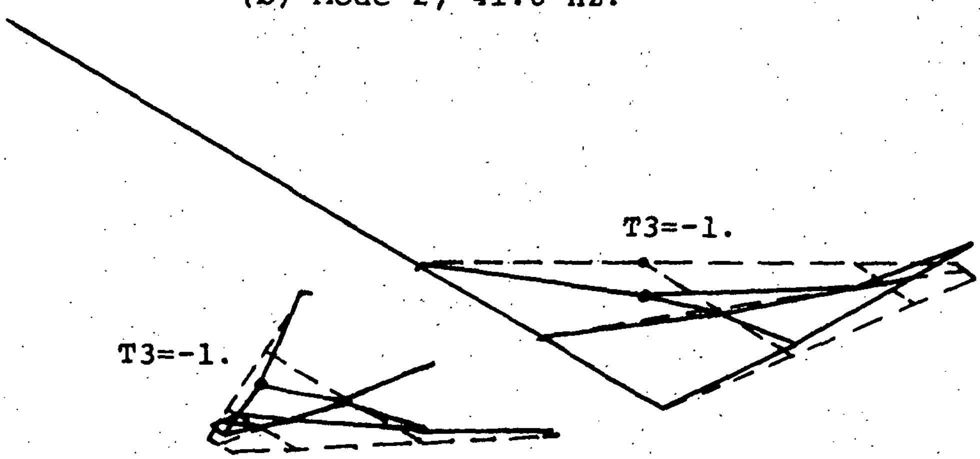

(c) Mode 3, 70.6 HZ.

Figure 27.- Mode shapes of orbiter airplane. Liftoff weight distribution.

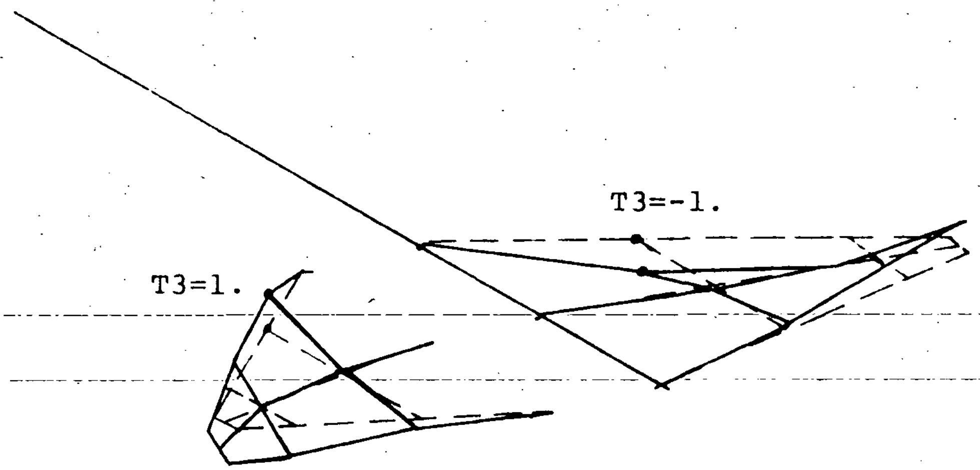

(d) Mode 4, 71.7 HZ.

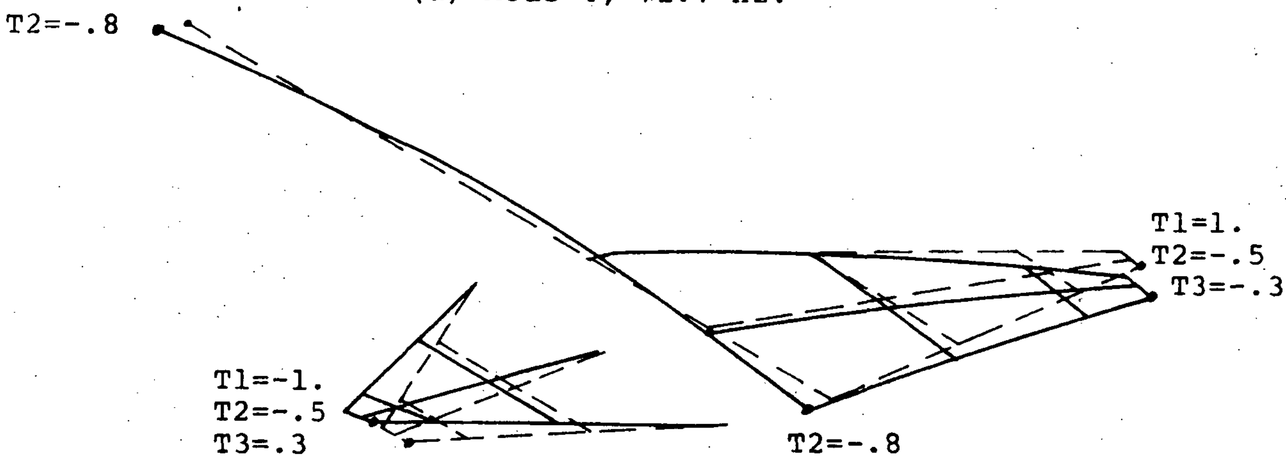

(e) Mode 5, 76.1 HZ.

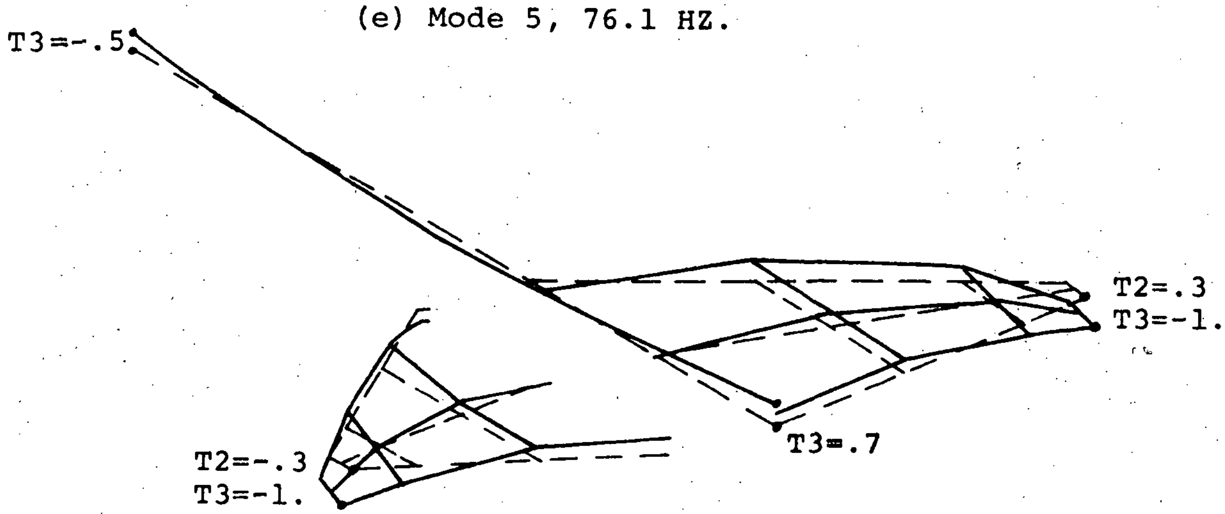

(f) Mode 6, 79.6 HZ.

Figure 27 (concluded).- Mode shapes of orbiter airplane.
Liftoff weight distribution.

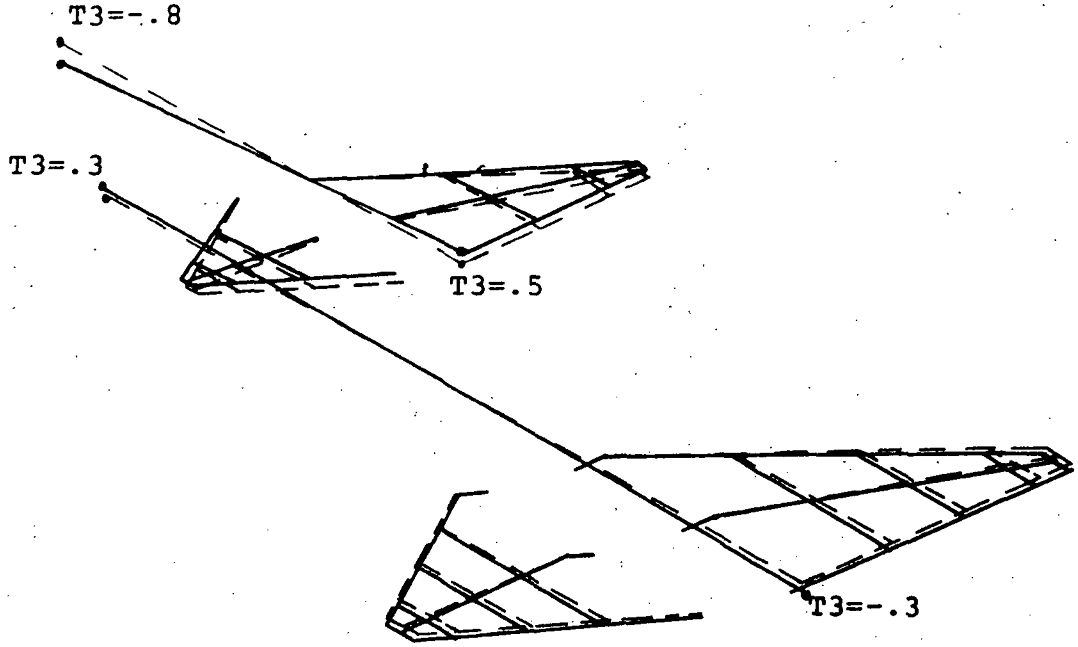

(a) Mode 1, 10.9 HZ.

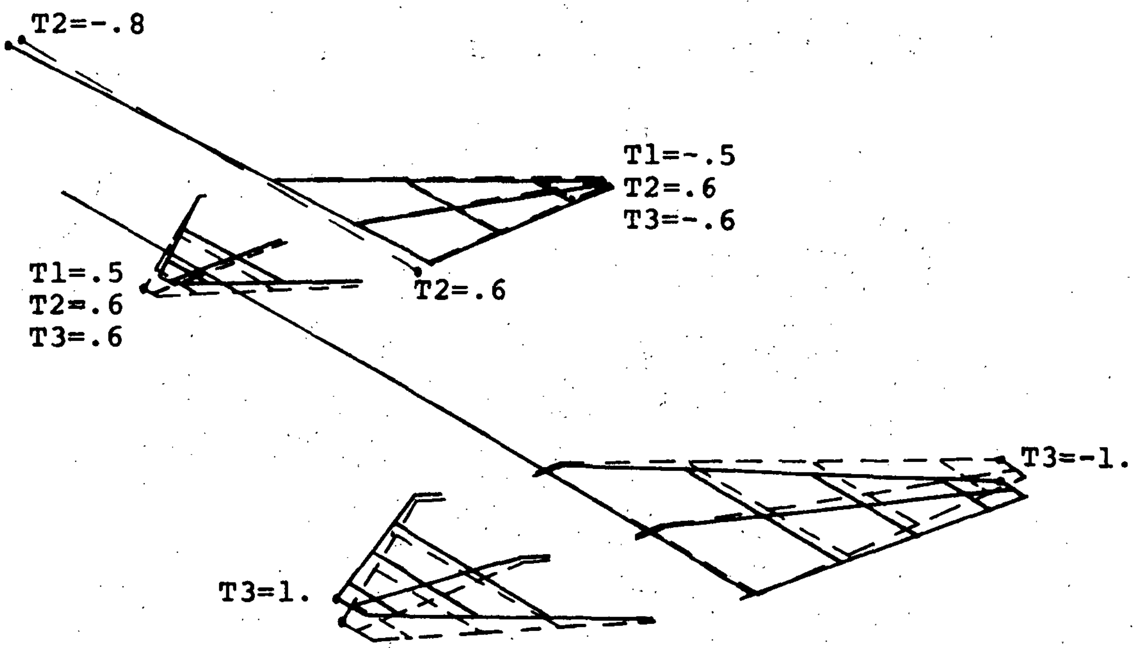

(b) Mode 2, 13.8 HZ.

Figure 28.- Mode shapes of complete model. 10^3 lb/in theoretical flexibility matrix. Liftoff weight distribution.

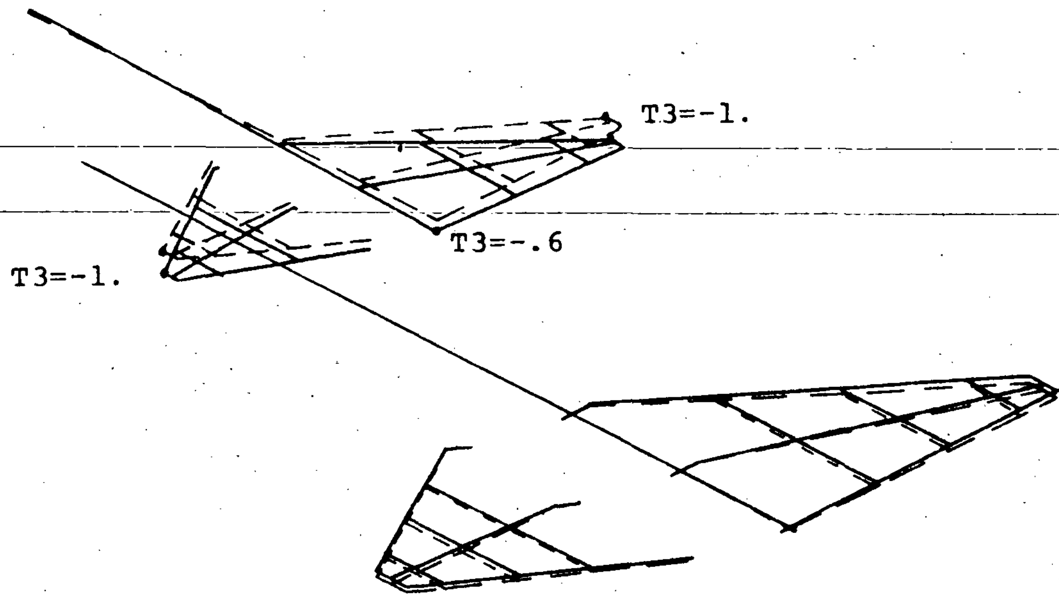

(c) Mode 3, 20.9 HZ.

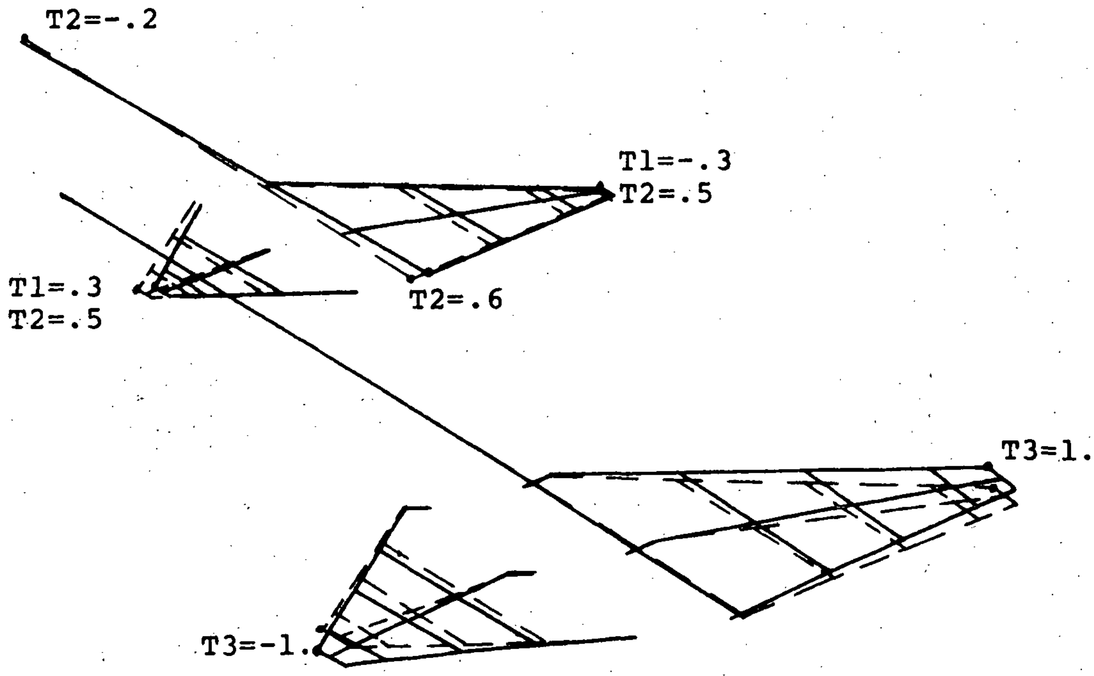

(d) Mode 4, 23.7 HZ

Figure 28 (continued).- Mode shapes of complete model. 10^3 lb/in theoretical flexibility matrix. Liftoff weight distribution.

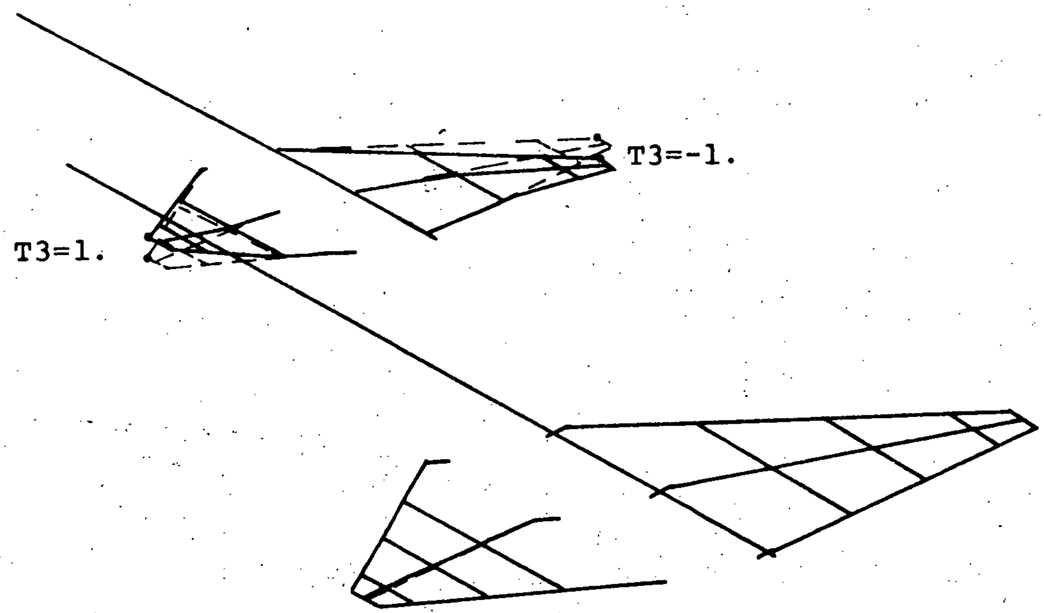

(e) Mode 5, 30.2 HZ.

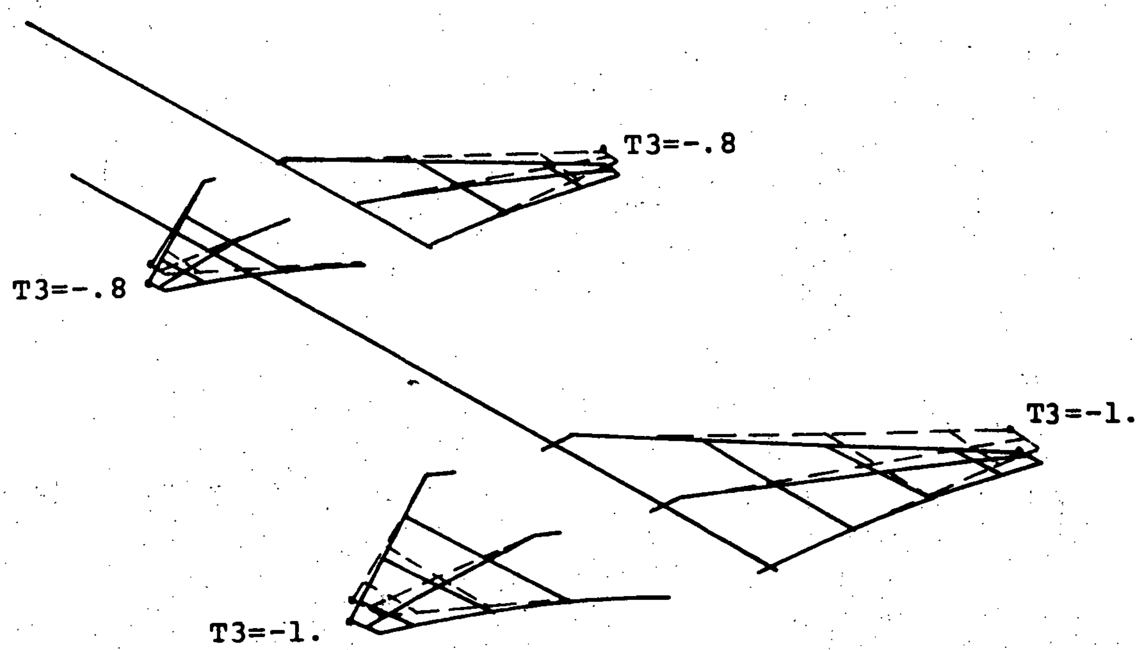

(f) Mode 6, 30.9 HZ.

Figure 28 (continued).- Mode shapes of complete model. 10^3 lb/in theoretical flexibility matrix. Liftoff weight distribution.

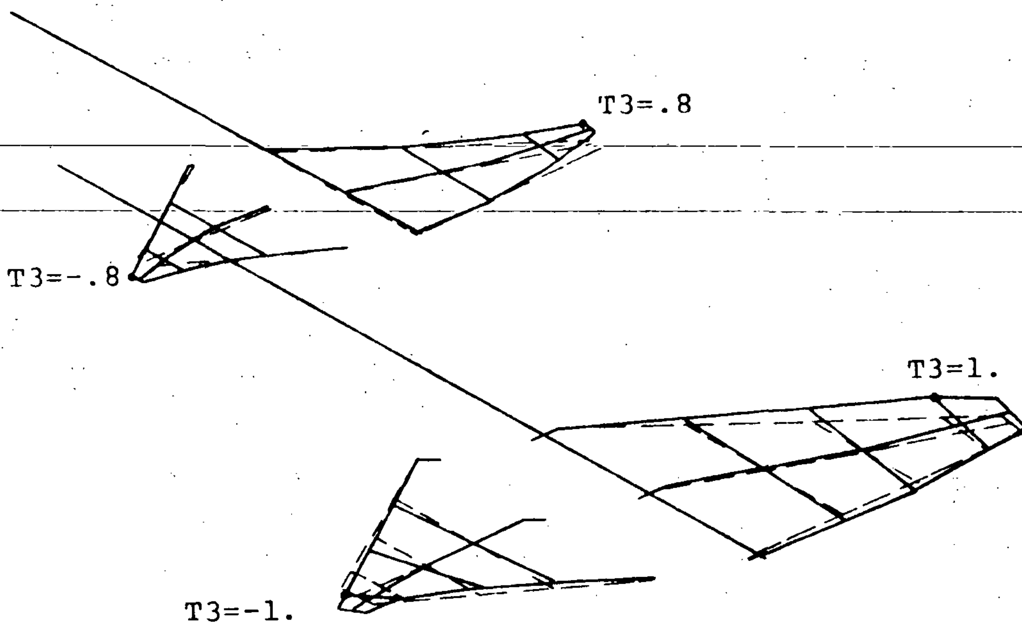

(g) Mode 10, 47.2 HZ

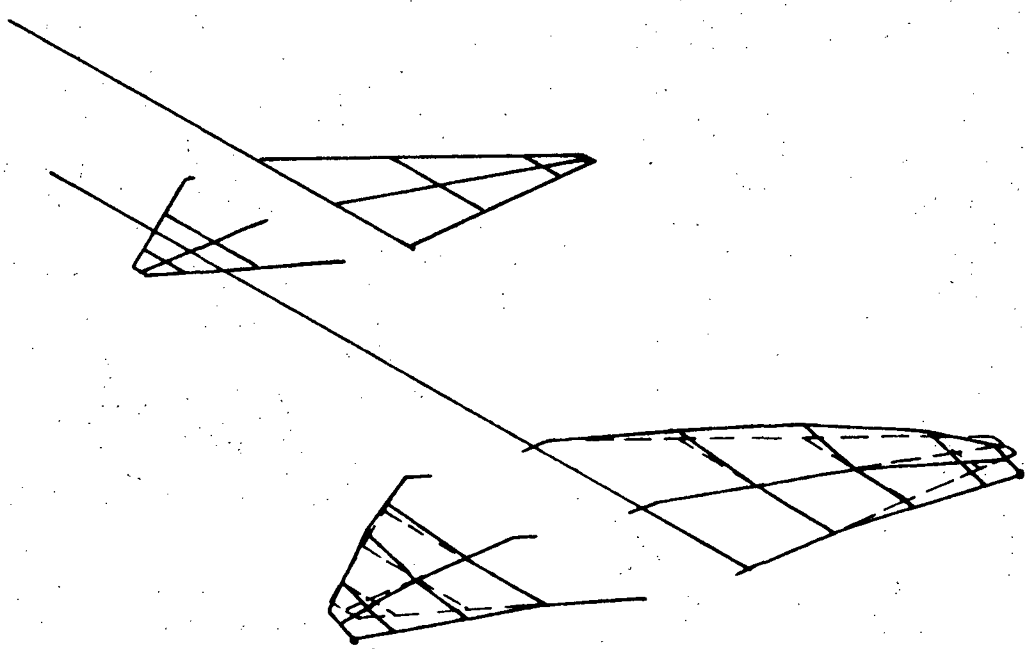

(h) Mode 13, 65.6 HZ.

Figure 28 (continued).- Mode shapes of complete model. 10^3 lb/in theoretical flexibility matrix. Liftoff weight distribution.

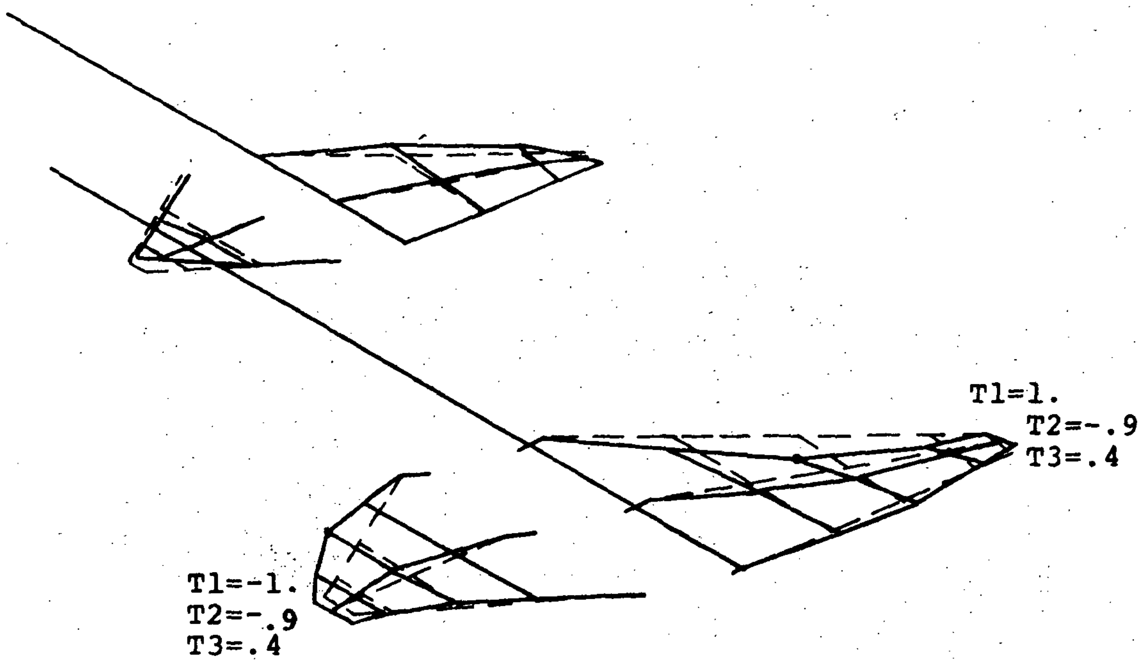

(i) Mode 14, 69.6 HZ.

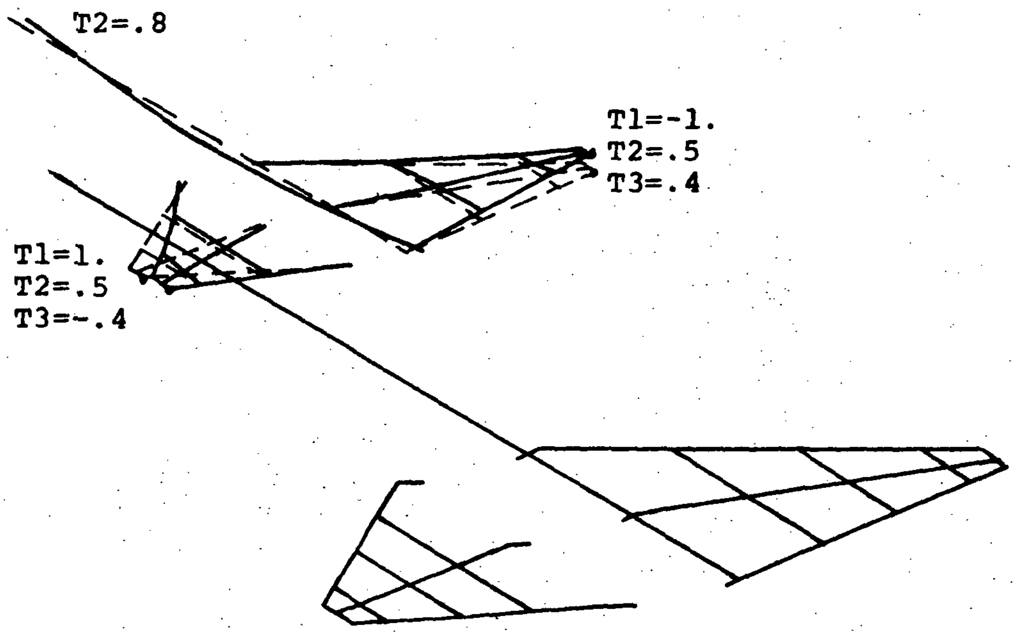

(j) Mode 18, 78.7 HZ.

Figure 28 (concluded).- Mode shapes of complete model. 10^3 lb/in theoretical flexibility matrix. Liftoff weight distribution.

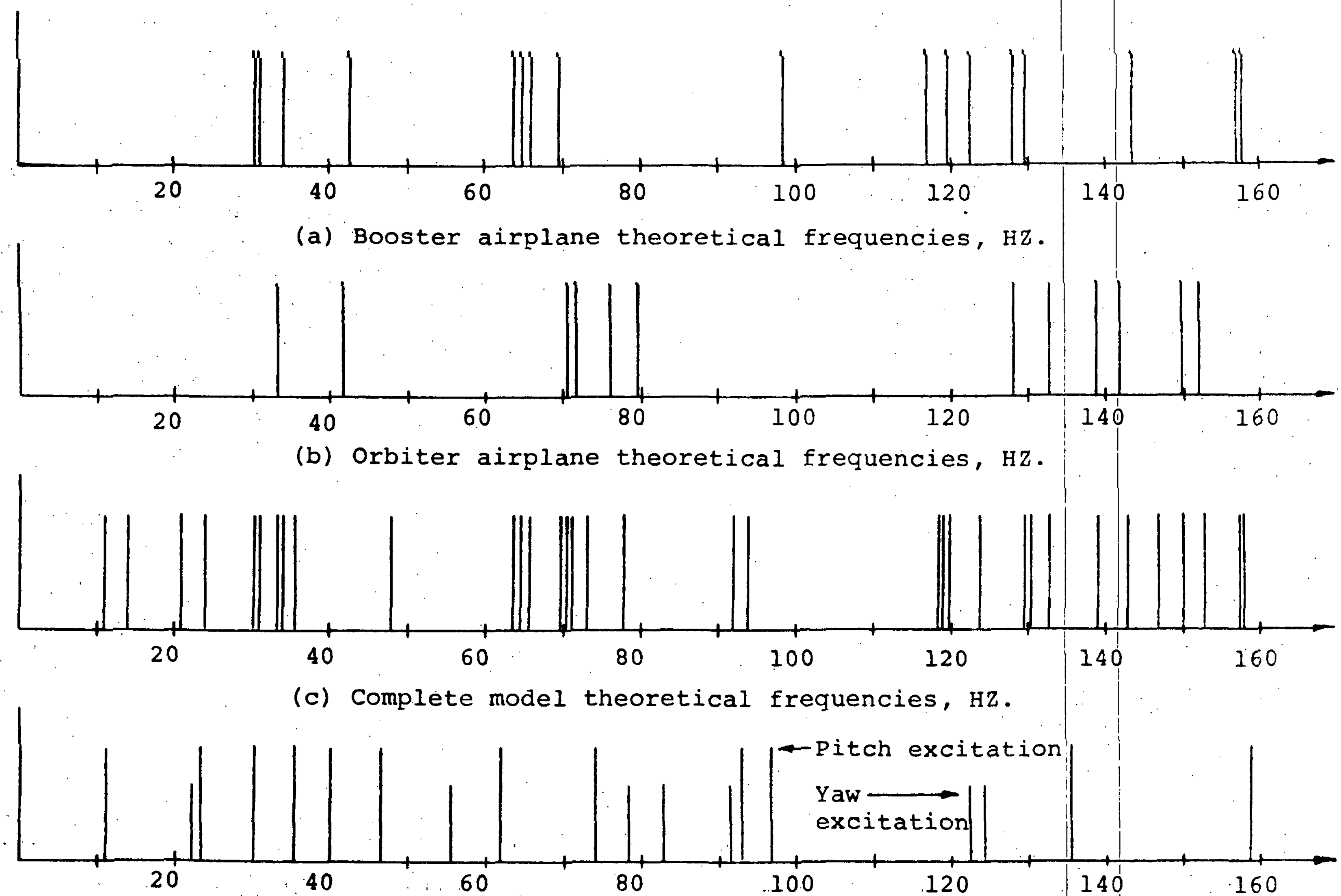

(a) Booster airplane theoretical frequencies, HZ.

(b) Orbiter airplane theoretical frequencies, HZ.

(c) Complete model theoretical frequencies, HZ.

(d) Complete model experimental frequencies, HZ.

Figure 29.- Frequency spectrums for booster and orbiter airplanes and complete model. 10 lb/in theoretical flexibility matrix. Liftoff weight distribution.

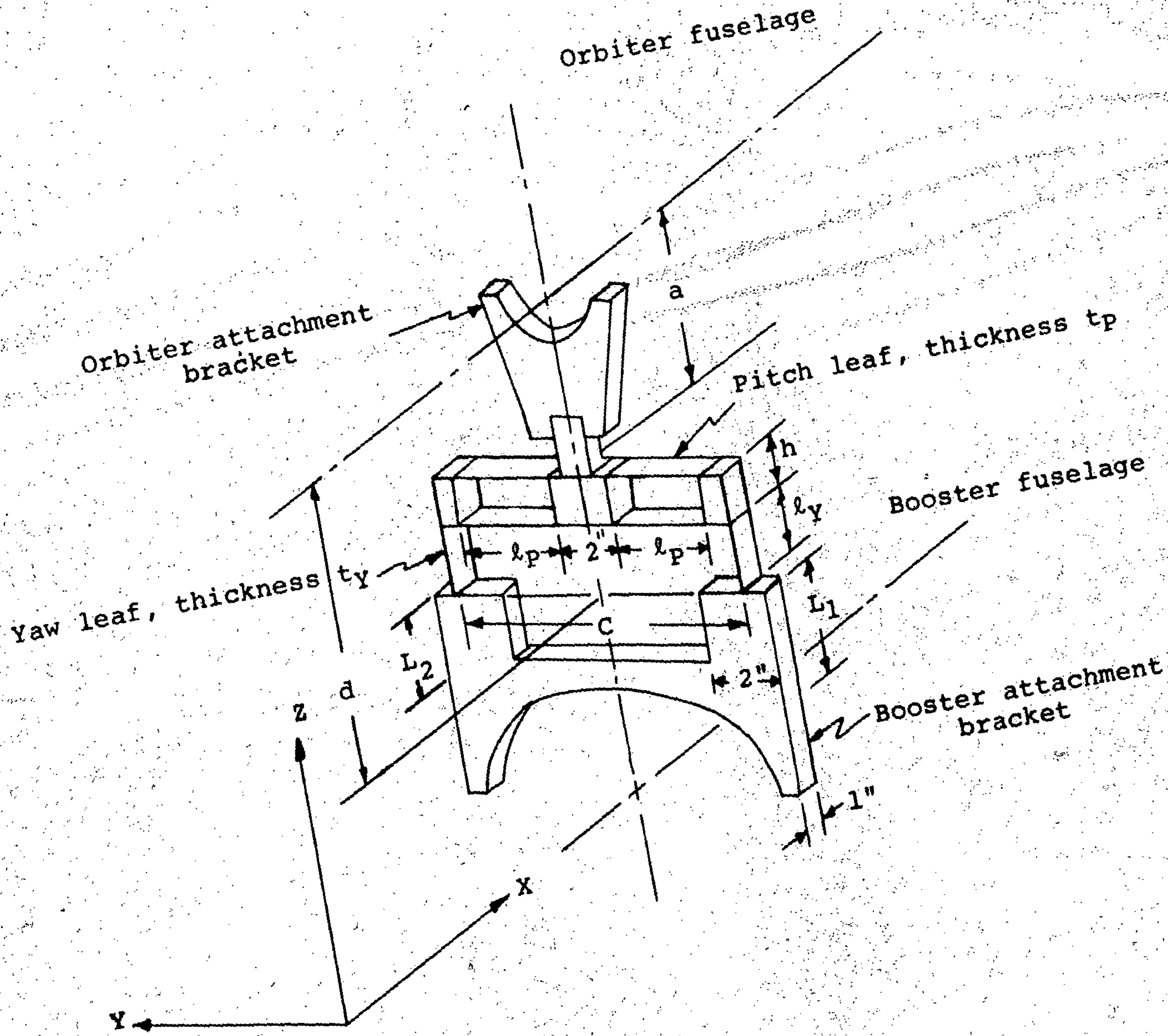

Figure A-1.- Schematic of elastic interface.

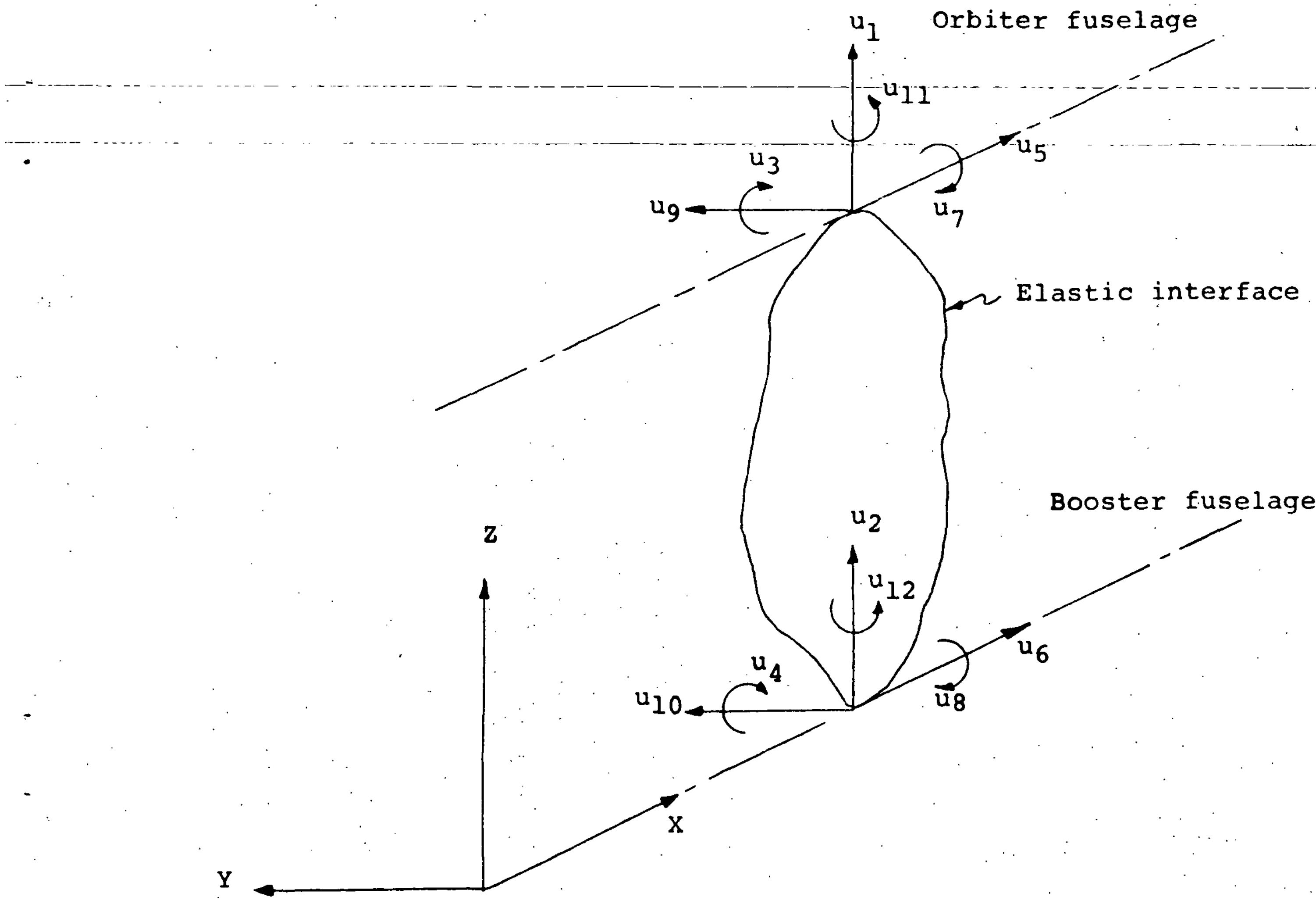

Figure A-2.- Displacement components of elastic interface.

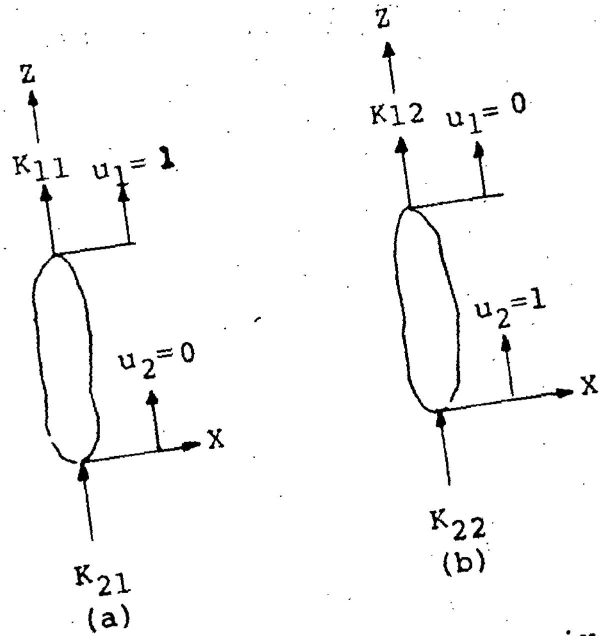

Figure A-3.- Elements of matrix $[K_Z]$.

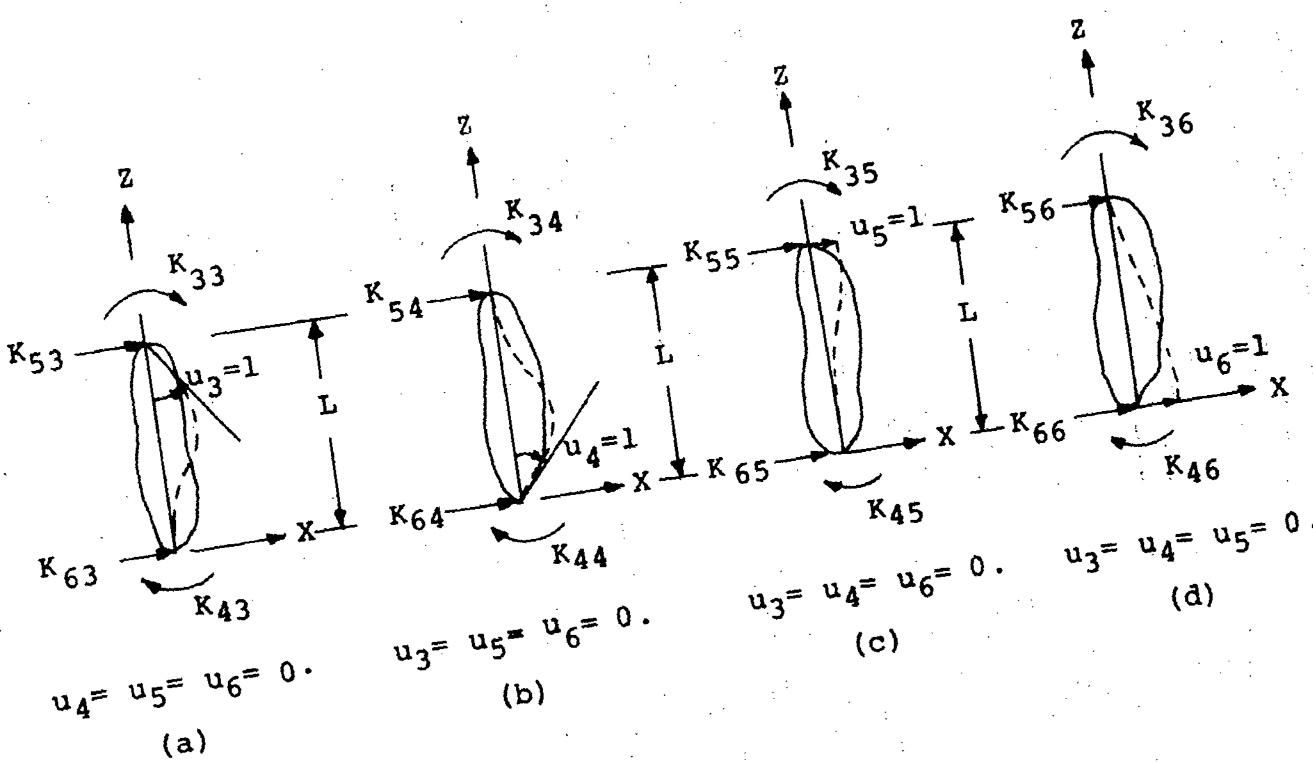

Figure A-4.- Elements of matrix $[K_{XZ}]$.

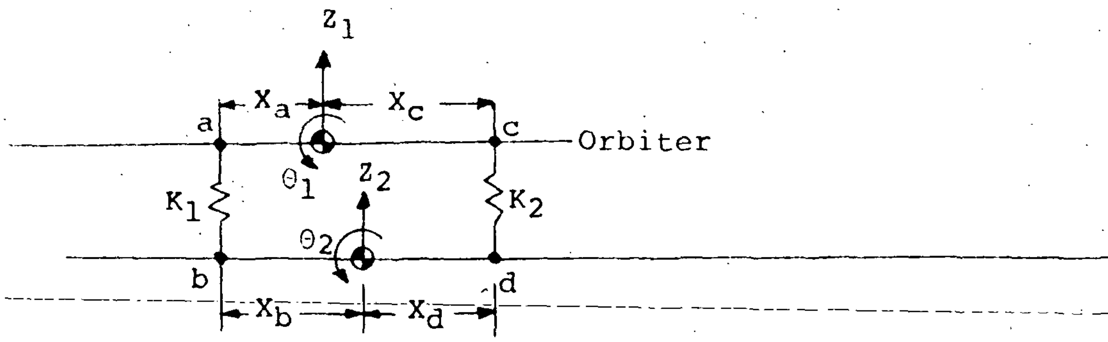

Figure B-1.- Plane motion rigid body model.

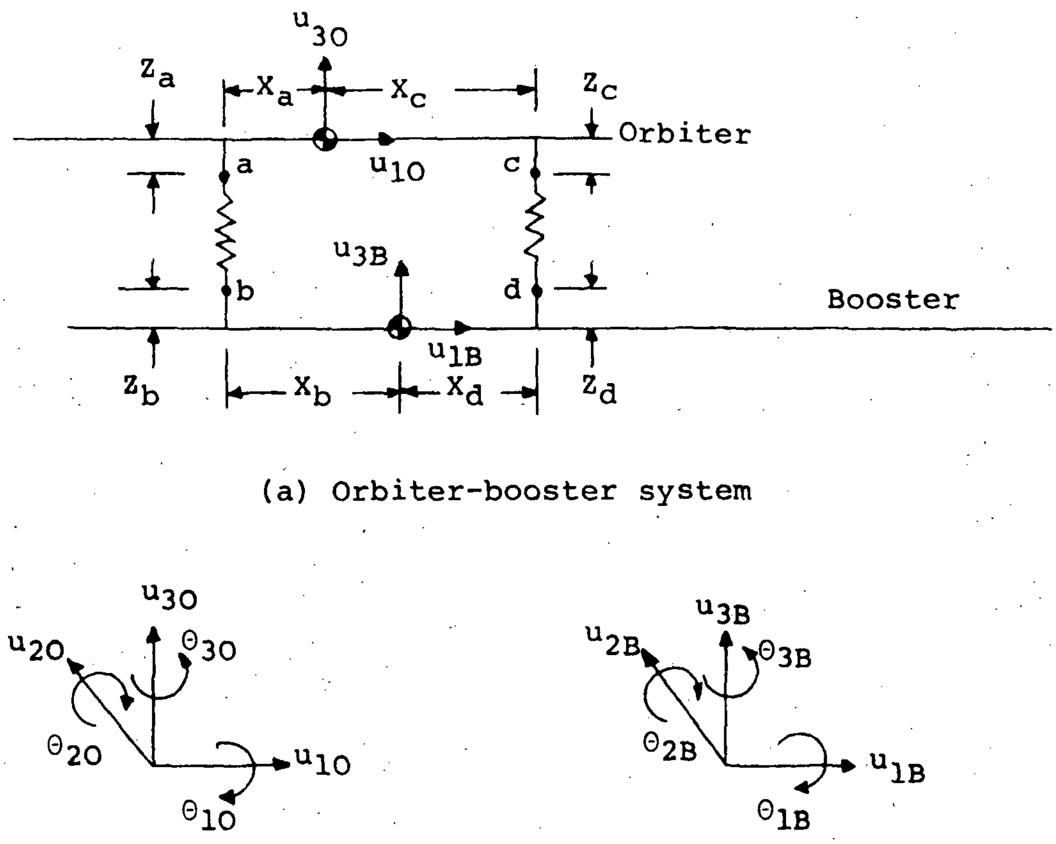

(a) Orbiter-booster system

(b) Orbiter displacement (c) Booster displacements.

Figure B-2.- General motion rigid body model.

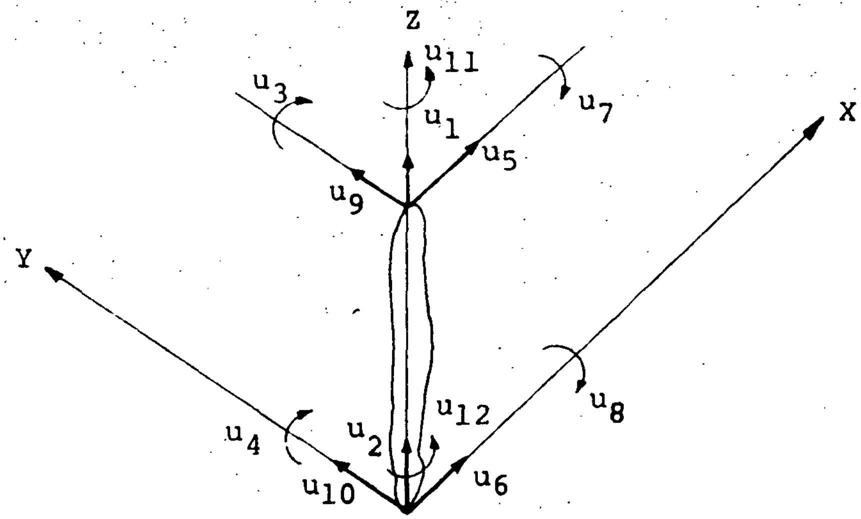

$$[K_1] = \begin{array}{c} \begin{array}{cccccccccccc} u_1 & u_2 & u_3 & \cdot & \cdot & \cdot & \cdot & \cdot & \cdot & \cdot & u_{11} & u_{12} \end{array} \\ \left[\begin{array}{c|c|c|c} K_Z & & & \\ \hline & K_{XZ} & & \\ \hline & & K_{YZ} & \\ \hline & & & K_T \end{array}\right] \end{array} \begin{array}{c} u_1 \\ u_2 \\ u_3 \\ \cdot \\ \cdot \\ \cdot \\ \cdot \\ \cdot \\ \cdot \\ \cdot \\ u_{11} \\ u_{12} \end{array}$$

Figure B-3.- Stiffness matrix in interface coordinates.

$$
\begin{array}{cc}
\begin{array}{cccccccccccc}
u_{1a} & u_{2a} & u_{3a} & \theta_{1a} & \theta_{2a} & \theta_{3a} & u_{1b} & u_{2b} & u_{3b} & \theta_{1b} & \theta_{2b} & \theta_{3b}
\end{array} & \\
\left[\begin{array}{cccccc|cccccc}
K_{33}{}^{*} & & & & K_{13} & & K_{34} & & & & K_{23} & \\
 & K'_{33}{}^{**} & & K'_{13} & & & & K'_{34} & & K'_{23} & & \\
 & & K_Z & & & & & & -K_Z & & & \\
 & K'_{13} & & K'_{11} & & & & K'_{14} & & K'_{12} & & \\
K_{13} & & & & K_{11} & & K_{14} & & & & K_{12} & \\
 & & & & & K_T & & & & & & -K_T \\
\hline
K_{34} & & & & K_{14} & & K_{44} & & & & K_{24} & \\
 & K'_{34} & & K'_{14} & & & & K'_{44} & & K'_{24} & & \\
 & & -K_Z & & & & & & K_Z & & & \\
 & K'_{23} & & K'_{12} & & & & K'_{24} & & K'_{22} & & \\
K_{23} & & & & K_{12} & & K_{24} & & & & K_{22} & \\
 & & & & & -K_T & & & & & & K_T
\end{array}\right] &
\begin{array}{c}
u_{1a} \\ u_{2a} \\ u_{3a} \\ \theta_{1a} \\ \theta_{2a} \\ \theta_{3a} \\ u_{1b} \\ u_{2b} \\ u_{3b} \\ \theta_{1b} \\ \theta_{2b} \\ \theta_{3b}
\end{array}
\end{array}
$$

*K_{ij} denotes an element of $[K_{XZ}]$.

**K'_{ij} denotes an element of $[K_{YZ}]$.

Figure B-4.- Stiffness matrix $[K_1]$ in attachment coordinates.

$$K_{1,1} = K_{33}$$
$$K_{1,4} = K_{13} - Z_a K_{33}$$
$$K_{1,1} = K_{34}$$
$$K_{1,11} = K_{23} + Z_b K_{34}$$
$$K_{2,2} = K'_{33}$$
$$K_{2,4} = K'_{13} + Z_a K'_{33}$$
$$K_{2,6} = -X_a K'_{33}$$
$$K_{2,8} = K_{34}$$
$$K_{2,10} = K'_{23} - Z_b K'_{34}$$
$$K_{2,12} = -X_b K'_{34}$$
$$K_{3,3} = K_A$$
$$K_{3,5} = X_a K_A$$
$$K_{3,9} = -K_A$$
$$K_{3,11} = -X_b K_A$$
$$K_{4,4} = Z_a^2 K'_{33} + 2Z_a K'_{13} + K'_{11}$$
$$K_{4,6} = -X_a Z_a K'_{33} - X_a K'_{13}$$
$$K_{4,8} = K'_{14} + Z_a K'_{13}$$
$$K_{4,10} = Z_a K'_{23} - Z_a Z_b K'_{34} + K'_{12} - Z_b K'_{14}$$

Figure B-5.- Elements of $[K_1]$ in generalized coordinates

$K_{4,12} = -Z_a X_b K'_{34} - X_b K'_{14}$

$K_{5,5} = Z_a^2 K_{33} + X_a^2 K_Z - 2Z_a K_{13} + K_{11}$

$K_{5,7} = K_{14} - Z_a K_{34}$

$K_{5,9} = -X_a K_Z$

$K_{5,11} = -Z_a K_{23} - Z_a Z_b K_{34} - X_a X_b K_Z + K_{12} + Z_b K_{14}$

$K_{6,6} = X_a^2 K'_{33} + K_T$

$K_{6,8} = -X_a K'_{34}$

$K_{6,10} = -X_a K'_{23} + X_a Z_b K'_{34}$

$K_{6,12} = X_a X_b K'_{34} - K_T$

$K_{7,7} = K_{44}$

$K_{7,11} = K_{24} + Z_b K_{44}$

$K_{8,8} = K'_{44}$

$K_{8,10} = K'_{24} - Z_b K'_{44}$

$K_{8,12} = -X_b K'_{44}$

$K_{9,9} = K_Z$

$K_{10,10} = Z_b^2 K'_{44} - 2Z_b K'_{24} + K'_{22}$

$K_{10,12} = X_b Z_b K'_{44} - X_b K'_{24}$

$K_{11,11} = 2Z_b K_{24} + X_b^2 K_Z + K_{22} + Z_b^2 K_{44}$

$K_{12,12} = X_b^2 K_{44} + K_T$

Figure B-5 (continued).- Elements of $[K_1]$ in generalized coordinates

TABLE I
Booster and orbiter simulated propellant weights

(a) Booster add-on weights
(Pounds)

Weight No. (See Figure 2)	Liftoff	Max Q	Burnout
1	138.7	138.7	0
2	22.4	22.4	0
3	80.6	0	0
4	13.9	0	0

(b) Orbiter add-on weights
(Pounds)

Position	Liftoff	Empty
Forward	60.4	0
Aft	9.9	0

Table II
Booster fuselage
Element properties

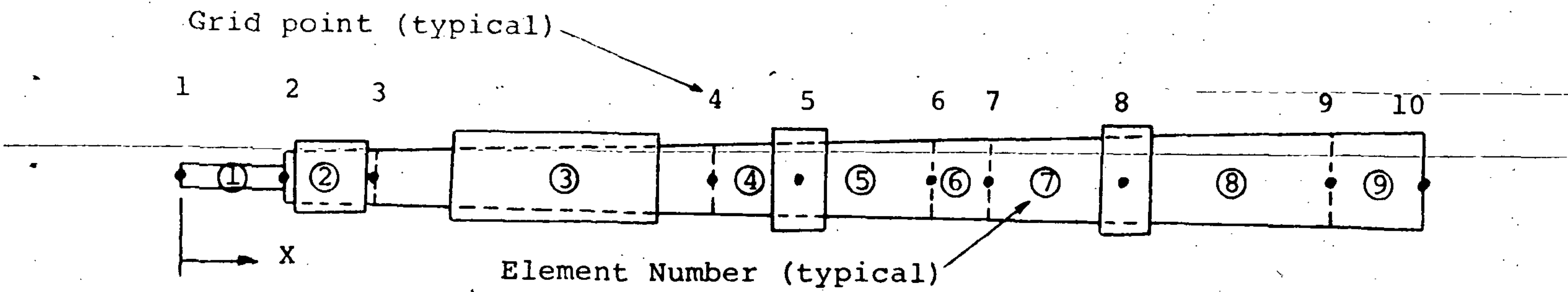

	Cross Section Properties			NSM ($lb\text{-}sec^2/in/in$)	
Element	$A(in^2)$	$I(in^4)$	$J(in^4)$	Liftoff	Max Q
1	1.305	0.7882	1.576	0	0
2	1.261	3.964	7.928	2.243-2*	0
3	1.707	9.843	19.69	0.965-2	0.965-2
4	2.072	17.61	35.22	0	0
5	2.092	18.21	36.42	0	0
6	2.113	18.77	37.54	0	0
7	2.203	21.27	42.54	0	0
8	2.416	28.04	56.08	0	0
9	2.602	35.04	70.08	0	0

*The notation 2.243-2 represents 2.243×10^{-2}.

Table III

Booster fuselage

Concentrated mass properties

Liftoff

		Nominal Values		Test Values	
Grid Point	Station x(in)	M lb-sec^2/in	I_{xx} in-lb-sec^2	M lb-sec^2/in	I_{xx} in-lb-sec^2
1	0.0	0.233-3	0.0023	0.233-3	0.0023
2	11.0	0.207-2	1.366	0.207-2	1.47
3	20.3	0.184-2	4.937	0.174-1	4.28
4	57.5	0.298-2	3.636	0.139-1	2.86
5	66.0	0.360-1	0.906	0.360-1	0.83
6	80.97	0.362-2	0.135	0.362-2	0.135
7	87.0	0.373-2	0.148	0.373-2	0.148
8	101.7	0.580-1	1.734	0.580-1	1.69
9	124.2	0.455-2	0.325	0.455-2	0.325
10	134.8	0.142-1	0.345	0.246-1	0.345

		Nominal			
		Max Q		Burnout	
Grid Point	Station x(in)	M lb-sec^2/in	I_{xx} in-lb-sec^2	M lb-sec^2/in	I_{xx} in-lb-sec^2
1	0	0.233-3	0.0023	0.233-3	0.0023
2	11.0	0.207-2	0.0172	0.207-2	0.0172
3	20.3	0.184-2	3.588	0.184-2	0.110
4	57.5	0.298-2	3.636	0.298-2	0.158
5	66.0	0	0.107	0	0.107
6	80.97	0.362-2	0.135	0.362-2	0.135
7	87.0	0.373-2	0.148	0.373-2	0.148
8	101.7	0.580-1	1.734	0	0.240
9	124.2	0.455-2	0.325	0.455-2	0.325
10	134.3	0.142-1	0.345	0.142-;	0.345

Table IV
Orbiter fuselage
Element properties

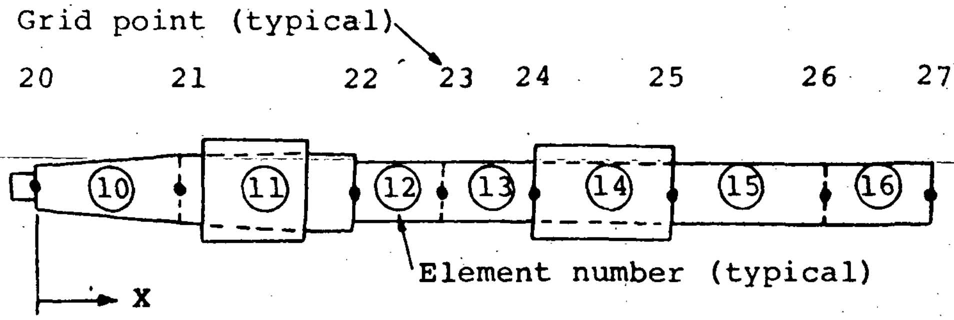

Element	Cross section properties A(in^2)	I(in^4)	J(in^4)	NSM ($lb\text{-}sec^2/in/in$) Liftoff	Empty
10	1.169	3.160	6.32	0	0
11	1.458	6.138	12.28	1.042-2	0
12	1.272	4.072	8.14	0	0
13	1.272	4.072	8.14	0	0
14	1.272	4.072	8.14	0.214-2	0
15	1.272	4.072	8.14	0	0
16	1.272	4.072	8.14	0	0

Table V
Orbiter Fuselage
Concentrated Mass Properties

Grid Point	x (inches)	Liftoff				Empty	
		Nominal Values		Test Values		Nominal Values	
		M $lb\text{-}sec^2/in$	I_{xx} $in\text{-}lb\text{-}sec^2$	M $lb\text{-}sec^2/in$	I_{xx} $in\text{-}lb\text{-}sec^2$	M $lb\text{-}sec^2/in$	I_{xx} $in\text{-}lb\text{-}sec^2$
20	0	1.345-2	0.0152	1.345-2	0.0152	1.345-2	0.0152
21	12.0	0.197-2	1.700	0.197-2	1.290	0.197-2	1.700
22	27.0	0.295-2	1.707	1.855-2	1.298	0.295-2	1.707
23	32.84	0.166-2	0.0408	0.166-2	0.0408	0.166-2	0.0408
24	40.5	0	0.144	0	0.128	0	0.144
25	52.5	0	0.144	0	0.128	0	0.144
26	65.2	0.166-2	0.0563	1.266-2	0.0563	0.166-2	0.0563
27	76.0	0.124-2	0.0150	0.124-2	0.0150	0.124-2	0.0150

Table VI
Booster wing grid point coordinates

Coordinate System 1

Grid Point	X_1 (inches)	Y_1 (inches)	Z_1 (inches)
1	41.33	0	0
2	20.66	0	0
3	0	0	0
4	41.33	-9.42	1.62
5	20.66	-9.42	1.62
6	0	-9.42	1.62
7	41.33	9.42	1.62
8	20.66	9.42	1.62
9	0	9.42	1.62
34*	41.33	-5.82	1.00
35*	20.66	-5.82	1.00
36*	0	-5.82	1.00
37*	41.33	5.82	1.00
38*	20.66	5.82	1.00
39*	0	5.82	1.00

*Grid points 34-39 were used only for attaching the wing to the fuselage.

Coordinate System 2

Grid Point	X_2 (inches)	Y_2 (inches)	Z_2 (inches)
10	10.0	41.33	0
11	10.0	25.82	0
12	10.0	10.31	0
16	20.0	41.33	0
17	20.0	30.97	0
18	20.0	20.62	0
22	30.0	41.33	0
23	30.0	36.13	0
24	30.0	30.94	0
28	35.0	41.33	0
29	35.0	38.71	0
30	35.0	36.10	0

Table VI continued

Coordinate System 3

Grid Point	X_3 (inches)	Y_3 (inches)	Z_3 (inches)
13	41.33	10.0	0
14	25.82	10.0	0
15	10.31	10.0	0
19	41.33	20.0	0
20	30.97	20.0	0
21	20.62	20.0	0
25	41.33	30.0	0
26	36.73	30.0	0
27	30.94	30.0	0
31	41.33	35.0	0
32	38.71	35.0	0
33	36.10	35.0	0

Table VII
Booster wing element properties

Element	A in^2	I1 in^4	I2 in^4	J in^4	I12 in^4
1,11,24,10,20,33	0.307	0.596-2	0.129-1	0.106-1	0
2,12,25,9,19,32	0.419	0.299-1	0.169-1	0.119-1	0
3,13,26,8,18,31	0.559	0.118	0.200-1	0.136-1	0
4,14,27,7,17,30	0.695	0.299	0.219-1	0.152-1	0
40,41	0.714-1	0.281-3	0.720-2	0.900-4	-0.895-3
50,51	0.714-1	0.396-2	0.720-2	0.900-4	+0.895-3
42,43	0.936-1	0.296-2	0.980-2	0.111-3	-0.308-2
52,53	0.936-1	0.296-2	0.980-2	0.111-3	+0.308-2
44,45	0.116	0.114-1	0.114-1	0.139-3	-0.622-2
54,55	0.116	0.114-1	0.114-1	0.139-3	+0.622-2
5,15,28,6,16,29	1.33	0.857	0.143	0.320-1	0
35,36,37,38	0.25	0.130-2	0.208-1	0.833-1	0

Table VIII
Orbiter wing grid point coordinates

Grid point	X (inches)	Y (inches)	Z (inches)
1	28.36	0	0
2	14.36	0	0
3	0	0	0
4	28.36	4.928	0.8468
5	14.36	4.928	0.8468
6	0	4.928	0.8468
7	28.36	-4.928	0.8468
8	14.36	-4.928	0.8468
9	0	-4.928	0.8468
10	28.36	14.78	2.540
11	19.34	14.78	2.540
12	10.31	14.78	2.540
13	28.36	-14.78	2.540
14	19.34	-14.78	2.540
15	10.31	-14.78	2.540
16	28.36	24.64	4.234
17	24.49	24.64	4.234
18	20.63	24.64	4.234
19	28.36	-24.64	4.234
20	24.49	-24.64	4.234
21	20.63	-24.64	4.234
22	28.36	29.57	5.081
23	27.08	29.57	5.081
24	25.78	29.57	5.081
25	28.36	-29.57	5.081
26	27.08	-29.57	5.081
27	25.78	-29.57	5.081
44*	28.36	-3.94	0.676
45*	14.18	-3.94	0.676
46*	0	-3.94	0.676
47*	28.36	3.94	0.676
48*	14.18	3.94	0.676
49*	0	3.94	0.676

*Grid points 44-49 were used only for attaching wing to the fuselage.

Table IX Orbiter wing element properties

Element	A	I1	I2	J	I12
	in^2	in^4	in^4	in^4	in^4
4,12,20,5,13,21	0.563	0.167	0.160	0.293-2	0
3,11,19,6,14,22	0.302	0.301-1	0.998-2	0.352-2	0
2,10,18,7,15,23	0.205	0.335-2	0.751-2	0.302-2	0
1,9,17,8,16,24	0.156	0.814-3	0.509-2	0.326-2	0
25,26,27,28	0.125	0.651-3	0.260-2	0.260-2	0
29,30,31,32	0.864-1	0.159-2	0.848-2	0.109-3	-0.618-3
33,34,35,36	0.864-1	0.159-2	0.848-2	0.109-3	-0.618-3

Table X
Theoretical and Experimental Flexibility
Matrices for elastic interface.

Nominal 10^3 Case

Eq. (AI-1)	NASTRAN	Z_{ij}*	
		Theoretical	Experimental
a_{55}	Z_{11}	0.1041-2	0.1035-2
a_{53}	Z_{15}	0.1344-3	0.1324-3
a_{99}	Z_{22}	0.1055-2	0.1215-2
a_{97}	Z_{24}	-0.0775-4	-0.216-4
$a_{11} = a_z$	Z_{33}	0.9962-3	0.976-3
a_{77}	Z_{44}	0.1112-5	0.233-5
a_{33}	Z_{55}	0.1814-4	0.1807-4
a_T	Z_{66}	0.5263-5	0.721-5

*$Z_{ij} = Z_{ji}$; all other elements are zero.

Table XI Resequencing of grid points for complete model.

SEQGP[a]	ID[b]	SEQID[c]	ID	SEQID	ID	SEQID	ID	SEQID	
. 1 ..	2 ..	3 ..	4 ..	5 ..	6 ..	7 ..	8 ..	9 ..	10 .
SEQGP	1	43	2	44	3	46	4	45	
SEQGP	5	42	6	37	7	38	8	39	
SEQGP	9	40	10	41	20	47	21	48	
SEQGP	22	49	23	52	24	54	25	53	
SEQGP	26	50	27	51	34	36	35	34	
SEQGP	36	32	37	35	38	33	39	31	
SEQGP	44	55	45	57	46	59	47	56	
SEQGP	48	58	49	60	400	30	500	28	
SEQGP	401	62	501	64	601	66	701	61	
SEQGP	600	26	700	29	800	27	900	25	
SEQGP	801	63	901	65	1001	68	1101	70	
SEQGP	1000	24	1100	22	1200	20	1300	23	
SEQGP	1201	72	1301	67	1401	69	1501	71	
SEQGP	1400	21	1500	19	1600	18	1700	16	
SEQGP	1601	74	1701	76	1801	78	1901	73	
SEQGP	1800	14	1900	17	2000	15	2100	13	
SEQGP	2001	75	2101	77	2201	80	2301	82	
SEQGP	2200	12	2300	10	2400	8	2500	11	
SEQGP	2401	84	2501	79	2601	81	2701	83	
SEQGP	2600	9	2700	7	2800	6	2900	4	
SEQGP	3000	2	3100	5	3200	3	3300	1	

[a]Denotes NASTRAN bulk data card for grid point resequencing.

[b]Original grid point number.

[c]Resequenced grid point number.

Table XII Natural frequencies of booster and orbiter fuselages.

(a) Booster fuselage frequencies, HZ.

	Mode	Weight distribution				
		Liftoff		Max Q	Burnout	
		Theory	Exper.	Theory	Theory	Exper.
Bending	1 2 3	36.8 117.2 198.7	36.3[a], 36.8[b] 95.2[a], 98.8[b] 181.9, 177.3	53.6 137.9 252.3	83.9 242.7	73.7
Torsion	1 2	114.3 243.4	88.9 161.8	116.8 247.5		
Axial	1	240.2		298.9		

[a] Pitch excitation
[b] Yaw excitation

(b) Orbiter fuselage frequencies, HZ.

	Mode	Weight distribution		
		Liftoff		Empty
		Theory	Exper.	Theory
Bending	1 2 3	103.5 229.7 460.3	103.4[a], 102.7[b] 205[c], 201[c]	141.5 451.6

[a] Pitch excitation
[b] Yaw excitation
[c] Approximate

Table XIII Natural frequencies of free-free booster and orbiter wings.

	Booster wing		Orbiter wing	
Mode	Theory	Exper.	Theory	Exper.
1	24.6	26.4	26.3	
2	26.4	24.8	29.3	
3	27.3	26.4	31.0	28.5,32.2
4	28.0	26.0	61.3	
5	49.4		63.2	66.9
6	54.4	60.4	67.5	74.5
7	65.0		69.1	
8	69.4		73.4	
9	69.6	73.8		100.7
10	96.1			112.5
11	101.0		118.4	
12	107.3			120.5
13	113.2		125.7	
14	125.2		128.9	
15	142.5		133.4	
16	142.8		139.3	
17	152.2		177.1	
18	155.2		183.8	
19	182.9		190.4	
20	194.2		223.2	

Table XV Frequencies of elastically connected fuselages.
Theoretical flexibility matrix.
Liftoff weight distribution.

	Nominal spring constant, lb/in							
	10^2		10^3 [a]		10^4		10^5	
Mode	HZ	Motion	HZ	Motion	HZ	Motion	HZ	Motion
1	4.09	Pitch[b]	11.21	Pitch	27.27	Pitch	30.53	Yaw
2	8.73	Yaw[b]	17.35	Yaw	28.65	Yaw	31.35	Pitch
3	8.97	Pitch	24.98	Pitch	39.73	Pitch	54.19	Yaw
4	13.84	Yaw	34.38	Yaw	44.43	Yaw	63.34	Pitch
5	35.37	Yaw	37.42	Pitch	70.97	Pitch-axial	83.51	Axial-pitch
6	35.62	Pitch	40.12	Yaw	82.51	Pitch-axial	104.6	Yaw
7	68.57	Pitch-axial[c]	75.22	Pitch-axial	83.88	Yaw	113.5	Yaw
8	86.84	Roll[d]	96.22	Yaw	112.3	Yaw	117.7	Pitch
9	93.79	Yaw	104.9	Pitch	115.2	Yaw	158.4	Pitch
10	101.1	Pitch	110.4	Roll-yaw	116.6	Pitch	169.5	Yaw
11	112.8	Yaw	113.1	Yaw	131.2	Pitch	177.1	Yaw
12	117.5	Pitch	118.7	Pitch	137.2	Yaw	193.7	Pitch
13	123.6	Roll	131.9	Roll	155.3	Yaw-roll	197.9	Yaw
14	195.0	Yaw	195.3	Yaw	196.9	Yaw	223.9	Yaw

a The first nine modes for the 10^3 lb/in case are plotted in Figure 22.
b Pitch refers to motion primarily in the XZ plane; yaw refers to motion in the YZ plane.
c Axial denotes displacement along the X axis.
d Roll denotes rotation about the X axis.

Table XVI Comparison of frequencies for elastically connected fuselages.
Nominal 10^3 lb/in interface.
Liftoff weight distribution.

Nominal Interface Scalar springs[a]		Interface Flexibility Matrix			
		Theoretical Matrix[b]		Experimental Matrix[b]	
HZ	Motion	HZ	Motion	HZ	Motion
10.7	Pitch	11.2	Pitch	11.3	Pitch
10.7	Yaw	17.4	Yaw	16.3	Yaw
25.9	Pitch	25.0	Pitch	25.1	Pitch
25.9	Yaw	34.4	Yaw	33.5	Yaw
36.3	Pitch	37.4	Pitch	37.3	Pitch
36.3	Yaw	40.1	Yaw	38.5	Yaw
93.8	Pitch	75.2	Pitch-axial	64.3	Pitch-axial
93.8	Yaw	96.2	Yaw	88.4	Roll
110.5	Pitch	104.9	Pitch	95.5	Yaw
110.5	Yaw	110.4	Roll-yaw	102.6	Pitch
191.0	Pitch	113.1	Yaw	112.9	Pitch
191.0	Yaw	118.7	Pitch	116.7	Pitch
		131.9	Roll	123.9	Roll

[a]Test weights. Inverse power method with consistent mass matrix.
[b]Test weights. Givens method with lumped mass matrix.

Table XVII Frequencies of booster and orbiter airplanes.

(a) Booster airplane.

Frequencies, HZ

Predominate motion			
Coupled fuselage and wing modes		Wing modes	
Pitch[a]	Yaw[b]	Symmetric[c]	Antisymmetric[c]
30.0[d] 33.9 122.3 128.1	30.7[d]	65.2[d] 65.9 117.4	42.5[d] 63.8[d] 69.5 67.5 119.8

[a] Pitch refers to displacements in the XZ plane.
[b] Yaw refers to displacements in the YZ plane.
[c] Symmetry and antisymmetry refer to the XZ plane.
[d] The mode shapes for these frequencies are plotted in Figure 28.

(b) Orbiter airplane.

Frequencies, HZ

Predominate motion			
Coupled fuselage and wing modes		Wing modes	
Pitch[a]	Yaw[b]	Symmetric[c]	Antisymmetric[c]
79.6[d]	76.1[d]	33.1[d] 70.6[d] 132.7 138.8 152.2	41.6[d] 71.7[d] 128.1 141.7 149.7 198.9

[a] Pitch refers to displacement in the XZ plane.
[b] Yaw refers to displacements in the YZ plane.
[c] Symmetry and antisymmetry refer to the XZ plane.
[d] The mode shapes for these frequencies are plotted in Figure 28.

Table XVIII Frequencies of complete model

Frequencies, HZ.

Nominal 10^3 lb/in case.

Coupled fuselage and wing modes		Booster wing modes		Orbiter wing modes		Coupled booster and orbiter wing modes		
Pitch[a]	Combined pitch and yaw[a]	Sym.[b]	Antisym.[b]	Sym.	Antisym.	Sym.	Antisym.	Combined[c]
10.9[d]	13.8[d]	65.6[d]	119.9	73.2	30.2[d]	30.9[d]	47.2[d]	64.4
20.9	23.7[d]	118.8		132.8	70.2	33.6	63.6	69.6[d]
130.3	32.9	123.8		139.1	71.0	35.5		93.8
	78.7[d]	129.4			132.9			118.5
	92.0				142.9			147.9
					150.2			

[a] Pitch refers to displacements in the XZ plane; yaw refers to displacements in the YZ pla

[b] Symmetric and antisymmetric refer to the XZ plane.

[c] Combined modes indicate mode in which one wing vibrates symmetrically and the other anti-symmetrically.

[d] The mode shapes for these frequencies are plotted in Figure 28.

Table A-I
Spring Interface Dimensions

Nominal Spring Constant (lb/in)	t_p inches	t_Y inches
10^2	0.0188	.0237
10^3	0.0406	.0511
10^4	0.0874	.1101
10^5	0.1882	.2371

Dimension	Value inches
a	6.5
h	1.6
ℓ_P	2.0[a]
ℓ_Y	2.0[b]
L_1	5.5
L_2	2.0
d	9.0
C	8.0

[a] In equations A-3c, 4b, 6, 7b, 8a, 11 an effective length ℓ_P = 3.0 inches was used.

[b] In equation A-11b and 11c an effective length ℓ_Y = 2.75 inches was used.

TABLE A-II

SPRING INTERFACE FLEXIBILITY MATRIX

NOMINAL 10^2 CASE

PITCH SPRING T=0.01880 YAW SPRING T=0.02370

EFFECTIVE LENGTHS

L1 = 5.5 , L2 = 2.0

XZ PLANE FLEXIBILITIES

A55= 0.19770360E-02 A53= 0.26752064E-03 A33= 0.37227770E-04

YZ PLANE FLEXIBILITIES

A99= 0.10118822E-01 A97=-0.15005651E-04 A77= 0.22277925E-05

AT= 0.74455364E-05 AZ= 0.10033101E-01

NASTRAN FLEXIBILITY MATRIX Z(I,J)

0.19770360E-02	0.00000000E 00	0.00000000E 00	0.00000000E 00	0.26752064E-03	0.00000000E 00
0.00000000E 00	0.10118822E-01	0.00000000E 00	-0.15005651E-04	0.00000000E 00	0.00000000E 00
0.00000000E 00	0.00000000E 00	0.10033101E-01	0.00000000E 00	0.00000000E 00	0.00000000E 00
0.00000000E 00	-0.15005651E-04	0.00000000E 00	0.22277925E-05	0.00000000E 00	0.00000000E 00
0.26752064E-03	0.00000000E 00	0.00000000E 00	0.00000000E 00	0.37227770E-04	0.00000000E 00
0.00000000E 00	0.00000000E 00	0.00000000E 00	0.00000000E 00	0.00000000E 00	0.74455364E-05

Page Intentionally Left Blank

TABLE A-II Continued

SPRING INTERFACE FLEXIBILITY MATRIX

NOMINAL 10^3 CASE

PITCH SPRING T=0.04060 YAW SPRING T=0.05110

EFFECTIVE LENGTHS
L1 = 5.5 , L2 = 2.0

XZ PLANE FLEXIBILITIES

A55= 0.10407350E-02 A53= 0.13438055E-03 A33= 0.18136963E-04

YZ PLANE FLEXIBILITIES

A99= 0.10549543E-02 A97=-0.77538485E-05 A77= 0.11121305E-05

AT= 0.52633350E-05 AZ= 0.99616353E-03

NASTRAN FLEXIBILITY MATRIX Z(I,J)

0.10407350E-02	0.00000000E 00	0.00000000E 00	0.00000000E 00	0.13438055E-03	0.00000000E 00
0.00000000E 00	0.10549543E-02	0.00000000E 00	-0.77538485E-05	0.00000000E 00	0.00000000E 00
0.00000000E 00	0.00000000E 00	0.99616353E-03	0.00000000E 00	0.00000000E 00	0.00000000E 00
0.00000000E 00	-0.77538485E-05	0.00000000E 00	0.11121305E-05	0.00000000E 00	0.00000000E 00
0.13438055E-03	0.00000000E 00	0.00000000E 00	0.00000000E 00	0.18136963E-04	0.00000000E 00
0.00000000E 00	0.00000000E 00	0.00000000E 00	0.00000000E 00	0.00000000E 00	0.52633350E-05

TABLE A-II Continued

SPRING INTERFACE FLEXIBILITY MATRIX

NOMINAL 10^3 CASE

PITCH SPRING T=0.04060 YAW SPRING T=0.05110

EFFECTIVE LENGTHS
L1 = 0.0 , L2 = 0.0

XZ PLANE FLEXIBILITIES

A55= 0.80877251E-03 A53= 0.11499305E-03 A33= 0.16486963E-04

YZ PLANE FLEXIBILITIES

A99= 0.10399043E-02 A97=-0.62538485E-05 A77= 0.96213054E-06

AT= 0.18838428E-05 AZ= 0.99616353E-03

NASTRAN FLEXIBILITY MATRIX Z(I,J)

0.80877251E-03	0.00000000E 00	0.00000000E 00	0.00000000E 00	0.11499305E-03	0.00000000E 00
0.00000000E 00	0.10399043E-02	0.00000000E 00	-0.62538485E-05	0.00000000E 00	0.00000000E 00
0.00000000E 00	0.00000000E 00	0.99616353E-03	0.00000000E 00	0.00000000E 00	0.00000000E 00
0.00000000E 00	-0.62538485E-05	0.00000000E 00	0.96213054E-06	0.00000000E 00	0.00000000E 00
0.11499305E-03	0.00000000E 00	0.00000000E 00	0.00000000E 00	0.16486963E-04	0.00000000E 00
0.00000000E 00	0.00000000E 00	0.00000000E 00	0.00000000E 00	0.00000000E 00	0.18838428E-05

TABLE A-II Continued

SPRING INTERFACE FLEXIBILITY MATRIX

NOMINAL 10^4 CASE

PITCH SPRING T=0.08740 YAW SPRING T=0.11010

EFFECTIVE LENGTHS
L1 = 5.5 , L2 = 2.0

XZ PLANE FLEXIBILITIES

A55= 0.60748188E-03 A53= 0.72781408E-04 A33= 0.93055150E-05

YZ PLANE FLEXIBILITIES

A99= 0.13383578E-03 A97=-0.44051058E-05 A77= 0.59693936E-06

AT= 0.42543296E-05 AZ= 0.99856064E-04

NASTRAN FLEXIBILITY MATRIX Z(I,J)

0.60748188E-03	0.00000000E 00	0.00000000E 00	0.00000000E 00	0.72781408E-04	0.00000000E 00
0.00000000E 00	0.13383578E-03	0.00000000E 00	-0.44051058E-05	0.00000000E 00	0.00000000E 00
0.00000000E 00	0.00000000E 00	0.99856064E-04	0.00000000E 00	0.00000000E 00	0.00000000E 00
0.00000000E 00	-0.44051058E-05	0.00000000E 00	0.59693936E-06	0.00000000E 00	0.00000000E 00
0.72781408E-04	0.00000000E 00	0.00000000E 00	0.00000000E 00	0.93055150E-05	0.00000000E 00
0.00000000E 00	0.00000000E 00	0.00000000E 00	0.00000000E 00	0.00000000E 00	0.42543296E-05

TABLE A-II Continued

SPRING INTERFACE FLEXIBILITY MATRIX

NOMINAL 10^4 CASE

PITCH SPRING T=0.08740 YAW SPRING T=0.11010

EFFECTIVE LENGTHS
L1 = 0.0 , L2 = 0.0

XZ PLANE FLEXIBILITIES

A55= 0.37551938E-03 A53= 0.53393908E-04 A33= 0.76555150E-05

YZ PLANE FLEXIBILITIES

A99= 0.11878578E-03 A97=-0.29051058E-05 A77= 0.44693936E-06

AT= 0.87483745E-06 AZ= 0.99856064E-04

NASTRAN FLEXIBILITY MATRIX Z(I,J)

0.37551938E-03	0.00000000E 00	0.00000000E 00	0.00000000E 00	0.53393908E-04	0.00000000E 00
0.00000000E 00	0.11878578E-03	0.00000000E 00	-0.29051058E-05	0.00000000E 00	0.00000000E 00
0.00000000E 00	0.00000000E 00	0.99856064E-04	0.00000000E 00	0.00000000E 00	0.00000000E 00
0.00000000E 00	-0.29051058E-05	0.00000000E 00	0.44693936E-06	0.00000000E 00	0.00000000E 00
0.53393908E-04	0.00000000E 00	0.00000000E 00	0.00000000E 00	0.76555150E-05	0.00000000E 00
0.00000000E 00	0.00000000E 00	0.00000000E 00	0.00000000E 00	0.00000000E 00	0.87483745E-06

TABLE A-II Continued

SPRING INTERFACE FLEXIBILITY MATRIX

NOMINAL 10^5 CASE

PITCH SPRING   T=0.18820   YAW SPRING   T=0.23710

EFFECTIVE LENGTHS
L1 = 5.5 , L2 = 2.0

XZ PLANE FLEXIBILITIES

A55= 0.40634561E-03   A53= 0.44182558E-04   A33= 0.52050779E-05

YZ PLANE FLEXIBILITIES

A99= 0.33822662E-04   A97=-0.28491299E-05   A77= 0.35755844E-06

AT= 0.37857546E-05   AZ= 0.10001148E-04

NASTRAN FLEXIBILITY MATRIX Z(I,J)

0.40634561E-03	0.00000000E 00	0.00000000E 00	0.00000000E 00	0.44182558E-04	0.00000000E 00
0.00000000E 00	0.33822662E-04	0.00000000E 00	-0.28491299E-05	0.00000000E 00	0.00000000E 00
0.00000000E 00	0.00000000E 00	0.10001148E-04	0.00000000E 00	0.00000000E 00	0.00000000E 00
0.00000000E 00	-0.28491299E-05	0.00000000E 00	0.35755844E-06	0.00000000E 00	0.00000000E 00
0.44182558E-04	0.00000000E 00	0.00000000E 00	0.00000000E 00	0.52050779E-05	0.00000000E 00
0.00000000E 00	0.00000000E 00	0.00000000E 00	0.00000000E 00	0.00000000E 00	0.37857546E-05

TABLE A-II Concluded

SPRING INTERFACE FLEXIBILITY MATRIX

NOMINAL 10^5 CASE

PITCH SPRING T=0.18820 YAW SPRING T=0.23710

EFFECTIVE LENGTHS
L1 = 0.0 , L2 = 0.0

XZ PLANE FLEXIBILITIES

A55= 0.17438311E-03 A53= 0.24795058E-04 A33= 0.35550779E-05

YZ PLANE FLEXIBILITIES

A99= 0.18772662E-04 A97=-0.13491299E-05 A77= 0.20755844E-06

AT= 0.40626247E-06 AZ= 0.10001148E-04

NASTRAN FLEXIBILITY MATRIX Z(I,J)

0.17438311E-03	0.00000000E 00	0.00000000E 00	0.00000000E 00	0.24795058E-04	0.00000000E 00
0.00000000E 00	0.18772662E-04	0.00000000E 00	-0.13491299E-05	0.00000000E 00	0.00000000E 00
0.00000000E 00	0.00000000E 00	0.10001148E-04	0.00000000E 00	0.00000000E 00	0.00000000E 00
0.00000000E 00	-0.13491299E-05	0.00000000E 00	0.20755844E-06	0.00000000E 00	0.00000000E 00
0.24795058E-04	0.00000000E 00	0.00000000E 00	0.00000000E 00	0.35550779E-05	0.00000000E 00
0.00000000E 00	0.00000000E 00	0.00000000E 00	0.00000000E 00	0.00000000E 00	0.40626247E-06

TABLE A-III

SPRING INTERFACE STIFFNESS MATRICES

NOMINAL 10^2 CASE

PITCH SPRING T=0.01880 YAW SPRING T=0.02370

EFFECTIVE LENGTHS
L1 = 5.5 , L2 = 2.0

STIFFNESS MATRIX KXZ

0.97230462E 06	0.10801315E 07	-0.13156641E 06	0.13156641E 06
0.10801315E 07	0.13230095E 07	-0.15404750E 06	0.15404750E 06
-0.13156641E 06	-0.15404750E 06	0.18308584E 05	-0.18308584E 05
0.13156641E 06	0.15404750E 06	-0.18308584E 05	0.18308584E 05

STIFFNESS MATRIX KYZ

0.45340370E 06	-0.46389271E 06	0.67237249E 03	-0.67237249E 03
-0.46389271E 06	0.49867460E 06	-0.22296084E 04	0.22296084E 04
0.67237249E 03	-0.22296084E 04	0.99822819E 02	-0.99822819E 02
-0.67237249E 03	0.22296084E 04	-0.99822819E 02	0.99822819E 02

KZ= 0.99670079E 02 KT= 0.13430865E 06

TABLE A-III Continued

SPRING INTERFACE STIFFNESS MATRICES

NOMINAL 10^2 CASE

PITCH SPRING T=0.01880 YAW SPRING T=0.02370

EFFECTIVE LENGTHS
L1 = 0.0 , L2 = 0.0

STIFFNESS MATRIX KXZ

0.33834323E 07	0.41216096E 07	-0.48109243E 06	0.48109243E 06
0.41216096E 07	0.51602935E 07	-0.59499379E 06	0.59499379E 06
-0.48109243E 06	-0.59499379E 06	0.68979886E 05	-0.68979886E 05
0.48109243E 06	0.59499379E 06	-0.68979886E 05	0.68979886E 05

STIFFNESS MATRIX KYZ

0.48549825E 06	-0.49562207E 06	0.64896258E 03	-0.64896258E 03
-0.49562207E 06	0.53004304E 06	-0.22064727E 04	0.22064727E 04
0.64896258E 03	-0.22064727E 04	0.99840397E 02	-0.99840397E 02
-0.64896258E 03	0.22064727E 04	-0.99840397E 02	0.99840397E 02

KZ= 0.99670079E 02 KT= 0.24593928E 06

TABLE A-III Continued

SPRING INTERFACE STIFFNESS MATRICES

NOMINAL 10^3 CASE

PITCH SPRING T=0.04060 YAW SPRING T=0.05110

EFFECTIVE LENGTHS
L1 = 5.5 , L2 = 2.0

STIFFNESS MATRIX KXZ

```
 0.12728518E 07 0.12910341E 07-0.16435166E 06 0.16435166E 06
 0.12910341E 07 0.15433108E 07-0.18168878E 06 0.18168878E 06
-0.16435166E 06-0.18168878E 06 0.22182080E 05-0.22182080E 05
 0.16435166E 06 0.18168878E 06-0.22182080E 05 0.22182080E 05
```

STIFFNESS MATRIX KYZ

```
 0.94774131E 06-0.10564084E 07 0.69658395E 04-0.69658395E 04
-0.10564084E 07 0.14082181E 07-0.22551905E 05 0.22551905E 05
 0.69658395E 04-0.22551905E 05 0.99910681E 03-0.99910681E 03
-0.69658395E 04 0.22551905E 05-0.99910681E 03 0.99910681E 03
```

KZ= 0.10038512E 04 KT= 0.18999360E 06

TABLE A-III Continued

SPRING INTERFACE STIFFNESS MATRICES

NOMINAL 10^3 CASE

PITCH SPRING T=0.04060 YAW SPRING T=0.05110

EFFECTIVE LENGTHS
L1 = 0.0 , L2 = 0.0

STIFFNESS MATRIX KXZ

0.72993245E 07	0.88908857E 07	-0.10378339E 07	0.10378339E 07
0.88908857E 07	0.11130374E 08	-0.12834141E 07	0.12834141E 07
-0.10378339E 07	-0.12834141E 07	0.14879795E 06	-0.14879795E 06
0.10378339E 07	0.12834141E 07	-0.14879795E 06	0.14879795E 06

STIFFNESS MATRIX KYZ

0.10816415E 07	-0.11831171E 07	0.65048505E 04	-0.65048505E 04
-0.11831171E 07	0.15281344E 07	-0.22116491E 05	0.22116491E 05
0.65048505E 04	-0.22116491E 05	0.10007462E 04	-0.10007462E 04
-0.65048505E 04	0.22116491E 05	-0.10007462E 04	0.10007462E 04

KZ= 0.10038512E 04 KT= 0.53082985E 06

TABLE A-III Continued

SPRING INTERFACE STIFFNESS MATRICES

NOMINAL 10^4 CASE

PITCH SPRING T=0.08740 YAW SPRING T=0.11010

EFFECTIVE LENGTHS

L1 = 5.5 , L2 = 2.0

STIFFNESS MATRIX KXZ

0.17073768E 07	0.14837283E 07	-0.20455802E 06	0.20455802E 06
0.14837283E 07	0.16899799E 07	-0.20344283E 06	0.20344283E 06
-0.20455802E 06	-0.20344283E 06	0.26153901E 05	-0.26153901E 05
0.20455802E 06	0.20344283E 06	-0.26153901E 05	0.26153901E 05

STIFFNESS MATRIX KYZ

0.22126411E 07	-0.33487493E 07	0.72827447E 05	-0.72827447E 05
-0.33487493E 07	0.68865542E 07	-0.22678236E 06	0.22678236E 06
0.72827447E 05	-0.22678236E 06	0.98689047E 04	-0.98689047E 04
-0.72827447E 05	0.22678236E 06	-0.98689047E 04	0.98689047E 04

KZ= 0.10014414E 05 KT= 0.23505465E 06

TABLE A-III Continued

SPRING INTERFACE STIFFNESS MATRICES

NOMINAL 10^4 CASE

PITCH SPRING T=0.08740 YAW SPRING T=0.11010

EFFECTIVE LENGTHS
L1 = 0.0 , L2 = 0.0

STIFFNESS MATRIX KXZ

0.15722104E 08	0.19151323E 08	-0.22354761E 07	0.22354761E 07
0.19151323E 08	0.23976566E 08	-0.27646082E 07	0.27646082E 07
-0.22354761E 07	-0.27646082E 07	0.32051823E 06	-0.32051823E 06
0.22354761E 07	0.27646082E 07	-0.32051823E 06	0.32051823E 06

STIFFNESS MATRIX KYZ

0.26603519E 07	-0.36753405E 07	0.65063373E 05	-0.65063373E 05
-0.36753405E 07	0.71263018E 07	-0.22121547E 06	0.22121547E 06
0.65063373E 05	-0.22121547E 06	0.10009749E 05	-0.10009749E 05
-0.65063373E 05	0.22121547E 06	-0.10009749E 05	0.10009749E 05

KZ= 0.10014414E 05 KT= 0.11430694E 07

TABLE A-III Continued

SPRING INTERFACE STIFFNESS MATRICES

NOMINAL 10^5 CASE

PITCH SPRING T=0.18820 YAW SPRING T=0.23710

EFFECTIVE LENGTHS
L1 = 5.5 , L2 = 2.0

STIFFNESS MATRIX KXZ

0.24934969E 07	0.17360000E 07	-0.27112160E 06	0.27112160E 06
0.17360000E 07	0.18075213E 07	-0.22714880E 06	0.22714880E 06
-0.27112160E 06	-0.22714880E 06	0.31940410E 05	-0.31940410E 05
0.27112160E 06	0.22714880E 06	-0.31940410E 05	0.31940410E 05

STIFFNESS MATRIX KYZ

0.85066257E 07	-0.19685199E 08	0.71657522E 06	-0.71657522E 06
-0.19685199E 08	0.52748733E 08	-0.21194573E 07	0.21194573E 07
0.71657522E 06	-0.21194573E 07	0.89928340E 05	-0.89928340E 05
-0.71657522E 06	0.21194573E 07	-0.89928340E 05	0.89928340E 05

KZ= 0.99988514E 05 KT= 0.26414812E 06

TABLE A-III Concluded

SPRING INTERFACE STIFFNESS MATRICES

NOMINAL 10^5 CASE

PITCH SPRING T=0.18820 YAW SPRING T=0.23710

EFFECTIVE LENGTHS
L1 = 0.0 , L2 = 0.0

STIFFNESS MATRIX KXZ

0.33856479E 08	0.41241298E 08	-0.48139600E 07	0.48139600E 07
0.41241298E 08	0.51632451E 08	-0.59534454E 07	0.59534454E 07
-0.48139600E 07	-0.59534454E 07	0.69021830E 06	-0.69021830E 06
0.48139600E 07	0.59534454E 07	-0.69021830E 06	0.69021830E 06

STIFFNESS MATRIX KYZ

0.90415186E 07	-0.19178155E 08	0.64978440E 06	-0.64978440E 06
-0.19178155E 08	0.53642719E 08	-0.22092669E 07	0.22092669E 07
0.64978440E 06	-0.22092669E 07	0.99966831E 05	-0.99966831E 05
-0.64978440E 06	0.22092669E 07	-0.99966831E 05	0.99966831E 05

KZ= 0.99988514E 05 KT= 0.24614629E 07

Table BI Mass properties of booster and orbiter rigid body models.

Body	Mass [a]	Center of Mass [b]			Mass Moments of Inertia		
	M	$\overline{X}$	$\overline{Y}$	$\overline{Z}$	I_{XX}	I_{YY}	I_{ZZ}
	lb-sec²/in	inches			in-lb-sec²		
Booster fuselage	0.799	60.7	0	0	12.1	847.6	847.6
Orbiter fuselage	0.230	34.0	0	15.7	2.97	68.0	68.0
Booster airplane	0.853	64.8	0	-0.23	39.9	1134.5	1160.6
Orbiter airplane	0.273	36.0	0	15.6	6.9	93.1	96.9

[a] Masses and moments of inertia are based on test weights.
[b] See Figure 2 for the coordinate system.